2017-08-01

Electrokinetically Operated Integrated Microfluidic Devices for Preterm Birth Biomarker Analysis

Mukul Sonker
Brigham Young University

Electrokinetically Operated Integrated Microfluidic Devices for Preterm Birth Biomarker Analysis

Mukul Sonker

A dissertation submitted to the faculty of
Brigham Young University
in partial fulfillment of the requirements for the degree of

Doctor of Philosophy

Adam T. Woolley, Chair
Kenneth A. Christensen
Steven W. Graves
Matthew R. Linford
Richard K. Watt

Department of Chemistry and Biochemistry

Brigham Young University

ABSTRACT

Electrokinetically Operated Integrated Microfluidic Devices for
Preterm Birth Biomarker Analysis

Mukul Sonker
Department of Chemistry and Biochemistry, BYU
Doctor of Philosophy

Microfluidics is a vibrant and expanding field that has the potential for solving many analytical challenges. Microfluidics shows promise to provide rapid, inexpensive, efficient, and portable diagnostic solutions that can be used in resource-limited settings. Microfluidic devices have gained immense interest as diagnostic tools for various diseases through biomarker analysis. My dissertation work focuses on developing electrokinetically operated integrated microfluidic devices for the analysis of biomarkers indicative of preterm birth risk. Preterm birth (PTB), a birth prior to 37 weeks of gestation, is the most common complication of pregnancy and the leading cause of neonatal deaths and newborn illnesses. In this dissertation, I have designed, fabricated and developed several microfluidic devices that integrate various sample preparation processes like immunoaffinity extraction, preconcentration, fluorescent labeling, and electrophoretic separation of biomarkers indicative of PTB risk.

I developed microchip electrophoresis devices for separation of selected PTB biomarkers. I further optimized multiple reversed-phase porous polymer monoliths UV-polymerized in microfluidic device channels for selective retention and elution of fluorescent dyes and PTB biomarkers to facilitate on-chip labeling. Successful on-chip fluorescent labeling of multiple PTB biomarkers was reported using these microfluidic devices. These devices were further developed using a pH-mediated approach for solid-phase extraction, resulting in a ~50 fold enrichment of a PTB biomarker. Additionally, this approach was integrated with microchip electrophoresis to develop a combined enrichment and separation device that yielded 15-fold preconcentration for a PTB peptide.

I also developed an immunoaffinity extraction device for analyzing PTB biomarkers directly from a human serum matrix. A glycidyl methacrylate monolith was characterized within microfluidic channels for immobilization of antibodies to PTB biomarkers. Antibody immobilization and captured analyte elution protocols were optimized for these monoliths, and two PTB biomarker proteins were successfully extracted using these devices. This approach was also integrated with microchip electrophoresis for combined extraction and separation of two PTB biomarkers in spiked human serum in <30 min.

In the future, these optimized microfluidic components can be integrated into a single platform for automated immunoaffinity extraction, preconcentration, fluorescent labeling, andseparation of PTB biomarkers. This integrated microfluidic platform could significantly improve human health by providing early diagnosis of PTBs.

Keywords: microfluidics, microchip electrophoresis, sample preparation, electrochromatography, monoliths, immunoaffinity extraction, solid-phase extraction, on-chip labeling, preconcentration, biomarker analysis

ACKNOWLEDGEMENTS

I would like to express my gratitude to all who helped me through this journey. First, I would like to thank my PhD advisor, Dr. Adam T. Woolley, for his excellent guidance and for motivating me throughout my PhD. I consider myself very fortunate to have the opportunity to hone my skills as a researcher under Adam's tutelage. I wouldn't have been able to get through my PhD. if it wasn't for Adam's consistent encouragement and optimism. I would also like to express my gratitude to my PhD committee members, Dr. Kenneth Christensen, Dr. Steven Graves, Dr. Matthew Linford and Dr. Richard Watt for their thought provoking questions and helpful recommendations.

I thank my colleagues in the ATW lab especially Dr. Vishal Sahore, Dr. Chad Rogers, Dr. Jayson Pagaduan, Dr. Debolina Chatterjee, Dr. Suresh Kumar, Dr. Radim Knob, Rui Yang, Michael Beauchamp, Anna Nielsen, Ellen Parker, Robert Hanson, Janice Darko, Basu Aryal, John Jensen and others for their help with my research and insightful ideas. I am thankful to Dr. Bibek Uprety for his help with SEM imaging and to Dr. Anubhav Diwan and Tuhin Roychowdhury for their help with contact angle measurements. I am also thankful to Dr. Vajira Weerasekara and Ashari Kannangara for their help with dot blot tests and to Prof. William Pitt for providing human serum samples for this research. I am also thankful to the Science Support Shop for their technical support. Financial support for this work was partially provided by the National Institutes of Health through grant R01 EB006124 and a Roland K. Robins Graduate Research Fellowship awarded to me by the Department of Chemistry and Biochemistry. I am very thankful to Brigham Young University for providing me such an excellent platform for conducting this research and the entire faculty and staff in the Department of Chemistry and Biochemistry, especially Janet Fonoimoana, Sue Mortensen, and Anna Kennington for their administrative help and for providing a home-like environment away from home.

In the last, I want to express my gratitude towards my family and friends. I have been blessed by the Almighty with a big loving family who regardless of the distance and lack of communication, never stopped supporting me and my educational pursuits. I will always be grateful to my late grandparents, Mr. Om Prakash Sonker and Mrs. Dhanwanti Devi, who rooted their strong traditions and morals within me and will live forever in my cherished memories. I am grateful to my parents Mr. Hari Shankar Sonker and Mrs. Kusum Sonker who despite their financial conditions never compromised my education and always motivated to do my best. I am thankful to my brothers Ravi, Gazal, Sumit, Ratul, Amit, Nitin, Sagar, Sameer, Raj and sisters Deepika, Ritika, Kajal, Kanchan, and Geetika, who have always been a pillar of support for me. I am very thankful to all of my uncles, aunts, cousins, nieces and nephews for their never ending love and support. I am also thankful to all my friends in the US (Shailesh, Pankaj, Anupriya, Ankur, Bhuppi, Supriya, Rohit, Chandramouli, Teva, Ramya, Michelle, and Amber) and India (Rahul, Geet, Anju, Rashmi, Aastha, Aarti, Kanchan) who always encouraged me to move forward and kept me going during my PhD.

TABLE OF CONTENTS

LIST OF FIGURES ..... **x**

LIST OF TABLES ..... **xii**

1. INTRODUCTION **1**

1.1 MICROFLUIDIC DEVICES AS DIAGNOSTIC TOOLS 1

1.2 PRETERM BIRTH 2

1.3 ON-CHIP SAMPLE PREPARATION METHODS 3

1.3.1 Molecular Affinity Extraction 3

1.3.2 Sample Preconcentration 12

1.3.3 Sample Labeling 15

1.4 MOLECULAR SEPARATION TECHNIQUES 16

1.5 DISSERTATION OVERVIEW 19

1.6 REFERENCES 20

2. MICROCHIP ELECTROPHORETIC SEPARATIONS OF SELECTED PRETERM BIRTH BIOMARKERS **30**

2.1 INTRODUCTION 30

2.2 EXPERIMENTAL SECTION 33

2.2.1 Materials and Reagents 33

2.2.2 Device Fabrication 33

2.2.3 Instrumentation Setup 36

2.2.4 Off-chip Fluorescent Labeling 36

2.2.5 Device Operation 37

2.3 RESULTS AND DISCUSSION 39

2.3.1 μCE of Model Amino Acids, Peptides, and Proteins 39

2.3.2 μCE of PTB Biomarkers 40

2.4 REFERENCES 42

3. ON-CHIP FLUORESCENT LABELING OF SELECTED PRETERM BIRTH BIOMARKERS USING REVERSED-PHASE MONOLITHS 46

3.1 INTRODUCTION 46

3.2 EXPERIMENTAL SECTION 48

3.2.1 Materials and Reagents 48

3.2.2 COC Device Fabrication 49

3.2.3 Monolith Fabrication 50

3.2.4 Data Analysis 52

3.2.5 Device Operation 52

3.3 RESULTS AND DISCUSSION 54

3.3.1 Monolith Optimization 54

3.3.2 Retention and Elution of P1 55

3.3.3 Retention of FITC on C8 58

3.3.4 On-chip Labeling of PTB Biomarkers 58

3.4 REFERENCES 61

4. INTEGRATED ELECTROKINETICALLY DRIVEN MICROFLUIDIC DEVICES WITH PH-MEDIATED SOLID-PHASE EXTRACTION COUPLED TO MICROCHIP ELECTROPHORESIS FOR PRETERM BIRTH BIOMARKERS 66

4.1 INTRODUCTION 66

4.2 EXPERIMENTAL SECTION 69

4.2.1 Chemicals and Materials 69

4.2.2 Device Design and Fabrication 70

4.2.3 Surface Modification with PEGDA 72

4.2.4 Monolith Fabrication 74

4.2.5 Data Analysis 74

4.2.6 Device Operation 75

4.3 RESULTS AND DISCUSSION 76

4.3.1 Surface Modification with PEGDA 76

4.3.2 Monolith Characterization 78

4.3.3 Optimization of pH-mediated SPE 79

4.3.4 pH-mediated SPE of PTB Biomarkers 81

4.3.5 Effect of Analyte Concentration on pH-mediated Elution 82

4.3.6 Analyte Enrichment 83

4.3.7 Monolith Capacity 85

4.3.8 Effects of Blood Serum on P1 Binding Capacity 87

4.3.9 Integrated SPE and μCE of a PTB Biomarker 87

4.4 REFERENCES 89

5. MICROFLUIDIC DEVICES FOR INTEGRATED IMMUNOAFFINITY EXTRACTION AND ELECTROPHORETIC SEPARATION OF PRETERM BIRTH BIOMARKERS 98

5.1 INTRODUCTION 98

5.2 EXPERIMENTAL SECTION 100

5.2.1 Materials and Reagents 100

5.2.2 Device Design and Fabrication 101

5.2.3 Monolith Fabrication 103

5.2.4 Antibody Characterization and Immobilization 104

5.2.5 Fluorescent Labeling 105

5.2.6 Data Analysis 105

5.2.7 Device Operation 106

5.3 RESULTS AND DISCUSSION 107

5.3.1 Monolith Characterization 107

5.3.2 Antibody Immobilization 108

5.3.3 Optimization of Immunoaffinity Extraction 110

5.3.4 Immunoaffinity Extraction of PTB biomarkers 111

5.3.5 Integrated Immunoaffinity Extraction and μCE 113

5.3.6 Extraction and μCE Separation of PTB Biomarkers in a Human Serum Matrix 114

5.4 REFERENCES 116

6. CONCLUSIONS AND FUTURE WORK 122

6.1 CONCLUSIONS 122

6.1.1 μCE OF Selected PTB Biomarkers 122

6.1.2 On-Chip Fluorescent Labeling of PTB Biomarkers 122

6.1.3 Integrated pH-mediated SPE and Electrophoretic Separation of PTB Biomarkers ... 123

6.1.4 Immunoaffinity Extraction and Separation of PTB Biomarkers 123

6.2 FUTURE WORK 124

6.2.1 Integration of Immunoaffinity Extraction, On-chip Labeling and μCE 124

6.2.2 Integrated Analysis for PTB Diagnosis 125

6.2.3 3D Printed Integrated Microfluidic Devices for PTB Diagnosis 126

6.3 REFERENCES 128

LIST OF FIGURES

Figure 2.1 Schematic showing microchip electrophoresis..... 32

Figure 2.2 Schematic of silicon template fabrication. 34

Figure 2.3 Schematic showing fabrication of PMMA device from a silicon template..... 35

Figure 2.4 LIF setup used for detection 37

Figure 2.5 (A) Device layout, (B) photograph, and operation of "T" shaped device for μCE.... 39

Figure 2.6 μCE of model amino acids, peptides, and proteins. 40

Figure 2.7 μCE of PTB biomarkers. 41

Figure 3.1 Overview of on-chip labeling. 48

Figure 3.2 Device layout, photograph, and operation. 50

Figure 3.3 Monolith fabrication. 52

Figure 3.4 Schematic summarizing on-chip fluorescent labeling on a monolithic column..... 54

Figure 3.5 SEM images of bulk monoliths.. 55

Figure 3.6 Background-subtracted CCD fluorescence signal obtained from 50 μM FITC-P1 retained on monoliths..... 56

Figure 3.7 Retention and elution of FITC on a C8 monolith.. 57

Figure 3.8 On chip labeling of P1. 59

Figure 3.9 On-chip labeling of PTB proteins..... 60

Figure 4.1 Overview of pH mediated SPE..... 68

Figure 4.2 Device layout, photograph, operation and SEM images. 71

Figure 4.3 PEGDA photografting. 77

Figure 4.4 Effect of eluent pH on electroelution. 80

Figure 4.5 Effect of eluent buffer concentration. 80

Figure 4.6 pH-mediated SPE of sample dyes and PTB biomarkers 82

Figure 4.7 Effect of loaded P1 concentration on eluted peaks..... 83

Figure 4.8 P1 (50 nM loaded) enrichment with injection time. 83

Figure 4.9 Signal from 50 nM P1 injected directly into a channel. 84

Figure 4.10 Monolith saturation..... 85

Figure 4.11 Migration velocity of 500 nM P1. 86

Figure 4.12 Effect of a serum matrix on P1 retention and elution. 86

Figure 4.13 Integration of pH-mediated SPE with μCE. 88

Figure 5.1 Device design and images. 102

Figure 5.2 Dot blots. 108

Figure 5.3 Background-subtracted fluorescence on a GMA-EGDMA monolith after immobilization of anti-Fer 109

Figure 5.4 Effect of repeating immobilization of anti-Fer (2 mg/mL) on a GMA-EGDMA column for three consecutive days (n=3). 110

Figure 5.5 Effect of pH on extracted Fer (50 nM, AF 488 labeled) elution from an anti-Fer monolith. 111

Figure 5.6 Elution traces after immunoaffinity extraction of PTB biomarkers on control and Ab-modified monoliths. 112

Figure 5.7 Integrated immunoaffinity extraction and μCE of PTB biomarkers. 114

Figure 5.8 Integrated immunoaffinity extraction and μCE of PTB biomarkers spiked in human blood serum. 115

Figure 6.1 Schematic for proposed integrated microfluidic device for PTB diagnosis. 125

Figure 6.2 3D printed microfluidic devices 127

LIST OF TABLES

Table 1.1 Preterm birth biomarker panel 3

Table 1.2 Microfluidic devices for affinity-based analysis. 6

Table 1.3 On-chip sample preconcentration. 13

Table 1.4: Molecular separation methods for biomarker analysis. 16

Table 3.1. Monolith pre-polymer mixture 51

Table 4.1: Reversed phase octyl methacrylate prepolymer mixture 73

Table 4.2: Contact angle measurements 78

1. INTRODUCTION*

1.1 MICROFLUIDIC DEVICES AS DIAGNOSTIC TOOLS

Disease diagnostics are important for improving human health, and the effective treatment of many life-threatening conditions is dependent upon the accuracy and speed of the diagnosis, which can result in improved human life expectancy. Technologies currently used in healthcare diagnostics often require expensive instrumentation or a modern testing laboratory, neither of which are feasible in many developing nations or in remote locations. Hence, low-cost, rapid, portable, and easy to use tools are desirable to advance clinical diagnostics, especially in developing countries or remote areas that lack appropriate infrastructure.

Analyses of biomarkers, biomolecular indicators of medical conditions, hold excellent potential for the clinical diagnosis of various diseases. These biomarkers are frequently found in complex biological matrices or bodily fluids, which almost always require sample preparation prior to analysis. Sample preparation steps often need large volumes (> mL) and experienced personnel, which further increase the analysis time and cost. Thus, fast and effective sample preparation techniques are necessary to facilitate early diagnosis.

Microfluidic systems offering advantages like low cost per device, rapid analysis, and small sample requirements[1] have potential to transform diagnostics, especially in developing countries or remote locations, due to amenability to point-of-care testing. Biomarker analysis has been one of the most actively pursued applications in miniaturization of chemical analyzers. A number of microfluidic systems have been reported recently that can perform sample preparation

*Portions of this chapter are adapted with permission from M. Sonker, V. Sahore, A.T. Woolley, Recent advances in microfluidic sample preparation and separation techniques for molecular biomarker analysis: A critical review, *Anal. Chim. Acta* (**2017**), doi: 10.1016/j.aca.2017.07.043.

steps like purification, preconcentration and labeling on a chip prior to quantitation.[1-3] Separation techniques have also advanced for the analysis of molecular biomarkers in a microfluidic setup.

1.2 PRETERM BIRTH

Preterm birth (PTB) is the birth of a baby prior to 37 weeks of pregnancy or three weeks before the estimated due date. It is the most common type of complication in pregnancy with a high incidence rate of 1 out of every 8 births, and more than 500,000 cases annually in the US. Complications from PTB are a major cause of neonatal deaths and newborn illnesses. The actual causes of PTB are not known but there are associations with lifestyle, race/ethnicity and diet. US health care expenditures on PTB management were estimated to be over 26 billion dollars in 2005, and are even higher now.[4-7] Presently, there is no effective clinical method available for PTB risk assessment, which hinders the application of possible therapeutic interventions that can delay birth in at-risk cases. Thus, there is a major need for an efficient clinical diagnosis method to evaluate PTB risk at an early stage.

Biomarkers used previously for detection of PTB included a glycoprotein, fetal fibronectin, in cervical fluid or vaginal secretions. One drawback of this approach is the difficulty and discomfort in obtaining the samples for analysis.[8-9] Six serum protein biomarkers have also been associated with PTB (see Table 1.1).[5] Furthermore, three additional serum peptides, fragments of a larger protein called inter-alpha-trypsin inhibitor heavy chain 4, (also shown in Table 1.1), were discovered. These peptides when combined with the six protein biomarkers in Table 1.1 provided 87% sensitivity and 81% specificity in predicting a PTB four weeks later at a gestational age of 28 weeks.[10-11] Currently available biomarker analysis approaches like liquid chromatography,[12]

ELISA[13] and mass spectrometry[14-15] offer accurate analysis but they take time, are expensive and are not suitable for point-of- care (POC) analysis. Thus, a simple and cheaper microfluidic analysis system for PTB biomarkers is greatly needed.

Table 1.1 Preterm birth biomarker panel

Peptide-1	QLGLPGPPDVPDHAAYHPF
Peptide-2	NVHSAGAAGSRMNFRPGVLSSRQLGLPGPPDVPDHAAYHPF
Peptide-3	NVHSAGAAGSRM(O)NFRPGVLSSRQLGLPGPPDVPDHAAYHPF
Proteins	ferritin, defensin, lactoferrin, thrombin-antithrombin complex, corticotropin-releasing factor, tumor necrosis factor-α receptor type 1

1.3 ON-CHIP SAMPLE PREPARATION METHODS

Microfluidics can be used to miniaturize and integrate sample preparation processes on a microchip platform. Typically, building these systems requires innovations in device design and manufacturing; fluid transport, automation and control; preparation of samples before analysis; separation; multiplexing; and detection.[16] Often sample specimens are limited in volume, contain matrix-related interferences, require multiplex analysis and have low target analyte concentrations;[17] therefore, sample preparation is a key part of analysis. Commonly used sample preparation processes include analyte purification, enrichment and labeling. In this section I focus on select techniques published in the past two years on microfluidic sample preparation.

1.3.1 Molecular Affinity Extraction

On-chip sample preparation can be used to selectively extract, preconcentrate and label selected analytes in an automated fashion. The ability to extract trace amounts of desired analytes

from a complex sample matrix such as blood significantly simplifies the analysis.[18] Such on-chip sample preparation could replace laborious benchtop processes, and thus decrease analysis time and potentially allow point-of-care usage. Affinity approaches using antibodies or aptamers on a solid support can purify target species in blood from undesired matrix components that complicate analysis. A summary of key information related to molecular affinity extraction work discussed in this section is given in Table 1.2.

1.3.1.1 Antibody-based Extraction

An antibody (Ab) offers high selectivity and specificity towards its target antigen, and can be used in microfluidic systems for the selective capture of desired molecules.[19-20] Antibodies can be placed in a microfluidic setup by device surface modification [21-22] or through a solid support like porous polymer monoliths,[23] beads[24-25] or nanoparticles[26-27] introduced into microchannels.

An immunosensor was developed on a PDMS treated glass microfluidic device using Ab-conjugated polyvinyl alcohol covered zinc oxide nanoparticles for the extraction of epithelial cell adhesion molecule (EpCAM), a biomarker for epithelial cancers.[28] Whole blood was centrifuged and lysed off-chip to prepare the supernatant that was introduced into the microfluidic devices. Bound EpCAM interacted with anti-EpCAM conjugated to horseradish peroxidase, which catalyzed the oxidation of non-fluorescent 10-acetyl-3,7-dihydroxyphenoxazine to fluorescent resorufin. Extraction results from blood samples obtained from cancer patients and healthy volunteers were compared to a commercially available test, and a linear correlation was obtained from 2-2000 pg mL^{-1} EpCAM with a detection limit of 1.3 pg mL^{-1}. Future work in correlation of measured EpCAM levels with cancer incidence with minimum off-chip sample preparation would be impactful.

In a different study, a paper microfluidic device was reported that utilized an antibody-based sandwich assay for detection of tumor necrosis factor alpha (TNFα), an inflammation biomarker.[29] Carbon electrodes were printed on the paper device and anti-TNFα immobilization through both covalent binding and physical adsorption was tested for immuno-capture and electrochemical detection. The limit of detection for TNFα was 4 ng mL^{-1}, and diluted human serum samples spiked with TNFα were analyzed down to 20 ng mL^{-1}, although further improvements in detection will be needed to analyze TNFα at native levels in blood. With further work in miniaturizing the electrochemical detection instrumentation, such disposable devices may show promise for detection of diseases, potentially in a point-of-care setting in developing countries. Ali et al.[30] also reported a microfluidic device for electrochemical detection of a breast cancer biomarker, epidermal growth factor receptor 2 protein family (ErbB2). Using carbodiimide linkage methods Anti-ErbB2 was covalently attached to graphene foam modified with titanium dioxide nanofibers, which served as an immuno-electrode inside a polydimethylsiloxane (PDMS)-glass microfluidic device. Detection by differential pulse voltammetry and electrochemical impedance spectroscopy worked for ErbB2 from 100 nM to 1 fM in the presence of interfering antigens. Experimental results were obtained in buffer solutions, so studies with cell lysate or serum samples as a next step would provide a greater impact.

Table 1.2 Microfluidic devices for affinity-based analysis. Additional abbreviations used: Carcinoembryonic antigen (CEA), recombinant avian influenza A virus (rH7N9), cancer antigen-125 (CA-125), cluster of differentiation 24 (CD24).

Affinity method	Biomarkers	Disease/condition	Immobilization	Detection	Concentration	Reference
Antibody	EpCAM	Epithelial cancer	Channel surface	Fluorescence	2-2000 pg/mL	28
	TNFα	Inflammation	Channel surface	Electrochemical	4-50 ng/mL	29
	ErbB2	Breast cancer	Covalent to TiO_2 nanofibers	Electrochemical	1 fM – 0.1 μM	30
	CEA, rH7N9	Influenza A	in-solution and in-gel	Colorimetric	1-100 pg/mL	32
	Influenza virus epitope	Influenza	in-solution	Colorimetric	1-100 μg/mL	33
	Bcl-2	Apoptosis	Covalent to tin oxide	Mass spectrometry	140 nM	34
	Gastric cancer biomarker panel	Gastric cancer	Channel surface	Electrochemical	pg/mL-ng/mL	34
	E. *coli*	E. *coli* infection	Channel surface	Fluorescence	10^5-10^7 cfu/mL	38
	PGA	Anthrax	Magnetic beads	SERS	100 pg/mL-100 μg/mL	39
	Apolipoprotein A1	Bladder cancer	Magnetic beads	Semiconductor based ion-sensitivity	12.5-1000 ng/mL	40
	CA-125, EpCAM, CD24	Ovarian cancer	Magnetic beads	Fluorescence	7.5×10^5 - 1×10^7 particles/mL	41
	Aβ peptides	Alzheimer's disease	Magnetic beads	Fluorescence	25-100 ng	42
	E. *coli*	Pathogens	Nanoparticle clusters	UV-Vis	100-10^5 cfu/mL	43
Aptamer	PSA	Prostate cancer	Channel surface	Chemiluminescence	3-50 ng/mL	46
	Hemoglobin	Diabetes	Magnetic beads	Fluorescence	0.7-14.8 g/dL	47
	VEGF	Cervical cancer	Channel surface	UV-Vis, Fluorescence	2-40 ng/mL	48
	Creatine kinase	Cardiac damage	Covalent to gold electrode	Electrochemical	10 pg/mL-100 ng/mL	49

With the advent of smartphones, diagnosis based on ubiquitous camera capabilities offers great potential for point-of-care[31] and microfluidics applications. One recent example used an on-chip complement fixation test for the detection of carcinoembryonic antigen and recombinant avian influenza A virus using a PDMS-glass microchip.[32] Fluidic-based and agar gel-based complement fixation tests were developed to indicate the presence of a specific antibody or antigen. Colorimetric changes for concentrations in the range of 1-100 pg/mL were easily imaged and analyzed using a smartphone, indicating strong potential for point-of-care application. Another study reported a smartphone-operated microfluidic colorimetric immunoassay for detection of influenza infection.[33] The PDMS microfluidic device contained nitrocellulose paper with influenza virus epitope spots to capture the corresponding primary antibodies present in the diluted sample. These primary antibodies were then detected using alkaline phosphatase conjugated secondary antibodies that induced a color change for a concentration range of 1-100 μg/mL in diluted serum. The device was battery operated and portable, and the total analysis time was 18 min. The results in both these studies involved colorimetric changes that were imaged and analyzed using a smartphone, which as shown previously[31] can be advantageous for point-of-care applications. Improved microfluidic devices that can effectively detect clinically relevant concentration of biomarkers in typical biological matrices with little to no sample preparation are needed to further advance smartphone-enabled diagnostics.

Yang et al.[34] reported a PDMS microfluidic device containing wells separated by pneumatic valves for affinity capture, tryptic digestion and isotopic labeling leading to mass spectrometric analysis of an apoptosis-related protein, Bcl-2. Anti-Bcl-2 antibodies were covalently linked to indium tin oxide on the bottom of the wells, and sequence coverage of 50% was reported for mass spectrometric analysis after tryptic digestion and iTRAQ labeling of

captured Bcl-2. Going forward, cell studies and multiplex biomarker capture are important capabilities that should be addressed for these systems to have greater impact in proteomics.

In a different study an electrochemical microfluidic chip for the multiplexed detection of gastric cancer biomarkers was reported.[35] Gold working electrodes were fabricated on glass, antibodies were covalently bound and the device was formed by bonding a PDMS mold cover. Six biomarkers for gastric cancer (carcinoembryonic antigen, carbohydrate antigen 19-9, H. *pylori* CagA protein, P53 oncoprotein, and pepsinogen I and II) were electrochemically detected from serum samples using these immunosensor chips with a linear correlation from clinically relevant pg/mL to ng/mL concentrations. Future work in developing a concentration-based assay would eventually allow early diagnosis and monitoring of gastric cancer.

PDMS has been widely used for making microfluidic devices but it has disadvantages like hydrophobicity and poor fabrication scalability.[36-37] Thus, a thiol-acrylate resin that exhibits low background fluorescence was reported for making microfluidic devices at room temperature.[38] Simple electrostatic interaction between the channel walls and an Ab to E. *coli* was used for immobilization. Using these devices, 10^5 cfu mL^{-1} of fluorescently labeled E. *coli* were detected. Although this resin shows promise as a material for microfluidic devices, improvement in the detection limit, immobilization method and ability to detect unlabeled bacteria will be needed for utility in disease diagnosis.

Beads are routine solid supports for antibodies and can be easily manipulated within fluidic networks;[24] thus, microfluidic systems that utilize beads for immuno-capture and detection of disease biomarkers are being developed.[25] Gao et al.[39] used antibody-conjugated magnetic beads for the detection of an anthrax biomarker, poly-γ-D-glutamic acid (PGA), in human serum using surface-enhanced Raman scattering (SERS) in a microfluidic setup. Detection was done using

competition between PGA and PGA-conjugated gold nanoparticles for anti-PGA linked magnetic beads in a PDMS microdevice. A linear decrease in SERS signal was observed for clinically relevant PGA concentrations ranging from 100 pg/mL to 100 μg/mL in human serum. Future work should focus on extension of the approach to additional biomarkers and developing multiplexing methods.

Another study reported a magnetic bead-based immunoassay for urinary protein biomarker detection in a microfluidic device.[40] Magnetic beads with epoxy groups were conjugated with antibodies to capture apolipoprotein A1, a bladder cancer biomarker. Addition of negatively charged DNA on the antigen-antibody complex increased charge, resulting in signal enhancement on the semiconductor sensor platform within the microdevice. Apolipoprotein A1 was measured in urine samples within 20% error compared to established methods, with a limit of detection of 10 ng/mL. Although this microfluidic device shows promising results for quantitation of clinically useful levels of a urine biomarker, the error in concentration measurement has room for improvement.

Zhao et al.[41] also used magnetic beads to capture intact exosomes from human serum for the detection of three ovarian cancer biomarkers (see Table 1.2). A microchip containing a serpentine channel with Y-shaped inlets was fabricated in PDMS for mixing beads and capturing exosomes. These beads were then collected in a microchamber using a magnet, incubated with fluorescent antibodies for three ovarian cancer exosomal markers and detected by multi-color fluorescence imaging. Comparable results to a conventional assay for cancer vs. healthy samples were obtained using the microchip in a 40 min analysis time. Future efforts to correlate detected biomarker concentrations with occurrence of cancer will be needed for diagnostic applications.

Another group developed a PDMS microfluidic device that used antibody-coated magnetic beads for selective capture of Aβ peptides, biomarkers of Alzheimer's disease.[42] The device had a nanoporous hydrogel membrane for peptide preconcentration, and a microchip electrophoresis (μCE) channel for separation of Aβ peptides. Using this integrated device 25 ng of Aβ peptide spiked in 100 μL cerebrospinal fluid (CSF) was detected. To further improve this method, mixing of Ab-coated magnetic beads with CSF could be done on-chip and analysis of patient CSF samples instead of spiked ones should be done. Lee et al.[43] used antibody-conjugated magnetic nanoparticle clusters in a 3D printed helical channel device to capture E. *coli* in milk. The concentration of captured bacteria was determined by UV-Vis absorption, and the limit of detection was 100 cfu/mL in milk. This study indicates the potential of 3D printed fluidic devices for biomarker analysis; however, the channel dimensions are larger than traditional microfluidic dimensions.

1.3.1.2 Aptamer-based Extraction

Aptamers are short oligonucleotides that have high affinity for their target molecule; they have been used for capture and extraction in microfluidics. Compared to antibodies, aptamers offer advantages like easy synthesis, high stability and low cross-reactivity,[44-45] but aptamer research has not been pursued as deeply as the research of antibodies.

Jolly et al.[46] reported aptamer-based microfluidic immunoassays for prostate cancer biomarker measurement. Amine-linked aptamers covalently attached to PDMS channels derivatized with (3-glycidyloxypropyl) trimethoxysilane were used to capture prostate specific antigen (PSA) from buffer solution. In one immunoassay, free PSA was measured by introducing secondary antibodies, followed by chemiluminescence detection with a limit of detection of 0.5 ng/mL. Additionally, detection of glycosylated PSA was done using a biotinylated lectin after

aptamer capture, with a limit of detection of 3 ng/mL. This device shows a novel aptamer-based assay that can detect clinical levels of free PSA; however, multiplexed experiments using serum samples still need to be evaluated for greater impact. In a different report aptamers were used for sandwich immunoassays in a PDMS microfluidic device for potential diagnosis of diabetes.[47] Two parallel assays were conducted for quantitation of glycated hemoglobin and total hemoglobin. Analytes were captured from pretreated blood samples by incubating with aptamer-coated magnetic beads. After capture, a second labeled aptamer was added for fluorescence detection. This assay showed good correlation in the quantitation of typical human blood hemoglobin levels compared with benchtop HPLC results, in a shorter analysis time. Going forward, hemoglobin concentrations should be assayed on control vs. diabetic blood samples.

Lin et al.[48] reported a PDMS microfluidic device for cell culture and used aptamer-functionalized microchannels for analysis of vascular endothelial growth factor (VEGF). Amine-modified aptamers were attached to the carboxy-silane derivatized surface via carbodiimide coupling. Cell-cell communication was studied under different low oxygen conditions and for various distances between cell cultures. The results showed faster cell migration under oxidative stress, and captured VEGF (indicating tumor development) was detected using fluorescence and UV-Vis absorption. Another group developed an aptamer-based electrochemical microfluidic biosensor for the detection of creatine kinase, a cardiac biomarker.[49] A gold electrode surface was coated with a carboxy-terminated thiol, which was then functionalized with amine-linked aptamers via carbodiimide coupling. Impedance signal for creatine kinase was linear from 10 pg/mL to 100 ng/mL (relevant to clinical concentrations) in both buffer and culture media samples. A heart–on-chip cardiac bioreactor was integrated with this device, and doxorubicin-induced cardiac damage was assessed through changes in creatine kinase concentration. Both these studies demonstrate

microfluidic cell culture devices that detect secreted proteins; future work enabling detection of multiple biomarkers for diagnostic purposes would be impactful.

To summarize, a variety of microfluidic platforms have been reported recently for affinity capture of targeted biomarkers using antibodies and aptamers. A key area of improvement needed for many of these systems is the ability to maintain good detection limits with biological matrices. Multiplexing is another pursuit that could improve disease diagnosis in these microfluidic devices. Finally, efforts are needed to design diagnostic assays that are well suited for point-of-care applications.

1.3.2 Sample Preconcentration

To achieve rapid analysis in a point-of-care setup, a system must measure analytes from blood or other specimens with minimal sample preparation. Since biomarkers are often present in trace amounts, a preconcentration step can be desirable to improve detection.[50] Sample preconcentration on a microfluidic platform can be achieved through electrokinetic means, filtration or chromatographic interactions, as summarized in Table 1.3.

Ge et al.[51] developed an approach to concentrate DNA in a PDMS microchannel, where temperature gradient focusing (TGF) occurred at the interface of a channel that expanded rapidly, supplementing electrokinetic concentration. A combination of high-frequency AC with DC voltage reduced the backpressure due to electroosmosis and improved efficiency. DNA preconcentration of 500-fold was achieved in 40 s of operation. This device showed a good preconcentration efficiency for model DNA; however, device performance with real samples still needs to be evaluated.

Table 1.3 On-chip sample preconcentration.

Mechanism	Medium	Device material	Analytes	Enrichment	References
Electrokinetic	Liquid phase	PDMS	DNA	500	51
	Nanoporous membrane	PDMS	Angiotensin	450	52
		Paper	Bovine serum albumin	800	53
		PDMS	Lipid vesicles	160	54
SPE	Size selective membrane	PDMS	Albumin	500	55
	Porous polymer monolith	PDMS-COC	Ferritin	100	56

Combining hydrodynamic control with electrokinetic methods can be beneficial. Indeed, Cong et al.[52] developed an electrokinetic sample preconcentration microfluidic device with electrokinetic or hydrodynamic injection, a pneumatic valve for preconcentration and μCE separation. With the valve closed during electrokinetic injection, current flowed but bulk flow was blocked, allowing ion concentration polarization for sample preconcentration at the closed valve interface. A preconcentrated sample was hydrodynamically injected for μCE, showing 450-fold enrichment. This initial demonstration with model analytes in buffer solution could be improved upon with analysis of biomarkers in a complex sample matrix.

Paper microfluidics can provide inexpensive but often low performance devices. Paper microfluidics for electrokinetic preconcentration of model analytes were demonstrated by forming a cation selective Nafion membrane to induce ion concentration polarization.[53] Preconcentration was further enhanced by decreasing channel depth through a two-sided wax-printing process, resulting in an 800-fold increase in the concentration of bovine serum albumin. In future efforts this method should be tested on disease-related biomarkers in blood or other sample matrices.

Similarly, Lee et al.[54] fabricated an ion-selective Nafion membrane inside PDMS microfluidic channels to electrokinetically concentrate lipid vesicles. Under an applied voltage ion concentration polarization occurred at the interface of the microchannel with the Nafion, causing a 160-fold lipid vesicle enrichment. Further development is needed to achieve greater preconcentration as well as for application to specific biomarkers.

To provide analyte selectivity a PDMS microfluidic device was developed with integrated polycarbonate track etched membranes having different sized nanopores.[55] This double-membrane microfluidic device processed a urine sample, with the 100 nm pore membrane excluding particles and cells in human urine, but passing proteins, small molecules and ions. A second 10 nm pore membrane passed small molecules and ions but excluded albumin, which was then analyzed by μCE. This approach took 2 min to process a urine sample, and yielded a 6-100 μg/mL linear range and 1.5 μg/mL limit of detection for albumin. This work shows promise in analyzing proteins in a real sample matrix; future efforts to detect additional biomarkers in more complex matrices would be desirable.

On-chip pneumatic pumps and valves offer advantages such as reproducibility and precise control of fluids. Woolley's group developed a microfluidic device integrating solid phase extraction (SPE) and μCE to analyze for a preterm birth biomarker.[56] In this device, SPE was performed in a reversed-phase porous polymer monolith made inside cyclic olefin copolymer (COC) material, and the hydrodynamic controls were formed in PDMS. An integrated SPE-μCE analysis was performed on a preterm birth protein biomarker, ferritin, and a 100-fold enrichment factor was achieved relative to μCE without on-chip SPE, which makes this device amenable for detection of serum levels of ferritin. Although a real sample matrix was not tested, this work lays a foundation for the development of pneumatically operated integrated microfluidic systems for

biomarker analysis, potentially integrating additional sample preparation steps like analyte labeling.

1.3.3 Sample Labeling

In addition to preconcentration and purification, analyte labeling is an important sample preparation step that can be performed on a chip to save time. On-chip labeling requires loading, reacting and purifying, and typically uses a support inside the microchannels; fluorescent labeling is the most common approach being explored.

Herzog et al.[57] developed an integrated microfluidic device on a glass substrate for electrokinetic labeling and separation of peptides and proteins. The integrated device had a reactor for fluorescent labeling with Atto 425, a separation compartment for free flow isoelectric focusing, and a pH sensor layer to calibrate pI values. This device allowed the analysis of proteins and peptides in 5 min, offering process integration and speed; however, the resolution of the separated mixture still needs to be improved.

Woolley's group used reversed-phase porous polymer monolith SPE for the preconcentration and fluorescent labeling of model proteins with fluorescein isothiocyanate (FITC) and Alexa Fluor 488.[58] Different reversed-phase monolith recipes and eluent compositions were optimized for selective elution of fluorescent dye and labeling of bovine serum albumin and heat shock protein 90. This study indicate the potential of microfluidic devices to integrate preconcentration and labeling to minimize off-chip sample preparation time and effort. Future efforts should focus on lowering biomarker concentrations detected, subsequent integration with separation by μCE and on-chip processing of samples in complex matrices.

1.4 MOLECULAR SEPARATION TECHNIQUES

Multiple biomarkers are often analyzed simultaneously in clinical diagnostic applications; thus, separation is an integral part of biomarker panel analysis. Various separation techniques have been developed and explored in microfluidic systems for analysis of biomarkers.[3, 59] Molecular separation techniques in microfluidics discussed in this section are summarized in Table 1.4.

Table 1.4: Molecular separation methods for biomarker analysis.

Technique	Analytes	Device material	Concentration	Reference
Gel electrophoresis	Bovine serum albumin, ovalbumin, trypsin inhibitor, parvalbumin	PDMS-glass	0.05 mg/mL	60
	DNA fragments	PMMA	10-20 ng/µL	61
Electrophoresis	mAbs	Glass	0.5-1 mg/mL	62
	D-amino acids	Glass	0.3-0.5 mM	63
	TK1	PMMA	2-25 µg/mL	64
	Ferritin, preterm birth peptide biomarker	PDMS-COC	100-500 nM	65
	Myoglobin, carbonic anhydrase, catalase	Glass	0.1-0.3 µg/µL	66

Shameli and Ren[60] developed a PDMS-glass microfluidic chip for two-dimensional separation of proteins by combining TGF with sodium dodecyl sulfate-polyacrylamide gel electrophoresis. Initially a mixture of bovine serum albumin, ovalbumin, trypsin, and parvalbumin was injected and separated by TGF in the first dimension; subsequently, the TGF peaks were analyzed by denaturing gel electrophoresis in a different channel. In an 8 min analysis time a 70%

improvement in the peak resolution of a model protein sample was achieved compared to a separation with only TGF. However, further improvement in separation efficiency to achieve baseline resolution is desirable for quantitative applications. Another group reported a gel-based microchip for preconcentration, separation and extraction of DNA fragments.[61] The device was fabricated by thermally bonding 4 PMMA layers, agarose gel electrophoresis was used to separate DNA and a cellulose ester membrane was used for extraction of DNA fragments. Sample was preconcentrated prior to isotachophoresis, and two parallel channels were used for separation with one channel containing a reference DNA ladder. PCR products were analyzed and an extraction efficiency of 50% was reported. With further work in biological matrices, this device could be used for separation of nucleic acid biomarkers in the future. Redman et al.[62] reported an integrated μCE-electrospray ionization device for separation of monoclonal antibodies (mAbs). A T-shaped device had a separation channel with tapered turns and which extended to the edge of the device to produce an electrospray. This microchip was further combined with mass spectrometry for identification of separated mAbs, showing potential for rapid mass spectrometric analysis of biomarkers using microfluidics, provided more complex sample matrices can be analyzed.

In a different study a T-shaped electrophoresis device for separation of D-amino acids (biomarkers of *Vibrio cholerae* infection) followed by electrochemical detection was reported.[63] A graphene electrode at the end of the separation channel allowed the amperometric detection of liberated H_2O_2 when D-amino acids reacted with D-amino acid oxidase; in contrast L-amino acids showed no amperometric signal. Although this work utilized a novel signal generating mechanism, further improvements in analyte concentration are needed for potential clinical applications. Pagaduan et al.[64] reported a μCE device for determination of thymidine kinase 1 (TK1), a cancer biomarker. A microchip immunoaffinity assay was reported for measuring Ab-TK1 complex after

separating it from the unbound mAb. Although this study reported separation of purified TK1 in buffer incubated with mAb off-chip, there is potential for translation to clinical application if the assay can be performed with adequate detection limits in a relevant matrix like blood.

Sahore et al.[65] reported a pressure-actuated microfluidic device for separation of biomarkers associated with preterm birth. A three-layer PDMS device was fabricated with integrated valves and a peristaltic pump for pressure-actuated injection for μCE of these biomarkers. Injection was optimized for valve spacing and actuation rate, eliminating bias and yielding an increase in signal, resolution and number of theoretical plates compared to electrokinetic injection. Although this device was used to separate off-chip-labeled biomarkers in buffer, further integration with on-chip sample preparation should enable analysis in more complex matrices. Another study reported a two-dimensional electrophoresis microdevice for separation of proteins using pH gradient isoelectric focusing and zone electrophoresis.[66] The device was constructed with glass and used acidic and basic buffers driven through a voltage difference to create a multilayer pH gradient for isoelectric focusing of proteins. Using this setup, a mixture of proteins (myoglobin, carbonic anhydrase, and catalase) was separated at concentrations ranging from 0.1 to 0.3 μg/μL. Although not shown in this work, native proteins could be utilized for separation and studying protein interactions in the future.

Microfluidics show promise to provide rapid, inexpensive, efficient, and portable diagnostic solutions that can be used in resource-limited settings. Further research that leads to improvements in limits of detection, sample purification, multiplexing and ability to rapidly analyze samples directly from biological matrices is still needed. Improved integration of sample preparation with separation and other analyses on-chip would also be highly beneficial for development of sample-to-answer diagnostic devices.

1.5 DISSERTATION OVERVIEW

This dissertation focuses on the development of electrokinetically operated integrated microfluidic devices for on-chip sample preparation and separation of PTB biomarkers. In chapters 2-5, integrated microfluidic devices specific to PTB biomarkers are reported for various on-chip sample preparation and analysis processes like immunoaffinity extraction, preconcentration, purification, fluorescent labeling and μCE. A brief overview of chapters 2-6 of this dissertation is given below.

In chapter 2, I report microfluidic devices for microchip electrophoresis of various biomolecules. Device fabrication protocols, off-chip sample preparation, device operation and instrument setup are also described. Additionally, microchip electrophoretic separations of several off-chip-labeled amino acids, peptides, and proteins including PTB biomarkers are reported in poly(methyl methacrylate) microfluidic devices.

In chapter 3, I report electrokinetically operated microfluidic devices for solid-phase extraction and fluorescent labeling of PTB biomarkers. Reversed-phase monoliths based on different acrylate monomers were photopolymerized in cyclic olefin copolymer microdevices and studied for the selective retention and elution of a fluorescent dye and PTB biomarkers. Octyl methacrylate-based monoliths with desirable retention and elution characteristics were chosen and used for on-chip fluorescent labeling of three PTB biomarkers. Purification of on-chip labeled samples was done by selective elution of unreacted dye prior to sample. Automated and rapid on-chip fluorescent labeling was achieved with similar efficiency to that obtained for samples labeled off chip.

In chapter 4, I describe a microfluidic device that uses pH-mediated SPE for the enrichment and elution of PTB biomarkers. Furthermore, this SPE module was integrated with microchip

electrophoresis for combined enrichment and separation of multiple analytes, including a PTB peptide biomarker. A reversed-phase octyl methacrylate monolith was polymerized as the SPE medium in polyethylene glycol diacrylate modified cyclic olefin copolymer microfluidic channels. Eluent for pH-mediated SPE of PTB biomarkers on the monolith was optimized using different pH values and ionic concentrations. Nearly 50-fold enrichment was observed in single channel SPE devices for a low nanomolar solution of a PTB peptide, with great elution time reproducibility (~7% RSD). The monolith binding capacity was determined to be 400 pg (0.2 pmol). A mixture of a model peptide and a PTB biomarker was extracted, eluted, injected, and then separated by μCE in the integrated device with ~15-fold enrichment.

In chapter 5, I report integrated immunoaffinity extraction and separation devices for analysis of preterm birth biomarkers in a human blood serum matrix. A reactive polymer monolith was used for immobilization of antibodies for selective extraction of target biomarkers. Microfluidic immunoaffinity extraction protocols were optimized and then integrated with microchip electrophoresis for separation. Using these integrated devices, a ~30 min analysis was carried out on low nanomolar concentrations of two preterm birth biomarkers spiked in a human serum matrix.

In chapter 6, I present the conclusions of these studies and possible future directions for extension of this work.

1.6 REFERENCES

1. Nge, P. N.; Rogers, C. I.; Woolley, A. T., Advances in Microfluidic Materials, Functions, Integration, and Applications. *Chem. Rev.* **2013,** *113* (4), 2550-2583.

2. Sackmann, E. K.; Fulton, A. L.; Beebe, D. J., The present and future role of microfluidics in biomedical research. *Nature* **2014,** *507* (7491), 181-189.

3. Tetala, K. K. R.; Vijayalakshmi, M. A., A review on recent developments for biomolecule separation at analytical scale using microfluidic devices. *Anal. Chim. Acta* **2016,** *906*, 7-21.

4. Goldenberg, R. L.; Culhane, J. F.; Iams, J. D.; Romero, R., Epidemiology and causes of preterm birth. *Lancet* **2008,** *371* (9606), 75-84.

5. Goldenberg, R. L.; Iams, J. D.; Mercer, B. M.; Meis, P. J.; Moawad, A.; Das, A.; Miodovnik, M.; VanDorsten, P. J.; Caritis, S. N.; Thurnau, G.; Dombrowski, M. P., The Preterm Prediction Study: Toward a multiple-marker test for spontaneous preterm birth. *Am. J. Obstet. Gynecol.* **2001,** *185* (3), 643-651.

6. Romero, R.; Dey, S. K.; Fisher, S. J., Preterm labor: One syndrome, many causes. *Science* **2014,** *345* (6198), 760-765.

7. Iams, J. D.; Romero, R.; Culhane, J. F.; Goldenberg, R. L., Primary, secondary, and tertiary interventions to reduce the morbidity and mortality of preterm birth. *Lancet* **2008,** *371* (9607), 164-175.

8. Lu, G. C.; Goldenberg, R. L.; Cliver, S. P.; Kreaden, U. S.; Andrews, W. W., Vaginal fetal fibronectin levels and spontaneous preterm birth in symptomatic women. *Obstet. Gynecol.* **2001,** *97* (2), 225-228.

9. Sanchez-Ramos, L.; Delke, I.; Zamora, J.; Kaunitz, A. M., Fetal Fibronectin as a Short-Term Predictor of Preterm Birth in Symptomatic Patients: A Meta-Analysis. *Obstet. Gynecol.* **2009,** *114* (3), 631-640.

10. Esplin, M. S.; Merrell, K.; Goldenberg, R.; Lai, Y.; Iams, J. D.; Mercer, B.; Spong, C. Y.; Miodovnik, M.; Simhan, H. N.; van Dorsten, P.; Dombrowski, M., Proteomic identification of

serum peptides predicting subsequent spontaneous preterm birth. *Am. J. Obstet. Gynecol.* **2011,** *204* (5), 391.e1-391.e8.

11. Graves, S. W.; Esplin, M. S., 80: Validation of predictive preterm birth biomarkers obtained by maternal serum proteomics. *Am. J. Obstet. Gynecol.* **2011,** *204* (1), S46.

12. Nováková, L.; Vlčková, H., A review of current trends and advances in modern bio-analytical methods: Chromatography and sample preparation. *Anal. Chim. Acta* **2009,** *656* (1), 8-35.

13. Mathonnet, M.; Descottes, B.; Valleix, D.; Labrousse, F.; Truffinet, V.; Denizot, Y., Quantitative analysis using ELISA of vascular endothelial growth factor and basic fibroblast growth factor in human colorectal cancer, liver metastasis of colorectal cancer and hepatocellular carcinoma. *World J. Gastroenterol.* **2006,** *12* (23), 3782-3783.

14. Diamandis, E. P., Mass Spectrometry as a Diagnostic and a Cancer Biomarker Discovery Tool: Opportunities and Potential Limitations. *Mol. Cell. Proteomics* **2004,** *3* (4), 367-378.

15. Howard, B. A.; Wang, M. Z.; Campa, M. J.; Corro, C.; Fitzgerald, M. C.; Patz, E. F., Identification and validation of a potential lung cancer serum biomarker detected by matrix-assisted laser desorption/ionization-time of flight spectra analysis. *Proteomics* **2003,** *3* (9), 1720-1724.

16. Wu, J.; He, Z.; Chen, Q.; Lin, J.-M., Biochemical analysis on microfluidic chips. *TrAC Trends Anal. Chem.* **2016,** *80*, 213-231.

17. Karle, M.; Vashist, S. K.; Zengerle, R.; von Stetten, F., Microfluidic solutions enabling continuous processing and monitoring of biological samples: A review. *Anal. Chim. Acta* **2016,** *929*, 1-22.

18. Cui, F.; Rhee, M.; Singh, A.; Tripathi, A., Microfluidic Sample Preparation for Medical Diagnostics. *Annu. Rev. Biomed. Eng.* **2015,** *17* (1), 267-286.

19. Mairhofer, J.; Roppert, K.; Ertl, P., Microfluidic Systems for Pathogen Sensing: A Review. *Sensors* **2009,** *9* (6), 4804-4823.

20. Wujcik, E. K.; Wei, H.; Zhang, X.; Guo, J.; Yan, X.; Sutrave, N.; Wei, S.; Guo, Z., Antibody nanosensors: a detailed review. *RSC Adv.* **2014,** *4* (82), 43725-43745.

21. Makamba, H.; Kim, J. H.; Lim, K.; Park, N.; Hahn, J. H., Surface modification of poly(dimethylsiloxane) microchannels. *Electrophoresis* **2003,** *24* (21), 3607-3619.

22. Bai, Y.; Koh, C. G.; Boreman, M.; Juang, Y.-J.; Tang, I.-C.; Lee, L. J.; Yang, S.-T., Surface Modification for Enhancing Antibody Binding on Polymer-Based Microfluidic Device for Enzyme-Linked Immunosorbent Assay. *Langmuir* **2006,** *22* (22), 9458-9467.

23. Knob, R.; Sahore, V.; Sonker, M.; Woolley, A. T., Advances in monoliths and related porous materials for microfluidics. *Biomicrofluidics* **2016,** *10* (3), 032901.

24. Gijs, M. A. M., Magnetic bead handling on-chip: new opportunities for analytical applications. *Microfluid. Nanofluid.* **2004,** *1* (1), 22-40.

25. Reverté, L.; Prieto-Simón, B.; Campàs, M., New advances in electrochemical biosensors for the detection of toxins: Nanomaterials, magnetic beads and microfluidics systems. A review. *Anal. Chim. Acta* **2016,** *908*, 8-21.

26. Cretich, M.; Daaboul, G. G.; Sola, L.; Ünlü, M. S.; Chiari, M., Digital detection of biomarkers assisted by nanoparticles: application to diagnostics. *Trends Biotechnol.* **2015,** *33* (6), 343-351.

27. Ng, E.; Chen, K.; Hang, A.; Syed, A.; Zhang, J. X. J., Multi-Dimensional Nanostructures for Microfluidic Screening of Biomarkers: From Molecular Separation to Cancer Cell Detection. *Ann. Biomed. Eng.* **2016,** *44* (4), 847-862.

28. Fernández-Baldo, M. A.; Ortega, F. G.; Pereira, S. V.; Bertolino, F. A.; Serrano, M. J.; Lorente, J. A.; Raba, J.; Messina, G. A., Nanostructured platform integrated into a microfluidic immunosensor coupled to laser-induced fluorescence for the epithelial cancer biomarker determination. *Microchem. J.* **2016,** *128*, 18-25.

29. Eletxigerra, U.; Martinez-Perdiguero, J.; Merino, S., Disposable microfluidic immuno-biochip for rapid electrochemical detection of tumor necrosis factor alpha biomarker. *Sens. Actuators, B* **2015,** *221*, 1406-1411.

30. Ali, M. A.; Mondal, K.; Jiao, Y.; Oren, S.; Xu, Z.; Sharma, A.; Dong, L., Microfluidic Immuno-Biochip for Detection of Breast Cancer Biomarkers Using Hierarchical Composite of Porous Graphene and Titanium Dioxide Nanofibers. *ACS Appl. Mater. Interfaces* **2016,** *8* (32), 20570-20582.

31. Martinez, A. W.; Phillips, S. T.; Carrilho, E.; Thomas III, S. W.; Sindi, H.; Whitesides, G. M., Simple Telemedicine for Developing Regions: Camera Phones and Paper-Based Microfluidic Devices for Real-Time, Off-Site Diagnosis. *Anal. Chem.* **2008,** *80* (10), 3699-3707.

32. Li, M.; Shi, Z.; Fang, C.; Gao, A.; Li, C. M.; Yu, L., Versatile microfluidic complement fixation test for disease biomarker detection. *Anal. Chim. Acta* **2016,** *916*, 67-76.

33. Garg, N.; Vallejo, D.; Boyle, D.; Nanayakkara, I.; Teng, A.; Pablo, J.; Liang, X.; Camerini, D.; Lee, A. P.; Felgner, P., Integrated On-Chip Microfluidic Immunoassay for Rapid Biomarker Detection. *Procedia Eng.* **2016,** *159*, 53-57.

34. Yang, M.; Nelson, R.; Ros, A., Toward Analysis of Proteins in Single Cells: A Quantitative Approach Employing Isobaric Tags with MALDI Mass Spectrometry Realized with a Microfluidic Platform. *Anal. Chem.* **2016,** *88* (13), 6672-6679.

35. Xie, Y.; Zhi, X.; Su, H.; Wang, K.; Yan, Z.; He, N.; Zhang, J.; Chen, D.; Cui, D., A Novel Electrochemical Microfluidic Chip Combined with Multiple Biomarkers for Early Diagnosis of Gastric Cancer. *Nanoscale Res. Lett.* **2015,** *10* (1), 477.

36. McDonald, J. C.; Whitesides, G. M., Poly(dimethylsiloxane) as a Material for Fabricating Microfluidic Devices. *Acc. Chem. Res.* **2002,** *35* (7), 491-499.

37. Zhou, J.; Ellis, A. V.; Voelcker, N. H., Recent developments in PDMS surface modification for microfluidic devices. *Electrophoresis* **2010,** *31* (1), 2-16.

38. Zhang, W.; Tullier, M. P.; Patel, K.; Carranza, A.; Pojman, J. A.; Radadia, A. D., Microfluidics using a thiol-acrylate resin for fluorescence-based pathogen detection assays. *Lab Chip* **2015,** *15* (21), 4227-4231.

39. Gao, R.; Ko, J.; Cha, K.; Jeon, J. H.; Rhie, G.-e.; Choi, J.; deMello, A. J.; Choo, J., Fast and sensitive detection of an anthrax biomarker using SERS-based solenoid microfluidic sensor. *Biosens. Bioelectron.* **2015,** *72*, 230-236.

40. Lin, Y.-H.; Peng, P.-Y., Semiconductor sensor embedded microfluidic chip for protein biomarker detection using a bead-based immunoassay combined with deoxyribonucleic acid strand labeling. *Anal. Chim. Acta* **2015,** *869*, 34-42.

41. Zhao, Z.; Yang, Y.; Zeng, Y.; He, M., A microfluidic ExoSearch chip for multiplexed exosome detection towards blood-based ovarian cancer diagnosis. *Lab Chip* **2016,** *16* (3), 489-496.

42. Mohamadi, R. M.; Svobodova, Z.; Bilkova, Z.; Otto, M.; Taverna, M.; Descroix, S.; Viovy, J.-L., An integrated microfluidic chip for immunocapture, preconcentration and separation of b-amyloid peptides. *Biomicrofluidics* **2015,** *9* (5), 054117.

43. Lee, W.; Kwon, D.; Choi, W.; Jung, G. Y.; Au, A. K.; Folch, A.; Jeon, S., 3D-Printed Microfluidic Device for the Detection of Pathogenic Bacteria Using Size-based Separation in Helical Channel with Trapezoid Cross-Section. *Sci. Rep.* **2015,** *5*, 7717.

44. Cox, J. C.; Hayhurst, A.; Hesselberth, J.; Bayer, T. S.; Georgiou, G.; Ellington, A. D., Automated selection of aptamers against protein targets translated in vitro: from gene to aptamer. *Nucleic Acids Res.* **2002,** *30* (20), e108.

45. Bunka, D. H. J.; Stockley, P. G., Aptamers come of age – at last. *Nat. Rev. Microbiol.* **2006,** *4* (8), 588-596.

46. Jolly, P.; Damborsky, P.; Madaboosi, N.; Soares, R. R. G.; Chu, V.; Conde, J. P.; Katrlik, J.; Estrela, P., DNA aptamer-based sandwich microfluidic assays for dual quantification and multi-glycan profiling of cancer biomarkers. *Biosens. Bioelectron.* **2016,** *79*, 313-319.

47. Li, J.; Chang, K.-W.; Wang, C.-H.; Yang, C.-H.; Shiesh, S.-C.; Lee, G.-B., On-chip, aptamer-based sandwich assay for detection of glycated hemoglobins via magnetic beads. *Biosens. Bioelectron.* **2016,** *79*, 887-893.

48. Lin, X.; Chen, Q.; Liu, W.; Zhang, J.; Wang, S.; Lin, Z.; Lin, J.-M., Oxygen-induced cell migration and on-line monitoring biomarkers modulation of cervical cancers on a microfluidic system. *Sci. Rep.* **2015,** *5*, 9643.

49. Shin, S. R.; Zhang, Y. S.; Kim, D.-J.; Manbohi, A.; Avci, H.; Silvestri, A.; Aleman, J.; Hu, N.; Kilic, T.; Keung, W.; Righi, M.; Assawes, P.; Alhadrami, H. A.; Li, R. A.; Dokmeci, M. R.;

Khademhosseini, A., Aptamer-Based Microfluidic Electrochemical Biosensor for Monitoring Cell-Secreted Trace Cardiac Biomarkers. *Anal. Chem.* **2016,** *88* (20), 10019-10027.

50. Giri, B.; Pandey, B.; Neupane, B.; Ligler, F. S., Signal amplification strategies for microfluidic immunoassays. *TrAC Trends Anal. Chem.* **2016,** *79*, 326-334.

51. Ge, Z.; Wang, W.; Yang, C., Rapid concentration of deoxyribonucleic acid via Joule heating induced temperature gradient focusing in poly-dimethylsiloxane microfluidic channel. *Anal. Chim. Acta* **2015,** *858*, 91-97.

52. Cong, Y.; Katipamula, S.; Geng, T.; Prost, S. A.; Tang, K.; Kelly, R. T., Electrokinetic sample preconcentration and hydrodynamic sample injection for microchip electrophoresis using a pneumatic microvalve. *Electrophoresis* **2016,** *37* (3), 455-462.

53. Yeh, S.-H.; Chou, K.-H.; Yang, R.-J., Sample pre-concentration with high enrichment factors at a fixed location in paper-based microfluidic devices. *Lab Chip* **2016,** *16* (5), 925-931.

54. Lee, S. J.; Rhee, H.; Jeon, T.-J.; Kim, D., Preconcentration of lipid vesicles using concentration polarization in a microfluidic chip. *Sens. Actuators, B* **2016,** *229*, 276-280.

55. Li, F.; Guijt, R. M.; Breadmore, M. C., Nanoporous Membranes for Microfluidic Concentration Prior to Electrophoretic Separation of Proteins in Urine. *Anal. Chem.* **2016,** *88* (16), 8257-8263.

56. Kumar, S.; Sahore, V.; Rogers, C. I.; Woolley, A. T., Development of an integrated microfluidic solid-phase extraction and electrophoresis device. *Analyst* **2016,** *141* (5), 1660-1668.

57. Herzog, C.; Poehler, E.; Peretzki, A. J.; Borisov, S. M.; Aigner, D.; Mayr, T.; Nagl, S., Continuous on-chip fluorescence labelling, free-flow isoelectric focusing and marker-free isoelectric point determination of proteins and peptides. *Lab Chip* **2016,** *16* (9), 1565-1572.

58. Yang, R.; Pagaduan, J. V.; Yu, M.; Woolley, A. T., On chip preconcentration and fluorescence labeling of model proteins by use of monolithic columns: device fabrication, optimization, and automation. *Anal. Bioanal. Chem.* **2015,** *407* (3), 737-747.

59. Pagaduan, J. V.; Sahore, V.; Woolley, A. T., Applications of microfluidics and microchip electrophoresis for potential clinical biomarker analysis. *Anal. Bioanal. Chem.* **2015,** *407* (23), 6911-6922.

60. Shameli, S. M.; Ren, C. L., Microfluidic Two-Dimensional Separation of Proteins Combining Temperature Gradient Focusing and Sodium Dodecyl Sulfate-Polyacrylamide Gel Electrophoresis. *Anal. Chem.* **2015,** *87* (7), 3593-3597.

61. Wu, R.; Seah, Y. P.; Wang, Z., Microfluidic chip for stacking, separation and extraction of multiple DNA fragments. *J. Chromatogr. A* **2016,** *1437*, 219-225.

62. Redman, E. A.; Batz, N. G.; Mellors, J. S.; Ramsey, J. M., Integrated Microfluidic Capillary Electrophoresis-Electrospray Ionization Devices with Online MS Detection for the Separation and Characterization of Intact Monoclonal Antibody Variants. *Anal. Chem.* **2015,** *87* (4), 2264-2272.

63. Batalla, P.; Martín, A.; López, M. Á.; González, M. C.; Escarpa, A., Enzyme-Based Microfluidic Chip Coupled to Graphene Electrodes for the Detection of D-Amino Acid Enantiomer-Biomarkers. *Anal. Chem.* **2015,** *87* (10), 5074-5078.

64. Pagaduan, J. V.; Ramsden, M.; O'Neill, K.; Woolley, A. T., Microchip immunoaffinity electrophoresis of antibody–thymidine kinase 1 complex. *Electrophoresis* **2015,** *36* (5), 813-817.

65. Sahore, V.; Kumar, S.; Rogers, C. I.; Jensen, J. K.; Sonker, M.; Woolley, A. T., Pressure-actuated microfluidic devices for electrophoretic separation of pre-term birth biomarkers. *Anal. Bioanal. Chem.* **2016,** *408* (2), 599-607.

66. Lin, F.; Yu, S.; Gu, L.; Zhu, X.; Wang, J.; Zhu, H.; Lu, Y.; Wang, Y.; Deng, Y.; Geng, L., In situ photo-immobilised pH gradient isoelectric focusing and zone electrophoresis integrated two-dimensional microfluidic chip electrophoresis for protein separation. *Microchim. Acta* **2015,** *182* (13), 2321-2328.

2. MICROCHIP ELECTROPHORETIC SEPARATIONS OF SELECTED PRETERM BIRTH BIOMARKERS[†]

2.1 INTRODUCTION

PTB, the most common complication in pregnancy, affects more than 500,000 births every year in the USA alone and is the leading cause of newborn deaths and illnesses.[1-3] An early diagnosis of PTB risk could allow therapeutic interventions to delay delivery and hence improve health outcomes for infants at risk; such a diagnosis could come through the measurement of specific biomarkers in maternal fluids.[4-5] Importantly, a recently characterized maternal serum biomarker panel showed ~87% sensitivity and ~81% specificity in predicting a PTB four weeks later at a gestational age of 28 weeks.[6-7] Although microfluidic systems have been developed for biomarkers[8-9] indicative of cancers,[10-13] and infectious diseases,[14-15] there remains an unmet need for a cost-effective and rapid analysis system for the analysis of PTBs.[16-17] In order to analyze a biomarker panel, the most crucial step is to be able to separate and quantify them on a microfluidic platform. In this chapter I have developed protocols for electrophoretic separation of selected PTB biomarkers that will eventually be used for detection and quantification of these biomarkers on an integrated microfluidic platform.

Microchip electrophoresis (μCE) is the miniaturized microchip version of capillary electrophoresis that utilizes the mass to charge ratio of analytes for separation in a buffered matrix under an applied voltage. μCE is one of the most commonly used separation techniques in a microfluidic setup.[18-20] μCE offers many advantages over its benchtop counterpart[8, 21] like low

[†] Portions of this chapter are adapted with permission from Sonker, M.; Yang, R.; Sahore, V.; Kumar, S.; Woolley, A. T., On-chip fluorescent labeling using reversed-phase monoliths and microchip electrophoretic separations of selected preterm birth biomarkers. *Anal. Methods* **2016,** *8* (43), 7739-7746.

volume requirement, low cost, portability, fast analysis, and ability to be integrated with multiple processes.

Electrophoresis refers to the movement of a charged species under the influence of applied electric field. The migration velocity (v) of an analyte is primarily governed by electrophoretic flow (μ_e) and electroosmotic flow (μ_{eof}) and can be represented by equation 2.1.

$$v = (\mu_e + \mu_{eof})E \tag{2.1}$$

where, μ_e is the electrophoretic mobility of the analyte, μ_{eof} is the EOF, and E is the applied electric field. The μ_e of an analyte is affected by its charge to mass ratio and can be represented by equation 2.2.

$$\mu_e = qE / 6\pi\eta r \tag{2.2}$$

where q is the charge of the analyte, E is the electric field, η is the viscosity of the medium, r is the hydrodynamic radius of the analyte. Since viscosity and hydrodynamic radius of an analyte stay constant for a given condition, the electrophoretic mobility of the analytes is primarily governed by the charge on the analyte. Thus, changing the charge on an analyte by changing the buffer pH may result in altered analyte mobility.

Analyte movement is also affected by electroosmotic flow which is the bulk flow of a liquid in a microchannel when an electric field is applied across the channel and primarily governed by the surface of the microchannel. When an electric field is applied across a charged microchannel filled with charged ionic species, the surface attracts and forms a thin layer of oppositely charged ions called an electric double layer. This electric double layer, on application of an electric field, drives the bulk flow of the solution towards the oppositely charged electrode forming the electroosmotic flow. μ_{eof} can be mathematically represented by equation 2.3.

$$\mu_{eof} = \varepsilon E\zeta / 4\pi\eta \quad (2.3)$$

where, ε is the dielectric constant of the fluid, E is the applied electric field, ζ is the zeta potential of liquid solid interface. As shown by equation 2.3, electroosmotic flow can be manipulated by altering the zeta potential and viscosity of the solution by surface modifications. Typically in microchip electrophoresis the electrophoretic mobility of analyte in conjunction with electroosmotic mobility aids in separation.

In this Chapter, I demonstrate a microfluidic device for the separation of PTB biomarkers (see schematic in Figure 2.1). Protocols for microchip electrophoresis of several off-chip-labeled model analytes and PTB biomarkers (including protein and peptide biomarkers) were developed in poly(methyl methacrylate) (PMMA) microfluidic devices. This study is an important step toward the development of integrated separation microfluidic devices for PTB biomarkers.

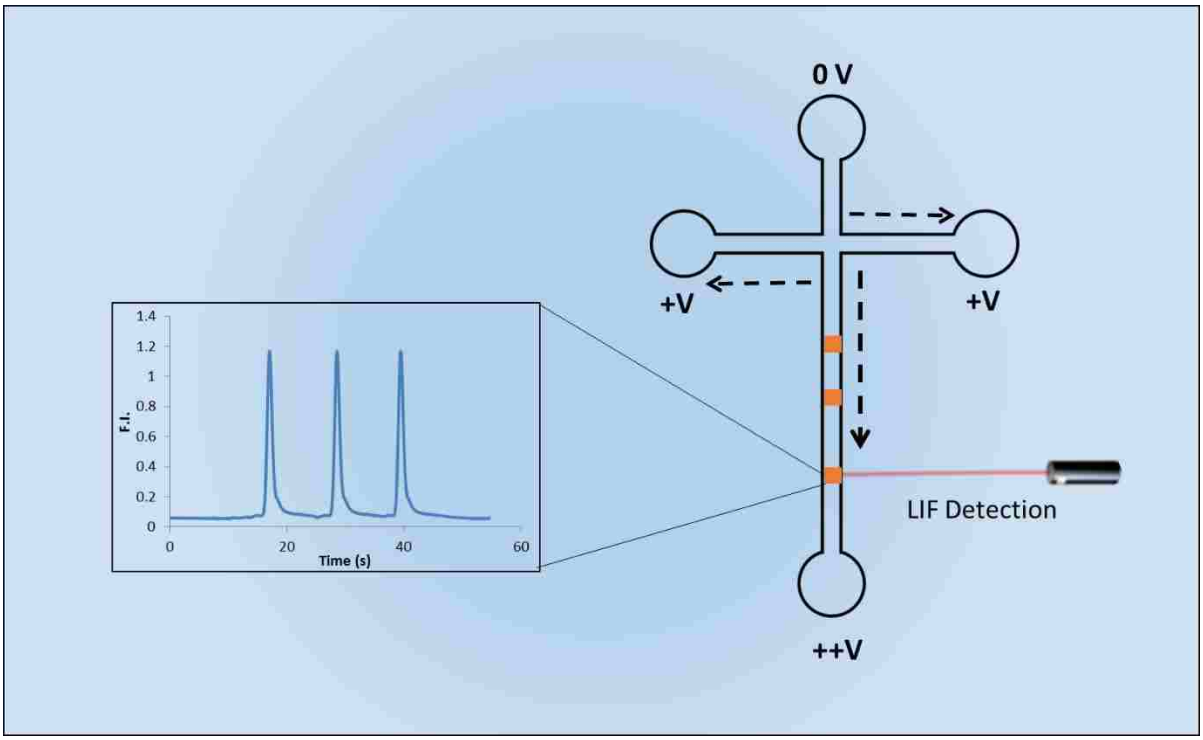

Figure 2.1 Schematic showing microchip electrophoresis.

2.2 EXPERIMENTAL SECTION

2.2.1 Materials and Reagents

PMMA sheets (1 mm and 3 mm thick) were from Evonik (Parsippany, NJ). Single side polished silicon wafers (4" diameter) were obtained from Desert Silicon (Tempe, AZ). C8 was purchased from Scientific Polymer Products (Ontario, NY). Hydroxypropylcellulose (HPC, M_w 100 kDa) were obtained from Sigma-Aldrich (St Louis, MO). Acetonitrile (ACN) was obtained from Fisher Scientific (Pittsburgh, PA). Potassium hydroxide was from Macron (Center Valley, PA). Sodium phosphate monohydrate, anhydrous sodium phosphate, anhydrous sodium carbonate, and sodium bicarbonate were from Merck (Darmstadt, Germany). Isopropyl alcohol (IPA), sodium chloride was purchased from Columbus Chemical (Columbus, WI). Buffers were prepared with deionized water (18.3 MΩ) purified by a Barnstead EASYpure UV/UF system (Dubuque, IA). Glycine was fro from Merck (Darmstadt, Germany) and phenylalanine was from Spectrum (Omaha, NE). Unlabeled and FITC-labeled PTB peptide P1 (QLGLPGPPDVPDHAAYHPF), and unlabeled PTB peptides, P2 (NVHSAGAAGSRMNFRPGVLSSRQLGLPGPPDVPDHAAYHPF) and P3 (NVHSAGAAGSRM(O)NFRPGVLSSRQLGLPGPPDVPDHAAYHPF)[6, 16] were synthesized by GenScript (Piscataway, NJ). Ferritin was purchased from EMD Millipore (Billerica, MA). Arginine, Phe-Ala (FA), Ala-Leu-Ala-Leu (ALAL), Gly-Gly-Tyr-Arg (GGYR), bovine serum albumin (BSA), cytochrome C (Cyt C) and lactoferrin was from Sigma-Aldrich (St Louis, MO). FITC used for sample labeling was obtained from Life Technologies (Carlsbad, CA).

2.2.2 Device Fabrication

First, device designs were patterned on a silicon wafer template using photolithography and wet etching processes described previously.[22] A schematic of silicon template fabrication process is shown in Figure 2.2. Briefly, a 4" silicon wafer was oxidized to grow a ~500 nm silicon oxide

layer in a Bruce Tube Furnace (Bruce Industrial Controls, New Castle, DE). This oxidized wafer was cleaned with IPA and acetone. A positive photoresist (S1805, Dow Chemical, Marlborough, MA) was spin coated on this wafer for 1 min at 3000 rpm using Laurell Spin Processor (Laurell Technologies Corporation, North Wales, PA) and baked 110˚C for 5 min. The device design was transferred to this baked wafer by photolithography using a Karl Suss UV aligner (Waterbury, VT) via exposure to UV radiation through a Cr mask.

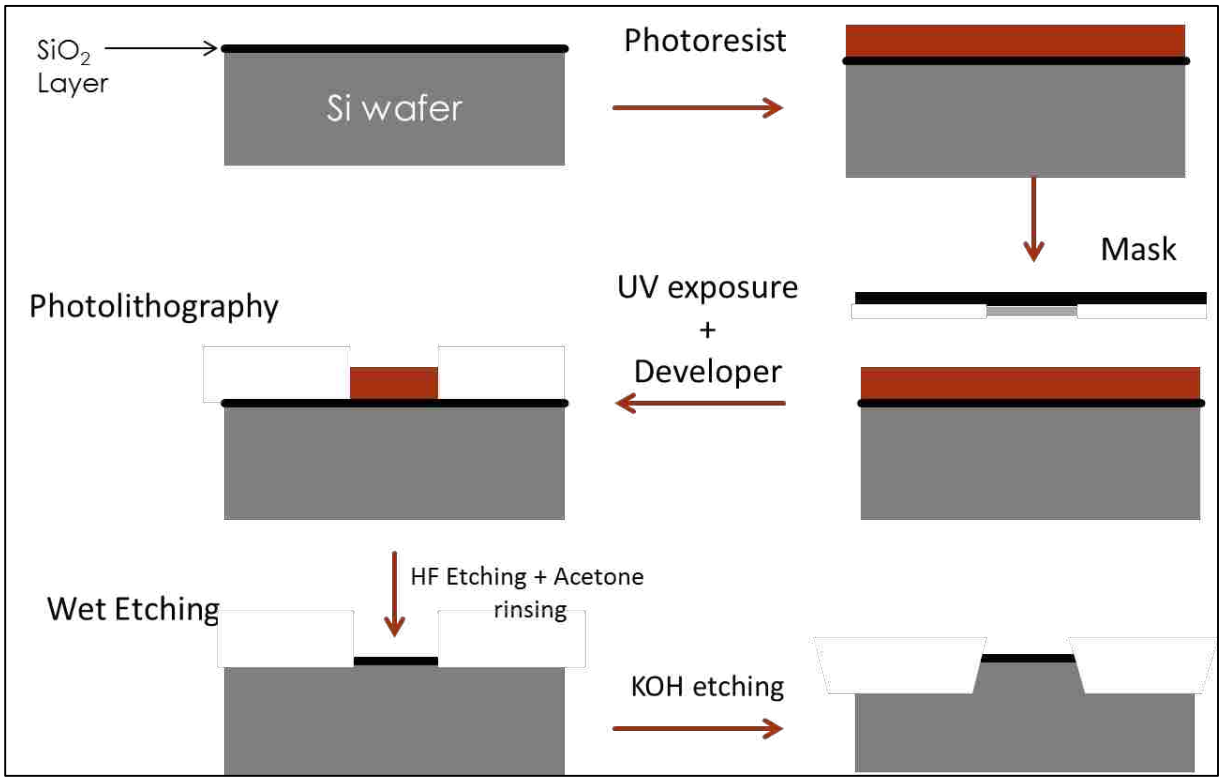

Figure 2.2 Schematic of silicon template fabrication.

After exposure, this wafer was baked again at 110˚C for 5 min and developed in MF26A, developer (Dow Chemical, Marlborough, MA) for ~1 min until the device design was visible on the wafer. This developed wafer was subjected to further baking at 110˚C for 5 min to improve the adhesion of photoresist to the wafer. This patterned silicon wafer was then subjected to wet etching using buffered HF for 5-6 min to etch the exposed silicon oxide layer. After HF etching, photoresist

is rinsed off using acetone and IPA. This wafer was then cut into a single device templates and subjected to etching under 40% KOH solution at 75˚C for 30 min to produce a feature height of 20-22 µm.

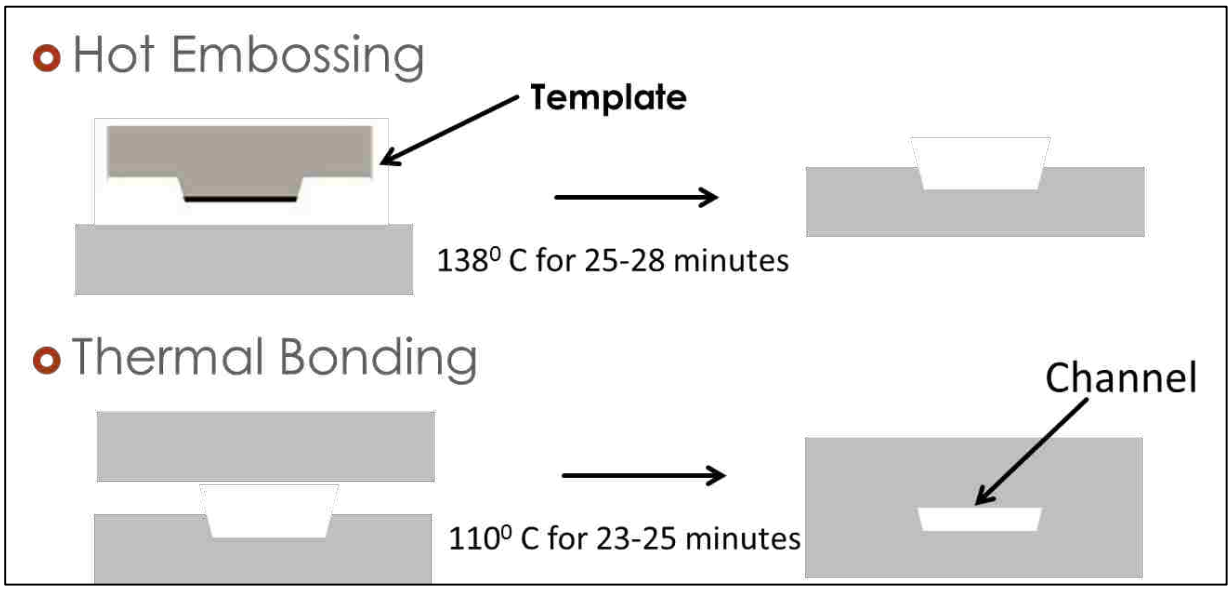

Figure 2.3 Schematic showing fabrication of PMMA device from a silicon template.

PMMA devices were made from these silicon templates roughly following hot embossing and thermal bonding techniques described previously.[22-23] Figure 2.3 briefly describes the fabrication procedure of PMMA device using previously fabricated silicon templates. Four-reservoir "T" shaped devices with ~50 µm × 20 µm channel dimensions were fabricated for µCE of PTB peptides. First, PMMA plates were cut into 5 cm × 2 cm pieces using a laser cutter (VLS 2.30 Versa Laser, Universal Laser Systems, Scottsdale, AZ). Holes for reservoirs were also cut into 3 mm thick PMMA cover plates with the laser cutter. Silicon templates were used to transfer the device design onto PMMA pieces by hot embossing at 138º C for 28 min. Drilled cover plates were thermally bonded to embossed channel pieces at 110º C for 25 min and chemically sealed around the device edges using ACN and channels were tested for adequate flow using DI water.

2.2.3 Instrumentation Setup

The experimental setup for laser induced fluorescence (LIF) detection (shown in Figure 2.4) has been described previously.[9, 24-26] A Nikon TE300 inverted microscope had a 488 nm laser (JDSU, Shenzhen, China) focused through a 20× objective (0.5 mW incident on the device, ~25 μm beam diameter) on a desired point in the channel to excite the fluorophores. The resulting fluorescence passed through a 505LD dichroic filter and a D535/40 band-pass filter (Chroma, Rockingham, VT) and was detected using a photomultiplier tube (PMT, Hamamatsu, Bridgewater, NJ). This signal was processed by a preamplifier (SR-560, Stanford Research Systems, Sunnyvale, CA). Fluorescence data were recorded at 20 Hz using LabVIEW software (National Instruments, Austin, TX) and digitized by a NI USB-6212 analog-to-digital converter (National Instruments). Voltages were applied to desired reservoirs using platinum electrodes connected to an in-house designed voltage switching box further connected to Stanford Research Systems power supplies (Sunnyvale, CA).

2.2.4 Off-chip Fluorescent Labeling

Off-chip labeled proteins were prepared by adding 10 μL of 10 mM FITC in DMSO to 100 μL of the unlabeled analyte and incubating overnight at room temperature. Unlabeled analyte solutions were prepared in bicarbonate buffer (100 mM BCB pH 9.5). Concentrations of unlabeled proteins were cytochrome C (1 mM), BSA (100 μM), lactoferrin (500 μM), and ferritin (50 μM). Off-chip labeling of amino acids and peptides was done similarly with 5 μL of 10 mM FITC in DMSO diluted to 50 μL in a 10 mM amino acid and peptide solution. After incubation unreacted FITC was removed from labeled proteins solutions using Amicon ultra centrifugal filters with a 10 kDa cutoff (EMD Millipore) in a centrifuge (Eppendorf, Denver, CO) at 14000 rpm for 15 min. A 3

kDa centrifugal filter was used for cytochrome C (M_w ~12 kDa). Excess FITC was not removed after labeling peptides and amino acids because of their lower molecular weight. The concentrations of labeled stock solutions were measured by a Nanodrop ND-1000 UV spectrophotometer (Wilmington, DE), and required dilutions were made in 10 mM BCB (pH 9.5).

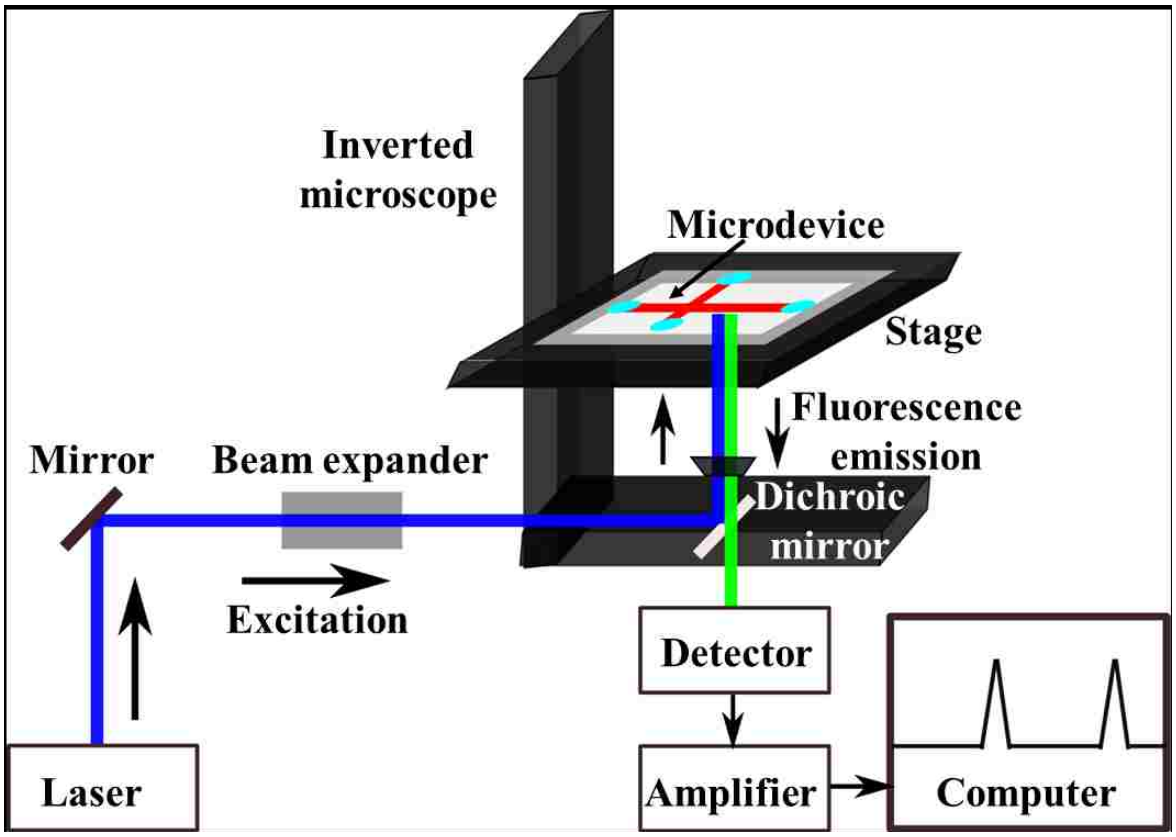

Figure 2.4 LIF setup used for detection (Adapted from Suresh Kumar, Design, Fabrication, and Optimization of Miniaturized Devices for Bioanalytical Applications, 2015, Brigham Young University)[26]

2.2.5 Device Operation

For µCE, the standard design shown in Figure 2.5 was used. The device was filled with separation buffer, and the sample (see Figure legends for concentration) was filled in reservoir 2. I used pinched injection[22, 27] for injecting fluorescently labeled samples, by applying a voltage on reservoir 3 and keeping all other reservoirs grounded (Figure 2.5C). This voltage difference

electrophoretically moves the negatively charged species in the sample towards reservoir 3. After the desired injection time, a higher separation voltage was applied to reservoir 4, reservoir 1 was grounded, and the injection voltage was applied to reservoirs 2 and 3 as shown in Figure 2.5 D. The injection voltage applied on reservoir 2 and 3 acts as a pullback voltage and prevents the sample from leaking back into the separation channel, making a plug of sample at the intersection of the "T". The separation voltage moves this sample plug into the separation channel, which results in the separation of different charged species present in sample based on their electrophoretic mobility.

For μCE shown in Figure 2.6, the separation buffer was 20 mM BCB (pH 9.3, 0.2% HPC, 20 mm NaCl), injection time was 60 s for 2.5A and 90 s for 2.6B, injection and separation voltages were +500V and +1500V, respectively and detection point was 2.5 cm from the injection intersection. For μCE shown in Figure 2.7A-B, the separation buffer was 20 mM BCB (pH 9.8, 0.2% HPC, 25 mM NaCl), the injection time was 90 s, injection voltage was +500V, the separation voltages were +1500V and +1200 V for Figure 2.7A and 2.7B, respectively, and the detection point 2.5 cm from the injection intersection. For μCE shown in Figure 2.7C, the separation buffer was 50 mM BCB (pH 10, 0.02% HPC), the injection time was 60 s, the separation voltage was +1200 V, and the LIF detection point was 0.5 cm from the injection intersection.

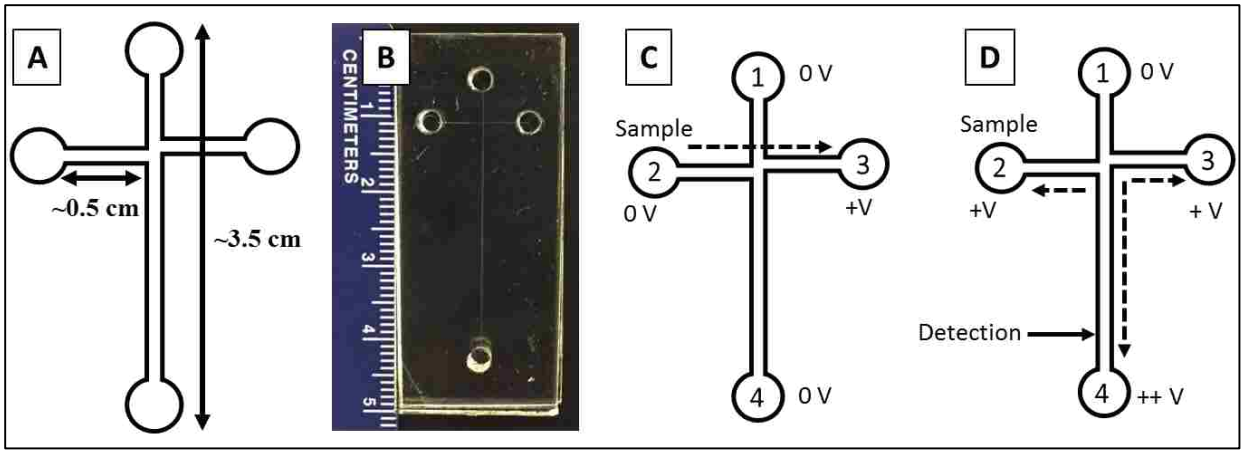

Figure 2.5 (A) Device layout, (B) photograph, and operation of "T" shaped device for µCE of PTB biomarkers showing (1) buffer, (2) sample, (3) sample waste, and (4) separation waste reservoirs along with voltage configuration and detection point for (C) injection and (D) separation in µCE.

2.3 RESULTS AND DISCUSSION

2.3.1 µCE of Model Amino Acids, Peptides, and Proteins

Model amino acids, peptides and proteins were used for separation prior to PTB biomarkers. Figure 2.6A shows an electropherogram for the baseline separation of a mixture of three amino acids (glycine, phenylalanine, and arginine) and three small peptides (FA, ALAL, and GGYR). Arg and GGYR are seen last as they contain extra primary amines which provide an extra site of dye attachment resulting in higher molecular mass. The rest of the amino acids and peptides due to presence of only one dye molecule possess lower molecular weight and move faster than Arg and GGYR and are observed according to their charge to mass ratio. A more complex sample mixture was also used for electrophoresis to see the feasibility of separating large PTB protein biomarkers using µCE. Figure 2.6B shows electrophoretic separation of three proteins, Cyt C (15 nM), BSA (1 µM) and ferritin (10 nM). A broader peak area was observed for ferritin (~450 kDa) and BSA (~65kDa) as they contain more sites for dye attachment. A baseline separation was not

observed in this case since larger proteins can adsorb on the walls of the microchannel and can induce a tailing effect.

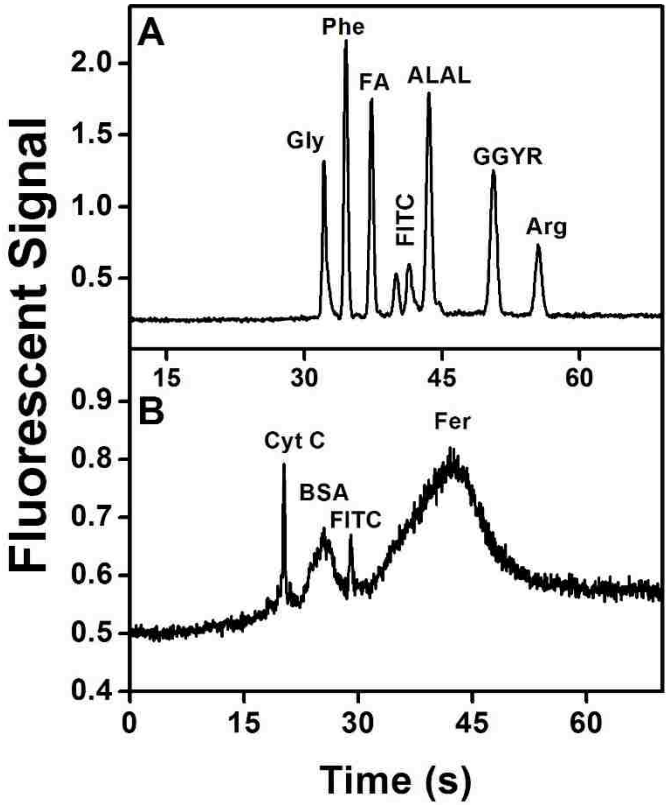

Figure 2.6 μCE of model amino acids, peptides, and proteins. (A) Electropherogram showing separation of a mixture of amino acids and peptides (167 nM each). (B) Electropherogram showing separation of model proteins, cytochrome C (Cyt C, 15 nM), bovine serum albumin (BSA, 1 μM), and ferritin (Fer, 10 nM).

2.3.2 μCE of PTB Biomarkers

Here, I show μCE of selected PTB biomarkers as a demonstration of improved resolution between the unattached dye and analyte for future studies where processes of immunoaffinity extraction, on-chip labeling, and μCE are integrated in a single device. In Figure 2.7A, μCE of two PTB peptide biomarkers (P1 and P3) is shown. P1 (pI=5) appears before P3 (pI=9.5) and has a narrower

peak due to its higher electrophoretic mobility owing to its lower molecular weight and higher net charge at pH 9.6.

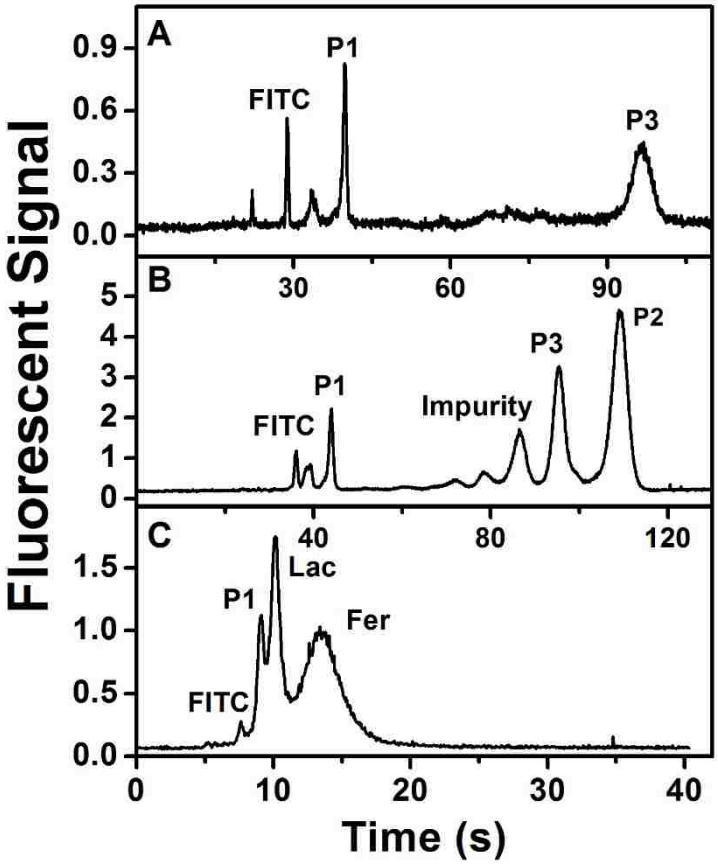

Figure 2.7 μCE of PTB biomarkers. (A) Electropherograms showing separation of P1 (50 nM), and P3 (1 μM). (B) Electropherogram showing separation of all three PTB peptides, P1 (66 nM), P2 (167 nM), and P3 (1.2 μM). (C) Electropherogram showing separation of P1 (100 nM), lactoferrin (Lac, 50 nM) and ferritin (Fer, 30 nM). Adapted from Sonker et al. *Anal. Methods* 2016, *8* (43), 7739-7746.[28]

Figure 2.7B shows the separation of all three PTB peptides. P2 and P3 appear close to each other as they have the same amino acid sequence except the oxidized methionine which makes the mass to charge ratio very similar. A number of impurity peaks are also observed in the electropherogram, which may have resulted due to breakdown of the larger peptide sequence during storage and labeling procedures. Figure 2.7C shows μCE of three PTB biomarkers (P1,

lactoferrin and ferritin). The separation peaks for the proteins are broadened because different numbers of amine-reactive sites are labeled with FITC in individual molecules during off-chip labeling, leading to acceptable but incomplete resolution.

2.4 REFERENCES

1. Blencowe, H.; Cousens, S.; Oestergaard, M. Z.; Chou, D.; Moller, A.-B.; Narwal, R.; Adler, A.; Vera Garcia, C.; Rohde, S.; Say, L.; Lawn, J. E., National, regional, and worldwide estimates of preterm birth rates in the year 2010 with time trends since 1990 for selected countries: a systematic analysis and implications. *Lancet* **2012,** *379* (9832), 2162-2172.

2. Romero, R.; Dey, S. K.; Fisher, S. J., Preterm labor: One syndrome, many causes. *Science* **2014,** *345* (6198), 760-765.

3. Goldenberg, R. L.; Culhane, J. F.; Iams, J. D.; Romero, R., Epidemiology and causes of preterm birth. *Lancet* **2008,** *371* (9606), 75-84.

4. Goldenberg, R. L.; Iams, J. D.; Mercer, B. M.; Meis, P. J.; Moawad, A.; Das, A.; Miodovnik, M.; VanDorsten, P. J.; Caritis, S. N.; Thurnau, G.; Dombrowski, M. P., The Preterm Prediction Study: Toward a multiple-marker test for spontaneous preterm birth. *Am. J. Obstet. Gynecol.* **2001,** *185* (3), 643-651.

5. Goldenberg, R. L.; Goepfert, A. R.; Ramsey, P. S., Biochemical markers for the prediction of preterm birth. *Am. J. Obstet. Gynecol.* **2005,** *192* (5), S36-S46.

6. Esplin, M. S.; Merrell, K.; Goldenberg, R.; Lai, Y.; Iams, J. D.; Mercer, B.; Spong, C. Y.; Miodovnik, M.; Simhan, H. N.; van Dorsten, P.; Dombrowski, M., Proteomic identification of serum peptides predicting subsequent spontaneous preterm birth. *Am. J. Obstet. Gynecol.* **2011,** *204* (5), 391.e1-391.e8.

7. Graves, S. W.; Esplin, M. S., 80: Validation of predictive preterm birth biomarkers obtained by maternal serum proteomics. *Am. J. Obstet. Gynecol.* **2011,** *204* (1), S46.

8. Pagaduan, J. V.; Sahore, V.; Woolley, A. T., Applications of microfluidics and microchip electrophoresis for potential clinical biomarker analysis. *Anal. Bioanal. Chem.* **2015,** *407* (23), 6911-6922.

9. Yang, W.; Yu, M.; Sun, X.; Woolley, A. T., Microdevices integrating affinity columns and capillary electrophoresis for multibiomarker analysis in human serum. *Lab Chip* **2010,** *10* (19), 2527-2533.

10. Chikkaveeraiah, B. V.; Mani, V.; Patel, V.; Gutkind, J. S.; Rusling, J. F., Microfluidic electrochemical immunoarray for ultrasensitive detection of two cancer biomarker proteins in serum. *Biosens. Bioelectron.* **2011,** *26* (11), 4477-4483.

11. Zhang, H.; Liu, L.; Fu, X.; Zhu, Z., Microfluidic beads-based immunosensor for sensitive detection of cancer biomarker proteins using multienzyme-nanoparticle amplification and quantum dotslabels. *Biosens. Bioelectron.* **2013,** *42*, 23-30.

12. Sardesai, N. P.; Kadimisetty, K.; Faria, R.; Rusling, J. F., A microfluidic electrochemiluminescent device for detecting cancer biomarker proteins. *Anal. Bioanal. Chem.* **2013,** *405* (11), 3831-3838.

13. Pagaduan, J. V.; Ramsden, M.; O'Neill, K.; Woolley, A. T., Microchip immunoaffinity electrophoresis of antibody–thymidine kinase 1 complex. *Electrophoresis* **2015,** *36* (5), 813-817.

14. Klostranec, J. M.; Xiang, Q.; Farcas, G. A.; Lee, J. A.; Rhee, A.; Lafferty, E. I.; Perrault, S. D.; Kain, K. C.; Chan, W. C. W., Convergence of Quantum Dot Barcodes with Microfluidics and Signal Processing for Multiplexed High-Throughput Infectious Disease Diagnostics. *Nano Lett.* **2007,** *7* (9), 2812-2818.

15. Lee, W. G.; Kim, Y.-G.; Chung, B. G.; Demirci, U.; Khademhosseini, A., Nano/Microfluidics for diagnosis of infectious diseases in developing countries. *Adv. Drug Delivery Rev.* **2010,** *62* (4–5), 449-457.

16. Sahore, V.; Kumar, S.; Rogers, C. I.; Jensen, J. K.; Sonker, M.; Woolley, A. T., Pressure-actuated microfluidic devices for electrophoretic separation of pre-term birth biomarkers. *Anal. Bioanal. Chem.* **2016,** *408* (2), 599-607.

17. Kumar, S.; Sahore, V.; Rogers, C. I.; Woolley, A. T., Development of an integrated microfluidic solid-phase extraction and electrophoresis device. *Analyst* **2016,** *141* (5), 1660-1668.

18. Dolník, V.; Liu, S.; Jovanovich, S., Capillary electrophoresis on microchip. *Electrophoresis* **2000,** *21* (1), 41-54.

19. Nordman, N.; Barrios-Lopez, B.; Laurén, S.; Suvanto, P.; Kotiaho, T.; Franssila, S.; Kostiainen, R.; Sikanen, T., Shape-anchored porous polymer monoliths for integrated online solid-phase extraction-microchip electrophoresis-electrospray ionization mass spectrometry. *Electrophoresis* **2015,** *36* (3), 428-432.

20. Tetala, K. K. R.; Vijayalakshmi, M. A., A review on recent developments for biomolecule separation at analytical scale using microfluidic devices. *Anal. Chim. Acta* **2016,** *906*, 7-21.

21. Nge, P. N.; Rogers, C. I.; Woolley, A. T., Advances in Microfluidic Materials, Functions, Integration, and Applications. *Chem. Rev.* **2013,** *113* (4), 2550-2583.

22. Kelly, R. T.; Woolley, A. T., Thermal Bonding of Polymeric Capillary Electrophoresis Microdevices in Water. *Anal. Chem.* **2003,** *75* (8), 1941-1945.

23. Nge, P. N.; Pagaduan, J. V.; Yu, M.; Woolley, A. T., Microfluidic chips with reversed-phase monoliths for solid phase extraction and on-chip labeling. *J. Chromatogr. A* **2012,** *1261*, 129-135.

24. Yu, M.; Wang, H. Y.; Woolley, A. T., Polymer microchip CE of proteins either off-or on-chip labeled with chameleon dye for simplified analysis. *Electrophoresis* **2009,** *30* (24), 4230-4236.

25. Sun, X.; Yang, W.; Pan, T.; Woolley, A. T., Affinity monolith-integrated poly (methyl methacrylate) microchips for on-line protein extraction and capillary electrophoresis. *Anal. Chem.* **2008,** *80* (13), 5126-5130.

26. Kumar, S., Design, Fabrication, and Optimization of Miniaturized Devices for Bioanalytical Applications. **2015**.

27. Jacobson, S. C.; Hergenroder, R.; Koutny, L. B.; Warmack, R. J.; Ramsey, J. M., Effects of Injection Schemes and Column Geometry on the Performance of Microchip Electrophoresis Devices. *Anal. Chem.* **1994,** *66* (7), 1107-1113.

28. Sonker, M.; Yang, R.; Sahore, V.; Kumar, S.; Woolley, A. T., On-chip fluorescent labeling using reversed-phase monoliths and microchip electrophoretic separations of selected preterm birth biomarkers. *Anal. Methods* **2016,** *8* (43), 7739-7746.

3. ON-CHIP FLUORESCENT LABELING OF SELECTED PRETERM BIRTH BIOMARKERS USING REVERSED-PHASE MONOLITHS‡

3.1 INTRODUCTION

Microfluidics is a vibrant and expanding research field.[1-4] An especially attractive feature of microfluidics is the ability to integrate multiple processes on a single device to achieve rapid, automated analysis.[2, 5] Many processes like preconcentration,[6-8] electrophoretic separation,[9-10] fluorescent labeling,[11-12] and solid phase extraction (SPE),[13-15] have been implemented in microfluidic setups. However, samples for analysis in microfluidic devices are generally prepared off-chip, making this one of the biggest obstacles in achieving complete automation.[2, 16-17] Off-chip sample preparation can extend total analysis time and is prone to errors that cause variation and irreproducibility. Sample preparation steps like purification, preconcentration and fluorescent labeling performed on-chip can potentially overcome these challenges and lead to truly automated and rapid analysis.[3] Microfluidic integration of sample preparation may also lead to cost reductions as reagent volumes and waste generation can be minimized.[2]

Sample purification and preconcentration can be achieved by SPE using a solid support in a microfluidic setup.[18-19] Solid supports can be made using packed materials,[18, 20] monoliths,[21-22] hydrogels,[23-24] or membranes.[6, 25] First introduced in microfluidics by Fréchet et al.,[21] monoliths have been used extensively for SPE, preconcentration and sample modification[26-27] due to their facile fabrication, low backpressure and surface modification capabilities.[27-28] Monoliths used for SPE in microfluidics include affinity[13-14, 20, 29] and reversed-phase.[11, 15, 30] Reversed-phase

‡ Adapted with Permission from Sonker, M.; Yang, R.; Sahore, V.; Kumar, S.; Woolley, A. T., On-chip fluorescent labeling using reversed-phase monoliths and microchip electrophoretic separations of selected preterm birth biomarkers. *Anal. Methods* **2016,** *8* (43), 7739-7746.

monoliths are used to retain analytes based on hydrophobic interactions, allowing preconcentration or separation.[26, 31] Reversed-phase monoliths are commonly made from cross-linked chains of alkyl methacrylates like methyl methacrylate, butyl methacrylate (C4), octyl methacrylate (C8), lauryl methacrylate (C12), or octadecyl methacrylate.[11-12, 32-34]

One of the slowest sample preparation steps in laser-induced fluorescence (LIF) analysis is the labeling of analytes, which can take hours to days.[35-36] Nge et al.[11] reported reversed-phase monoliths in cyclic olefin copolymer (COC) devices for SPE and on-chip fluorescent labeling of model proteins. The monoliths simultaneously enriched the protein and fluorescent dye, which increased their effective concentrations, enhancing labeling. This work was further validated by Yang et al.[12] for fluorescent labeling of proteins using fluorescein isothiocyanate (FITC) and Alexa Fluor 488. In both of these prior studies, only proteins were fluorescently labeled on-chip; additionally, these proteins were not collectively linked to a particular medical condition. Thus, in this Chapter I have advanced this approach for on-chip fluorescent labeling of a peptide and proteins that are preterm birth (PTB) biomarkers.

In this Chapter, I lay the foundation for a microfluidic system for the analysis of PTB biomarkers. I demonstrate an electrokinetically operated SPE device consisting of reversed-phase monoliths photopolymerized in COC microchips for selective retention, fluorescent labeling and elution of PTB biomarkers. A schematic overview of my approach is shown in Figure 3.1. Different monolith formulations were evaluated to optimize the retention and elution of a peptide PTB biomarker (P1) in the presence of a fluorescent label (FITC).[42, 43] Optimized monoliths were further used to achieve on-chip FITC labeling of three PTB biomarkers (one peptide and two proteins). Labeled analytes were further purified by removal of unreacted dye and were selectively

eluted from the column by changing eluent polarity. A comparison of elution profiles of unattached dye and off-chip labeled samples confirmed on-chip fluorescent labeling.

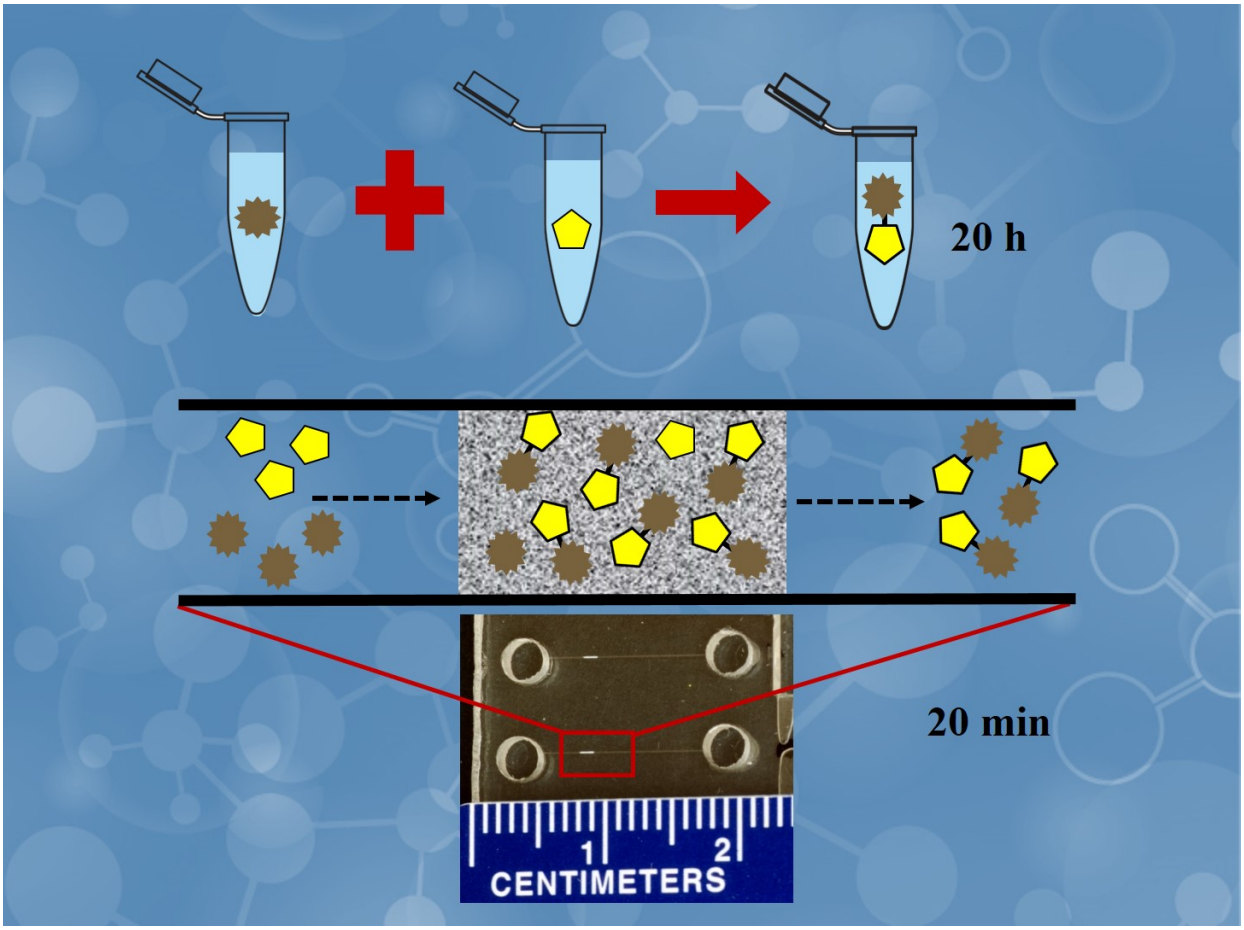

Figure 3.1 Overview of on-chip labeling.

3.2 EXPERIMENTAL SECTION

3.2.1 Materials and Reagents

Zeonor 1020R COC plates (6”×6”×1 mm thick and 6”×4”×2 mm thick) were purchased from Zeon Chemicals (Louisville, KY). Single side polished silicon wafers (4” diameter) were obtained from

Desert Silicon (Tempe, AZ). C8 was purchased from Scientific Polymer Products (Ontario, NY). C4, C12, 2,2-dimethoxy-2-phenylacetophenone (DMPA), ethylene dimethacrylate (EDMA), 1-dodecanol, dimethyl sulfoxide (DMSO), and hydroxypropylcellulose (HPC, M_w 100 kDa) were obtained from Sigma-Aldrich (St Louis, MO). Isopropyl alcohol (IPA) and acetonitrile (ACN) were obtained from Fisher Scientific (Pittsburgh, PA). Cyclohexanol was purchased from J. T. Baker (Phillipsburg, NJ). Sodium hydroxide and Tween 20 were from Mallinckrodt Baker (Paris, KY). Cyclohexane and potassium hydroxide were from Macron (Center Valley, PA). Sodium phosphate monohydrate, anhydrous sodium phosphate, anhydrous sodium carbonate, and sodium bicarbonate were from Merck (Darmstadt, Germany). Sodium chloride was purchased from Columbus Chemical (Columbus, WI). Buffers were prepared with deionized water (18.3 MΩ) purified by a Barnstead EASYpure UV/UF system (Dubuque, IA). Unlabeled and FITC-labeled P1 (QLGLPGPPDVPDHAAYHPF)[37-38] were synthesized by GenScript (Piscataway, NJ). Ferritin was purchased from EMD Millipore (Billerica, MA) and lactoferrin was from Sigma-Aldrich. FITC used for sample labeling was obtained from Life Technologies (Carlsbad, CA).

3.2.2 COC Device Fabrication

For device fabrication, silicon templates were made as described in section 2.2.2 following the protocols published previously.[11, 39] For monolith fabrication and on-chip labeling experiments, straight channel devices (Figure 3.2A-C) were made using COC plates roughly following the procedure described in Figure 2.3 and section 2.2.2. Briefly, COC plates were cut into device size pieces (5 cm × 3 cm) for fabrication using a bandsaw. A device design containing 6 straight channels was transferred from silicon templates to 1 mm thick COC pieces using hot embossing at 138º C for 26 min. A micro drill press (Cameron, Sonora, CA) was used to drill 2 mm diameter

holes for reservoirs in 2 mm thick COC cover plates. Drilled COC cover plates were thermally bonded to hot embossed COC plates at 110º C for 24 min. These bonded devices were then further sealed by applying cyclohexane around the edges. Channel dimensions were designed to be ~50 µm wide and ~20 µm deep.

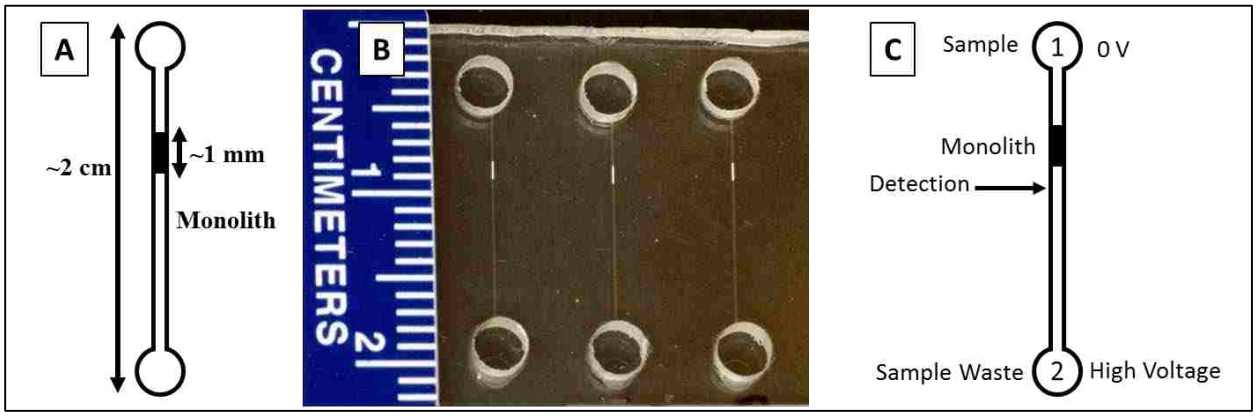

Figure 3.2 Device layout, photograph, and operation. (A) Device layout. (B) Device photograph. (C) Operation of straight channel design showing sample reservoir (1), sample waste reservoir (2), voltage configuration and detection point used for on-chip labeling/SPE of PTB biomarkers.

3.2.3 Monolith Fabrication

After device fabrication, channels were rinsed with IPA and dried using a vacuum pump. In this study, three different monomers (C4, C8 and C12) for monoliths were used to evaluate retention and elution of P1. Monoliths were fabricated following a similar protocol to that described by Nge et al.[11] Monolith pre-polymer solution was prepared by mixing monomers, porogens, Tween 20 and photoinitiator with the mass ratios indicated in Table 3.1. This mixture was sonicated for ~15 min until the photoinitiator was completely dissolved. After sonication, the mixture was purged for 5 min with nitrogen gas and then introduced into the reservoirs to fill the channel by capillary action. Electrical tape was used to seal the reservoirs, and a Cr mask was used to cover the channel, exposing only the desired region (~1 mm long). Monolith polymerization was carried out by UV

exposure at >100 $mWcm^{-2}$ for 11 min using a SunRay 600 UV lamp (Uvitron international, West Springfield, MA) as shown in Fig. 3.3A. Any unpolymerized mixture was then rinsed out with IPA flowed using a vacuum pump. A photograph of a monolith in a channel (Fig. 3.3B) was taken with a Nikon D90 digital camera.

Table 3.1. Monolith pre-polymer mixture

Name	Functional role	Mass (%)
C4, C8 or C12	monomer	25%
EDMA	cross-linker	15%
cyclohexanol	porogen	20%
1-dodecanol	porogen	20%
Tween 20	surfactant	19%
DMPA	photoinitiator	1%

Scanning electron microscopy (SEM) images of bulk monoliths were taken using a Phillips XL30 environmental scanning electron microscope (Hillsboro, OR) in high vacuum mode using a 5 kV electron beam potential. Bulk monoliths for SEM were prepared by adding ~250 µL of pre-polymer solution to a 1 mL Eppendorf tube and exposing the whole tube to UV light as above for 11 min. These polymerized monoliths were broken into pieces and stored in IPA for a few hours to dissolve any unpolymerized mixture. Then, the monolith pieces were held in a vacuum chamber overnight before placing on carbon-coated aluminum stubs. To reduce charging, all samples were sputtered with Au-Pd (~15 nm thickness) before imaging using a Q150T ES Sputterer (Quorum Technologies, Lewes, East Sussex, UK).

3.2.4 Data Analysis

Retention and elution data were collected using a Photometrics coolSNAP HQ2 (Tucson, AZ) CCD camera. A 488 nm laser directed through a 4× objective on a Nikon TE300 inverted microscope was used to illuminate a ~2 mm diameter area on and around the monolith. CCD images were collected with a 500 ms exposure time, and background-subtracted fluorescence was analyzed using NIH ImageJ software. Data were analyzed and plotted using Origin Pro software (OriginLab, Northampton, MA).

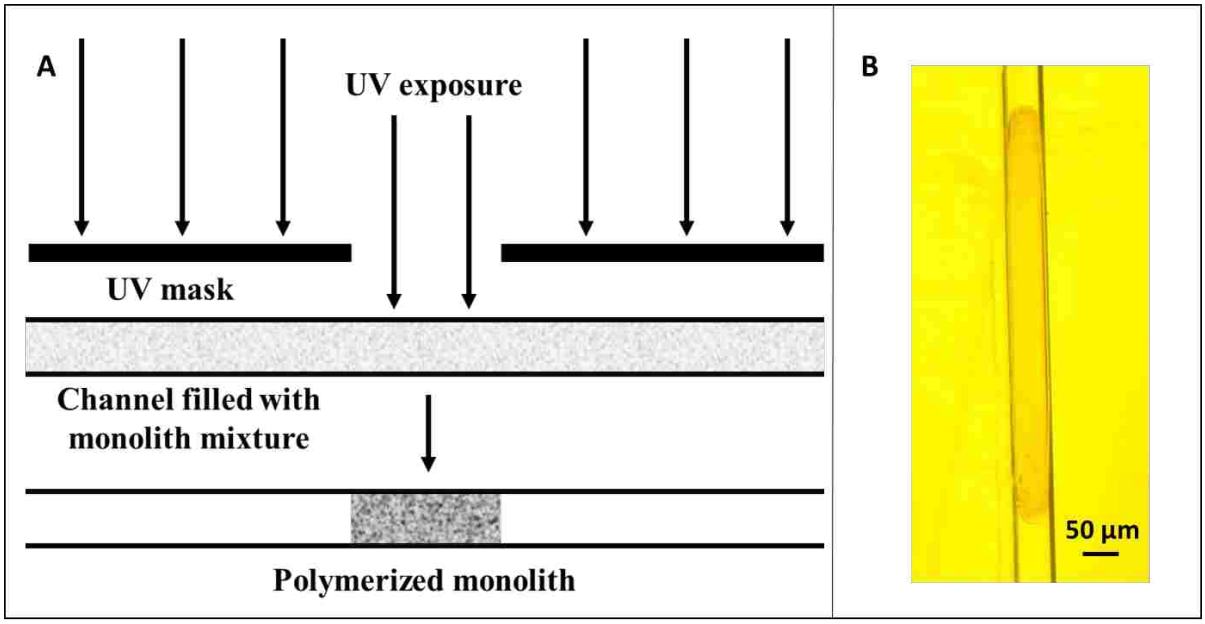

Figure 3.3 Monolith fabrication. (A) Schematic showing monolith fabrication via UV polymerization. (B) Photograph of a C8 monolith polymerized in a channel that has been filled with a 1:1 IPA:water mixture.

3.2.5 Device Operation

Before conducting experiments, monoliths in COC devices were cleaned several times using IPA, and channels in PMMA devices were cleaned with deionized water. Then, buffer was filled in channels by capillary action, and visual inspection was done for any trapped bubbles. For

monoliths, flushing was also done electrokinetically using 20 mM bicarbonate buffer (BCB, pH 9.6), by applying +400 V to reservoir 2 and grounding reservoir 1 to remove any air pockets trapped in the monolith.

3.2.5.1 Retention and Elution from Monoliths

FITC and FITC-labeled samples were retained and subsequently eluted from monoliths to optimize the conditions for on-chip labeling of PTB biomarkers. For retention and elution studies, the straight channel design described in Figure 3.2 was used. After flushing monoliths electrokinetically, buffer in reservoir 1 was replaced with off-chip labeled sample or FITC solution. To inject the sample, reservoir 1 was grounded and +500 V were applied on reservoir 2 for 5 min. The detection point was just after the monolith as indicated in Fig. 3.2C. After sample injection the content of reservoir 1 was removed, rinsed and replaced with fresh 20 mM BCB. Rinsing of unretained sample was carried out by applying +500 V on reservoir 2 and grounding reservoir 1 until the eluting LIF signal became low and steady (~2 min). Further rinsing steps were carried out with 20% ACN, 50% ACN, and 85% ACN using +1000 V at reservoir 2. A CCD image of the monolith was taken after every rinsing and elution step to determine sample retention.

3.2.5.2 On-chip Fluorescent Labeling

Figure 3.4 shows different steps required for on-chip labeling. First, unlabeled sample (see Figure legends for concentrations) was loaded on a buffer-rinsed monolith for 10 min by applying +500 V at reservoir 2 while grounding reservoir 1 (Figure 3.4A). After loading sample, reservoir 1 was rinsed with buffer, and 10 or 20 μM FITC was filled in reservoir 1. FITC was loaded on the

monolith by applying the same voltages for 5 min, followed by a no-voltage incubation time of 15-20 min to allow fluorescent labeling as shown in Figure 3.4B-C. After incubation, the reservoir was rinsed with buffer, which was loaded on the monolith for initial rinsing. Then, 50% ACN was filled in reservoir 1 and unreacted dye was eluted from the monolith by applying +1000 V at reservoir 2 and grounding reservoir 1 until the background signal became low and steady (~5 min). Finally, the labeled sample was eluted by replacing the content of reservoir 1 with 85% ACN and using the same voltage configurations for 2 min. This labeled analyte was then detected by LIF setup (Figure 3.4D).

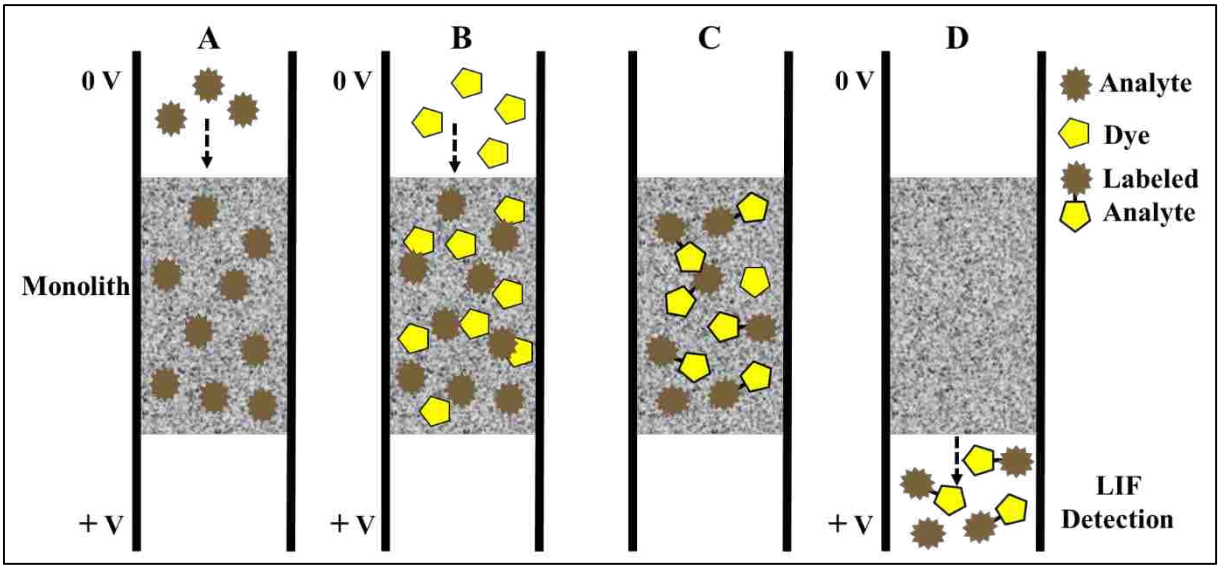

Figure 3.4 Schematic summarizing on-chip fluorescent labeling on a monolithic column.

3.3 RESULTS AND DISCUSSION

3.3.1 Monolith Optimization

In this study, monoliths fabricated in thermally bonded COC microchips were used for SPE of PTB biomarkers. COC was chosen as the device material due to its compatibility with organic

solvents like acetonitrile and IPA.[40-41] Monoliths were polymerized using a mixture containing 40% acrylate to ensure high porosity and sample retention as demonstrated previously.[11-12, 15] The exposure time for this polymer mixture was optimized to be 11 min for polymerizing high porosity monoliths in COC channels. Polymerized monoliths were found to be readily permeable to aqueous buffers by capillary action, so complicated preconditioning, surface modification or photografting steps[42] were not required.

Three different monomers (C4, C8, and C12) were used to fabricate monoliths to study the retention and elution of P1. SEM images of bulk monoliths (Fig. 3.5A-C) showed nodule sizes from 100-200 nm and pore sizes from 100-1500 nm, consistent with previous reports.[12, 22] Monolith porosity decreased with increasing length of alkyl chain going from C4 to C8 to C12. Additionally, pores were distributed randomly, aiding in sample mixing during flow. Monoliths did not dislocate during application of voltage across the channel, in accordance with previous reports.[11-12, 42]

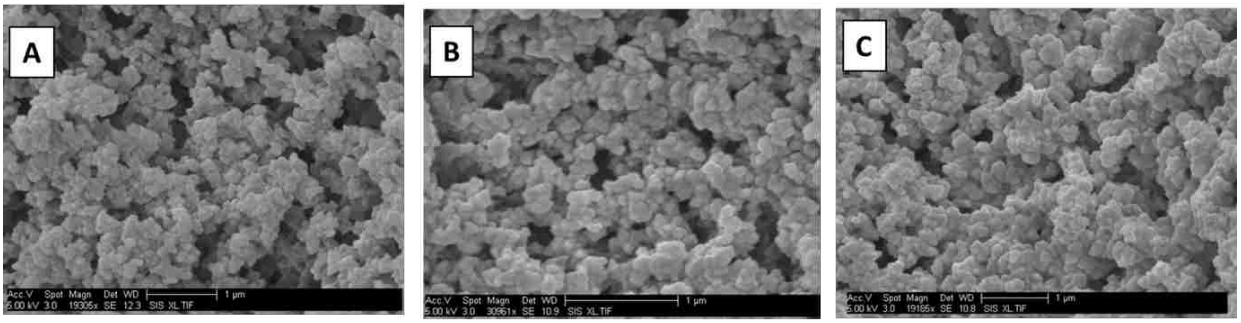

Figure 3.5 SEM images of bulk monoliths. (A) C4, (B) C8, and (C) C12.

3.3.2 Retention and Elution of P1

Yang et al.[12] previously found that monoliths made from C8 worked well for on-chip labeling of model proteins, showing good retention after rinsing with 50% ACN and efficient elution in 85%

ACN. Because on-chip SPE, labeling and elution of PTB peptides had not been shown previously, I tested monoliths made from C4, C8, and C12 to find the optimum composition for experiments with P1. The monomer to porogen ratio was the kept the same (40:60) in all cases to study the effect of the monomer itself on retention of P1. I measured background-subtracted fluorescence in CCD images of the monoliths to determine the retention of off-chip labeled FITC-P1 on these monoliths after rinsing with eluents of decreasing polarity. Fig. 3.6 shows the background-subtracted fluorescence on C4, C8 and C12 monoliths after injecting 50 μM FITC-P1 for 5 min and rinsing successively with buffer, 20%, 50% and 85% ACN solutions. P1 contains ten uncharged hydrophobic residues and four charged hydrophilic residues which makes it somewhat hydrophobic.[43]

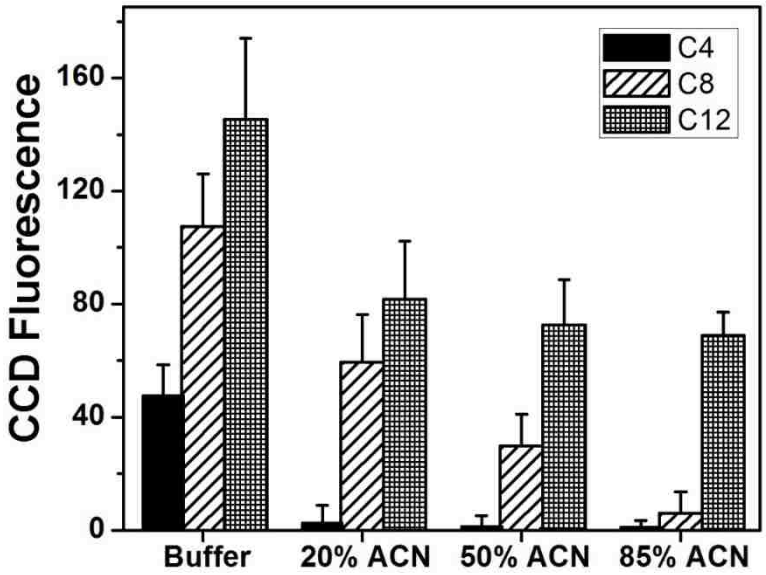

Figure 3.6 Background-subtracted CCD fluorescence signal obtained from 50 μM FITC-P1 retained on monoliths prepared from C4, C8 or C12 and eluted after successive electrokinetic flow of buffer, 20% ACN, 50% ACN, and 85% ACN (n=3). Error bars represent ±1 standard deviation.

C4 showed 3x lower retention of P1 than on C12 after an initial buffer rinse, which can be attributed to the lower hydrophobicity of C4. The retained P1 was also readily eluted in 20% ACN due to its limited hydrophobic interaction with C4. C8 monoliths had more than twice as much retained P1 as C4 monoliths after a buffer rinse, because of the greater hydrophobicity of C8

Additionally, in 85% ACN >90% of the initial retained P1 was eluted, which makes C8 monoliths well suited for selective retention followed by effective elution of P1. C12, due to its highly hydrophobic nature, showed the greatest retention of P1 (~40% more than on C8). However, elution of P1 from C12 monoliths was limited to ~50% of what was present following a buffer rinse, after a series of successive rinses containing 20%, 50%, and 85% ACN solutions. Thus, C8 monoliths showed the best retention and elution characteristics for on-chip labeling of P1, and were chosen for subsequent studies.

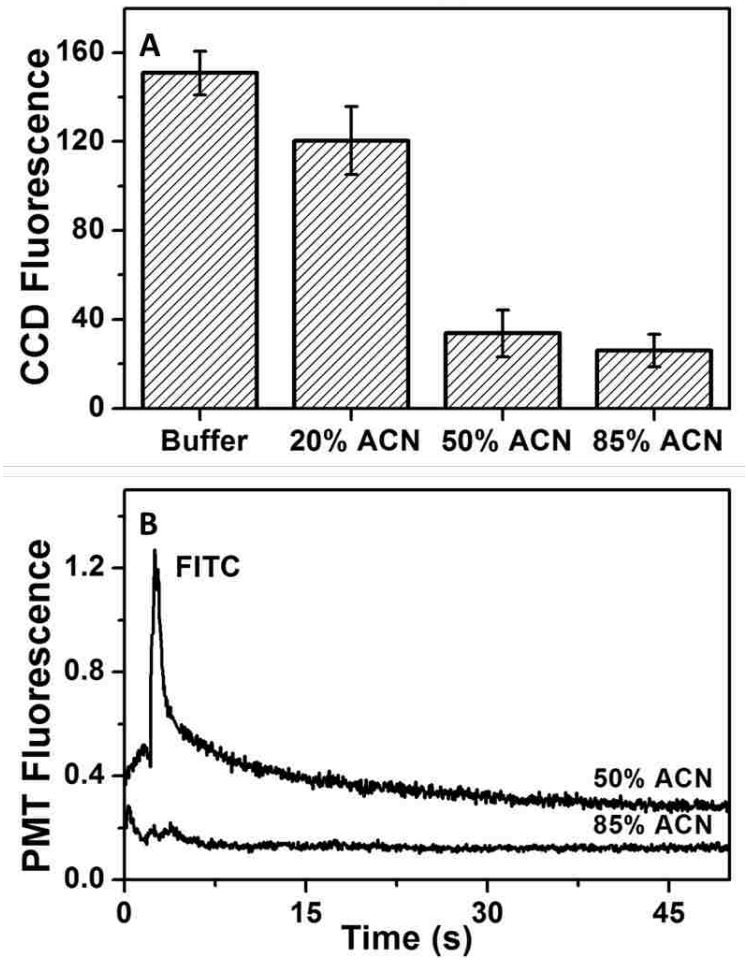

Figure 3.7 Retention and elution of FITC on a C8 monolith. (A) Background-subtracted CCD fluorescence from a C8 monolith after retention of 10 µM FITC and sequential rinsing with buffer, 20%, 50% and 85% ACN (n=3). Error bars represent ±1 standard deviation. (B) Sequential elution of 10 µM FITC from a C8 monolith after rinsing with 50% and then 85% ACN. Traces are offset vertically.

3.3.3 Retention of FITC on C8

Since C8 showed the best retention and elution characteristics for P1, retention of the widely used fluorescent tag, FITC, on a C8 monolith was studied. I injected 10 μM FITC on the monolith for 5 min and sequentially rinsed with buffer, 20%, 50% and 85% ACN solutions. Figure 3.7A shows the background-subtracted fluorescence on the monolith after each step, indicating a ~25% decrease in fluorescence between the buffer rinse and 25% ACN elution, with a further 3-fold decrease in fluorescence after a 50% ACN elution. Fig. 3.7B shows the electroelution profiles of 10 μM FITC in 50% ACN and 85% ACN recorded just past the end of the monolith (see Fig. 3.2C). During 50% ACN elution a sharp peak for eluted FITC is observed at ~5 s while only a small increase in signal (near the noise level) was noted in the successive 85% ACN elution, indicating that little additional FITC was eluted with 85% ACN.

3.3.4 On-chip Labeling of PTB Biomarkers

For on-chip labeling experiments C8 monoliths were prepared and the device was operated as described in sections 3.2.3 and 3.2.5. For labeling, mixing of sample and dye solution is necessary, but is also difficult to achieve with laminar flow typically observed in microfluidic channels.[44-45] However, the non-uniform and random porous flow paths in monoliths allow mixing to be achieved more efficiently.[19, 46]

3.3.4.1 P1

Blank experiments were done using FITC and off-chip labeled P1 to compare the elution profile in 85% ACN to that observed for on-chip labeled P1. Fig. 3.8A shows the elution of 20 μM FITC

in 85% ACN, showing a tailing peak at ~5 s indicating elution of remaining FITC from the column after the 50% ACN rinse. In Fig. 3.8B, the elution profile of off-chip-labeled 50 μM FITC-P1 is seen. In addition to the FITC peak at ~ 5 s, a second, larger peak is observed at ~15 s, indicating elution of FITC-P1 in the 85% ACN solution. A similar FITC-P1 peak is also observed in Fig. 3.8C after on-chip labeling of P1 with FITC and the same sequence of washing and elution steps. In both off-chip and on-chip labeled P1 elution (Fig. 3.8B-C), a broad peak corresponding to unreacted FITC at ~5 s is observed due to excess FITC used in labeling. The 1-mm length of the monolith is the principal cause of the broadness of the peaks in these electroelution experiments.

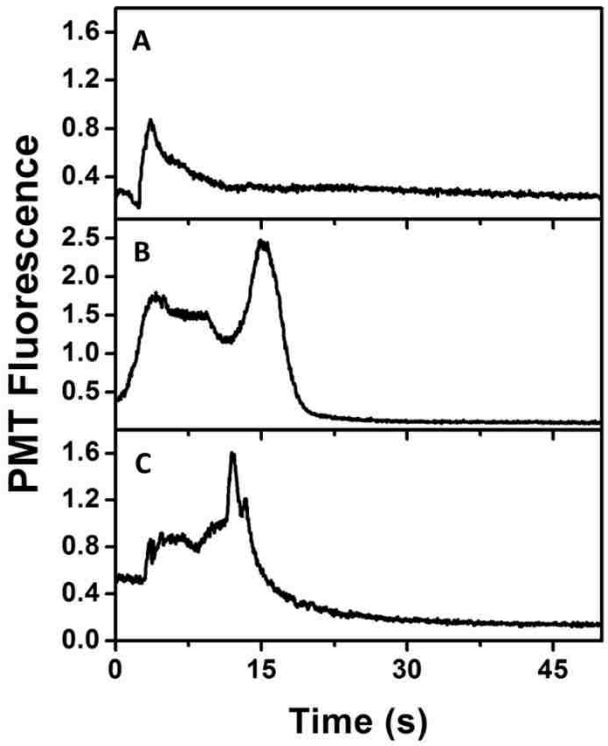

Figure 3.8 On chip labeling of P1. Electroelution profiles from C8 monolithic columns in 85% ACN of (A) 20 μM FITC, and FITC-P1 labeled (B) off-chip (50 μM), and (C) on-chip (15 μM).

3.3.4.2 PTB Proteins: Ferritin and Lactoferrin

Fig. 3.9A shows the 85% ACN elution traces of 10 μM FITC and 45 nM ferritin, labeled off-chip and on-chip. Only a small peak for FITC is observed at ~1 s in the blank experiment. For off-chip

labeled ferritin retained on and eluted from the column, a small FITC peak was seen at ~1 s and a larger peak corresponding to FITC-ferritin was observed at ~6 s. A similar set of peaks was observed when ferritin was labeled on-chip using FITC. Comparable peak height in 85% ACN elution of the off-chip and on-chip labeled ferritin indicates good efficiency for the on-chip labeling process. The difference in FITC peak heights for off-chip and on-chip labeled ferritin is likely due to the presence of excess FITC in on-chip labeled ferritin, unlike with the off-chip labeled ferritin sample, which was filtered before use. Lactoferrin was also used for on-chip labeling with a similar experimental procedure. Fig. 3.9B shows the elution profiles in 85% ACN for 20 μM FITC and 1.2 μM lactoferrin labeled on-chip. With only FITC loaded, a single peak corresponding to FITC was observed at ~3 s. When lactoferrin was labeled on-chip a second peak at ~7 s was observed, corresponding to on-chip-labeled FITC-lactoferrin.

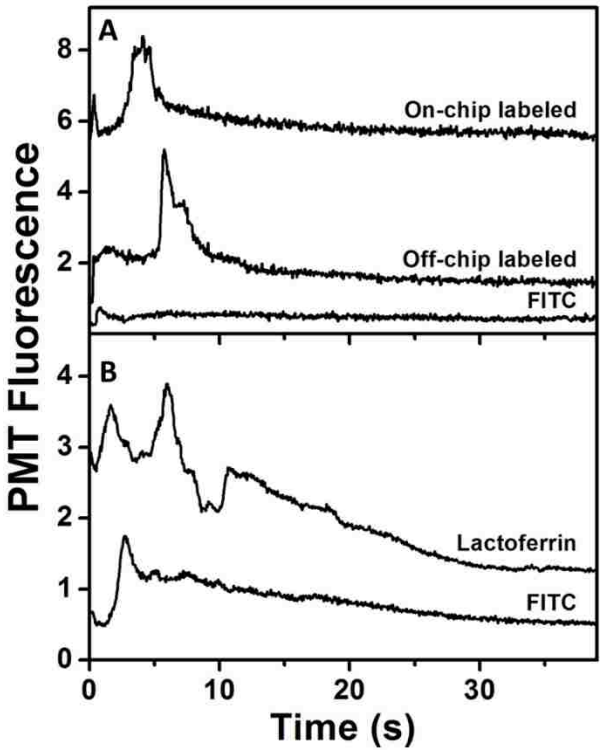

Figure 3.9 On-chip labeling of PTB proteins. Electroelution profiles from C8 monoliths in 85% ACN for (A) 10 μM FITC blank (*bottom*), and FITC-ferritin (45 nM) labeled off-chip (*middle*),

and on-chip (*top*); (B) 20 μM FITC blank (*bottom*), and 1.2 μM lactoferrin labeled on-chip (*top*). Traces are offset vertically.

3.4 REFERENCES

1. Arora, A.; Simone, G.; Salieb-Beugelaar, G. B.; Kim, J. T.; Manz, A., Latest Developments in Micro Total Analysis Systems. *Anal. Chem.* **2010,** *82* (12), 4830-4847.

2. Nge, P. N.; Rogers, C. I.; Woolley, A. T., Advances in Microfluidic Materials, Functions, Integration, and Applications. *Chem. Rev.* **2013,** *113* (4), 2550-2583.

3. Sackmann, E. K.; Fulton, A. L.; Beebe, D. J., The present and future role of microfluidics in biomedical research. *Nature* **2014,** *507* (7491), 181-189.

4. Pagaduan, J. V.; Sahore, V.; Woolley, A. T., Applications of microfluidics and microchip electrophoresis for potential clinical biomarker analysis. *Anal. Bioanal. Chem.* **2015,** *407* (23), 6911-6922.

5. Araci, I. E.; Brisk, P., Recent developments in microfluidic large scale integration. *Curr. Opin. Biotechnol.* **2014,** *25*, 60-68.

6. Nge, P. N.; Yang, W.; Pagaduan, J. V.; Woolley, A. T., Ion-permeable membrane for on-chip preconcentration and separation of cancer marker proteins. *Electrophoresis* **2011,** *32* (10), 1133-1140.

7. Giordano, B. C.; Burgi, D. S.; Hart, S. J.; Terray, A., On-line sample pre-concentration in microfluidic devices: A review. *Anal. Chim. Acta* **2012,** *718*, 11-24.

8. Song, H.; Wang, Y.; Garson, C.; Pant, K., Concurrent DNA preconcentration and separation in bipolar electrode-based microfluidic device. *Anal. Methods* **2015,** *7* (4), 1273-1279.

9. Castro, E. R.; Manz, A., Present state of microchip electrophoresis: State of the art and routine applications. *J. Chromatogr. A* **2015,** *1382*, 66-85.

10. Nuchtavorn, N.; Suntornsuk, W.; Lunte, S. M.; Suntornsuk, L., Recent applications of microchip electrophoresis to biomedical analysis. *J. Pharm. Biomed. Anal.* **2015,** *113*, 72-96.

11. Nge, P. N.; Pagaduan, J. V.; Yu, M.; Woolley, A. T., Microfluidic chips with reversed-phase monoliths for solid phase extraction and on-chip labeling. *J. Chromatogr. A* **2012,** *1261*, 129-135.

12. Yang, R.; Pagaduan, J. V.; Yu, M.; Woolley, A. T., On chip preconcentration and fluorescence labeling of model proteins by use of monolithic columns: device fabrication, optimization, and automation. *Anal. Bioanal. Chem.* **2015,** *407* (3), 737-747.

13. Sun, X.; Yang, W.; Pan, T.; Woolley, A. T., Affinity monolith-integrated poly (methyl methacrylate) microchips for on-line protein extraction and capillary electrophoresis. *Anal. Chem.* **2008,** *80* (13), 5126-5130.

14. Yang, W.; Yu, M.; Sun, X.; Woolley, A. T., Microdevices integrating affinity columns and capillary electrophoresis for multibiomarker analysis in human serum. *Lab Chip* **2010,** *10* (19), 2527-2533.

15. Kumar, S.; Sahore, V.; Rogers, C. I.; Woolley, A. T., Development of an integrated microfluidic solid-phase extraction and electrophoresis device. *Analyst* **2016,** *141* (5), 1660-1668.

16. Verbarg, J.; Kamgar-Parsi, K.; Shields, A. R.; Howell Jr., P. B.; Ligler, F. S., Spinning magnetic trap for automated microfluidic assay systems. *Lab Chip* **2012,** *12* (10), 1793-1799.

17. Hitzbleck, M.; Delamarche, E., Reagents in microfluidics: an 'in' and 'out' challenge. *Chem. Soc. Rev.* **2013,** *42* (21), 8494-8516.

18. Oleschuk, R. D.; Shultz-Lockyear, L. L.; Ning, Y.; Harrison, D. J., Trapping of Bead-Based Reagents within Microfluidic Systems: On-Chip Solid-Phase Extraction and Electrochromatography. *Anal. Chem.* **2000,** *72* (3), 585-590.

19. Quirino, J. P.; Dulay, M. T.; Zare, R. N., On-Line Preconcentration in Capillary Electrochromatography Using a Porous Monolith Together with Solvent Gradient and Sample Stacking. *Anal. Chem.* **2001,** *73* (22), 5557-5563.

20. Malmstadt, N.; Yager, P.; Hoffman, A. S.; Stayton, P. S., A Smart Microfluidic Affinity Chromatography Matrix Composed of Poly(N-isopropylacrylamide)-Coated Beads. *Anal. Chem.* **2003,** *75* (13), 2943-2949.

21. Yu, C.; Davey, M. H.; Svec, F.; Fréchet, J. M. J., Monolithic Porous Polymer for On-Chip Solid-Phase Extraction and Preconcentration Prepared by Photoinitiated in Situ Polymerization within a Microfluidic Device. *Anal. Chem.* **2001,** *73* (21), 5088-5096.

22. Ramsey, J. D.; Collins, G. E., Integrated Microfluidic Device for Solid-Phase Extraction Coupled to Micellar Electrokinetic Chromatography Separation. *Anal. Chem.* **2005,** *77* (20), 6664-6670.

23. Dhopeshwarkar, R.; Sun, L.; Crooks, R. M., Electrokinetic concentration enrichment within a microfluidic device using a hydrogel microplug. *Lab Chip* **2005,** *5* (10), 1148-1154.

24. Tokuyama, H.; Iwama, T., Temperature-Swing Solid-Phase Extraction of Heavy Metals on a Poly(N-isopropylacrylamide) Hydrogel. *Langmuir* **2007,** *23* (26), 13104-13108.

25. Long, Z.; Shen, Z.; Wu, D.; Qin, J.; Lin, B., Integrated multilayer microfluidic device with a nanoporous membrane interconnect for online coupling of solid-phase extraction to microchip electrophoresis. *Lab Chip* **2007,** *7* (12), 1819-1824.

26. Svec, F., Less common applications of monoliths: Preconcentration and solid-phase extraction. *J. Chromatogr. B* **2006,** *841* (1–2), 52-64.

27. Knob, R.; Sahore, V.; Sonker, M.; Woolley, A. T., Advances in monoliths and related porous materials for microfluidics. *Biomicrofluidics* **2016,** *10* (3), 032901.

28. Vázquez, M.; Paull, B., Review on recent and advanced applications of monoliths and related porous polymer gels in micro-fluidic devices. *Anal. Chim. Acta* **2010,** *668* (2), 100-113.

29. Yang, W.; Sun, X.; Wang, H.-Y.; Woolley, A. T., Integrated microfluidic device for serum biomarker quantitation using either standard addition or a calibration curve. *Anal. Chem.* **2009,** *81* (19), 8230-8235.

30. Karenga, S.; El Rassi, Z., Neutral octadecyl monolith for reversed phase capillary electrochromatography of a wide range of solutes. *J. Sep. Sci.* **2008,** *31* (14), 2677-2685.

31. Groarke, R. J.; Brabazon, D., Methacrylate Polymer Monoliths for Separation Applications. *Materials* **2016,** *9* (6), 446.

32. Stachowiak, T. B.; Rohr, T.; Hilder, E. F.; Peterson, D. S.; Yi, M.; Svec, F.; Fréchet, J. M. J., Fabrication of porous polymer monoliths covalently attached to the walls of channels in plastic microdevices. *Electrophoresis* **2003,** *24* (21), 3689-3693.

33. Aggarwal, P.; Tolley, H. D.; Lee, M. L., Monolithic bed structure for capillary liquid chromatography. *J. Chromatogr. A* **2012,** *1219*, 1-14.

34. Liu, K.; Aggarwal, P.; Lawson, J. S.; Tolley, H. D.; Lee, M. L., Organic monoliths for high-performance reversed-phase liquid chromatography. *J. Sep. Sci.* **2013,** *36* (17), 2767-2781.

35. Hermanson, G. T., *Bioconjugate techniques*. 3rd ed.; Academic press: 2013.

36. Rashidian, M.; Dozier, J. K.; Distefano, M. D., Enzymatic Labeling of Proteins: Techniques and Approaches. *Bioconjugate Chemistry* **2013,** *24* (8), 1277-1294.

37. Esplin, M. S.; Merrell, K.; Goldenberg, R.; Lai, Y.; Iams, J. D.; Mercer, B.; Spong, C. Y.; Miodovnik, M.; Simhan, H. N.; van Dorsten, P.; Dombrowski, M., Proteomic identification of serum peptides predicting subsequent spontaneous preterm birth. *Am. J. Obstet. Gynecol.* **2011,** *204* (5), 391.e1-391.e8.

38. Sahore, V.; Kumar, S.; Rogers, C. I.; Jensen, J. K.; Sonker, M.; Woolley, A. T., Pressure-actuated microfluidic devices for electrophoretic separation of pre-term birth biomarkers. *Anal. Bioanal. Chem.* **2016,** *408* (2), 599-607.

39. Kelly, R. T.; Woolley, A. T., Thermal Bonding of Polymeric Capillary Electrophoresis Microdevices in Water. *Anal. Chem.* **2003,** *75* (8), 1941-1945.

40. Ro, K. W.; Liu, J.; Knapp, D. R., Plastic microchip liquid chromatography-matrix-assisted laser desorption/ionization mass spectrometry using monolithic columns. *J. Chromatogr. A* **2006,** *1111* (1), 40-47.

41. Faure, K.; Albert, M.; Dugas, V.; Crétier, G.; Ferrigno, R.; Morin, P.; Rocca, J.-L., Development of an acrylate monolith in a cyclo-olefin copolymer microfluidic device for chip electrochromatography separation. *Electrophoresis* **2008,** *29* (24), 4948-4955.

42. Ladner, Y.; Crétier, G.; Faure, K., Electrochromatography in cyclic olefin copolymer microchips: A step towards field portable analysis. *J. Chromatogr. A* **2010,** *1217* (51), 8001-8008.

43. Kyte, J.; Doolittle, R. F., A simple method for displaying the hydropathic character of a protein. *J. Mol. Biol.* **1982,** *157* (1), 105-132.

44. Kamholz, A. E.; Yager, P., Theoretical Analysis of Molecular Diffusion in Pressure-Driven Laminar Flow in Microfluidic Channels. *Biophys. J.* **2001,** *80* (1), 155-160.

45. Junemo, K.; Clement, K., Liquid flow in microchannels: experimental observations and computational analyses of microfluidics effects. *J. Micromech. Microeng.* **2003,** *13* (5), 568-579.

46. Rohr, T.; Yu, C.; Davey, M. H.; Svec, F.; Fréchet, J. M. J., Porous polymer monoliths: Simple and efficient mixers prepared by direct polymerization in the channels of microfluidic chips. *Electrophoresis* **2001,** *22* (18), 3959-3967.

4. INTEGRATED ELECTROKINETICALLY DRIVEN MICROFLUIDIC DEVICES WITH PH-MEDIATED SOLID-PHASE EXTRACTION COUPLED TO MICROCHIP ELECTROPHORESIS FOR PRETERM BIRTH BIOMARKERS[§]

4.1 INTRODUCTION

Biomarker analysis in bodily fluids is important for the diagnosis of diseases like cancer,[1-3] and cardiovascular,[4-5] degenerative,[6-8] genetic,[9-11] and infectious[12-13] disorders. However, these biomarkers are typically found in low concentrations such that a sample preconcentration step is often required. Microfluidic devices offer advantages like integration, low cost, rapid analysis, portability, and low limits of detection for biomarker analysis.[14-15] Integration in microfluidics is a key advantage which can allow automated analysis of multiple analytes without sample loss and contamination.[14] Considering this potential, integrated microfluidic platforms have gained significant attention recently in diagnosing and monitoring the progression of diseases through biomarker analysis.[16-19] Devices have been developed recently that can integrate preconcentration, solid phase extraction (SPE) and electrophoretic separation.[20-22] However, these devices report data for model analytes, high (micromolar) concentrations or both. Here, I report an integrated microfluidic device for SPE and microchip electrophoresis (μCE) of multiple analytes including a preterm birth (PTB) biomarker, demonstrating enrichment for low nanomolar concentration samples that are typical of PTB biomarkers.[23-24]

PTB is birth before 37 weeks of pregnancy. It is the most common complication of pregnancy, affecting over 500,000 births in the United States every year.[25-26] Recently, Esplin et

[§]Adapted with permission from Sonker, M., Knob, R., Sahore, V., Woolley, A. T., Integrated electrokinetically driven microfluidic devices with pH-mediated solid-phase extraction coupled to microchip electrophoresis for preterm birth biomarkers, *Electrophoresis,* **2017**, 38 (13-14), 1743-1754.

al.[23-24] characterized and validated a biomarker panel in maternal serum, the analysis of which can provide a selective (81%) and sensitive (87%) diagnosis of PTB occurring four weeks in the future. One biomarker in this panel is a 19 amino acid, proline rich peptide (P1), which is a part of inter-alpha-trypsin inhibitor heavy chain 4, a glycoprotein previously indicated in inflammation. Although the serum concentration of P1 is not given in the literature, the concentrations of other PTB biomarkers in serum range from low nanomolar to micromolar levels.[23] Thus, a microfluidic analysis platform that detects nanomolar-level biomarker concentrations would allow the diagnosis of PTB risk and facilitate medical interventions to delay birth or increase fetus viability to improve outcomes.[27-28] This integrated microfluidic device that combines pH-mediated SPE of P1 with μCE is a step toward addressing this need.

SPE is a common method for sample enrichment in which the analyte is concentrated on a solid support and thereafter selectively eluted for further analysis.[29-31] Solid supports used for SPE in microfluidics include packed materials[17, 32] and porous polymer monoliths.[33-36] Monoliths are desirable SPE materials in microfluidics due to their ease of fabrication without the need for retaining frits,[37] high surface area, and low backpressures during fluid flow.[38-39] Reversed-phase monoliths are often used for sample enrichment by hydrophobic interaction with analytes.[40-41] Pruim et al.[42] used different methacrylate monoliths for preconcentration and gradient elution of peptides in a microfluidic setup. Ladner et al.[43] demonstrated electrochromatographic separations in lauryl methacrylate monoliths polymerized in cyclic olefin copolymer (COC) microchips. Although photopolymerization of monoliths in microfluidic systems requires additional device processing steps, masked UV exposure for controlled placement[39] makes monoliths amenable for scalable microfluidic production.

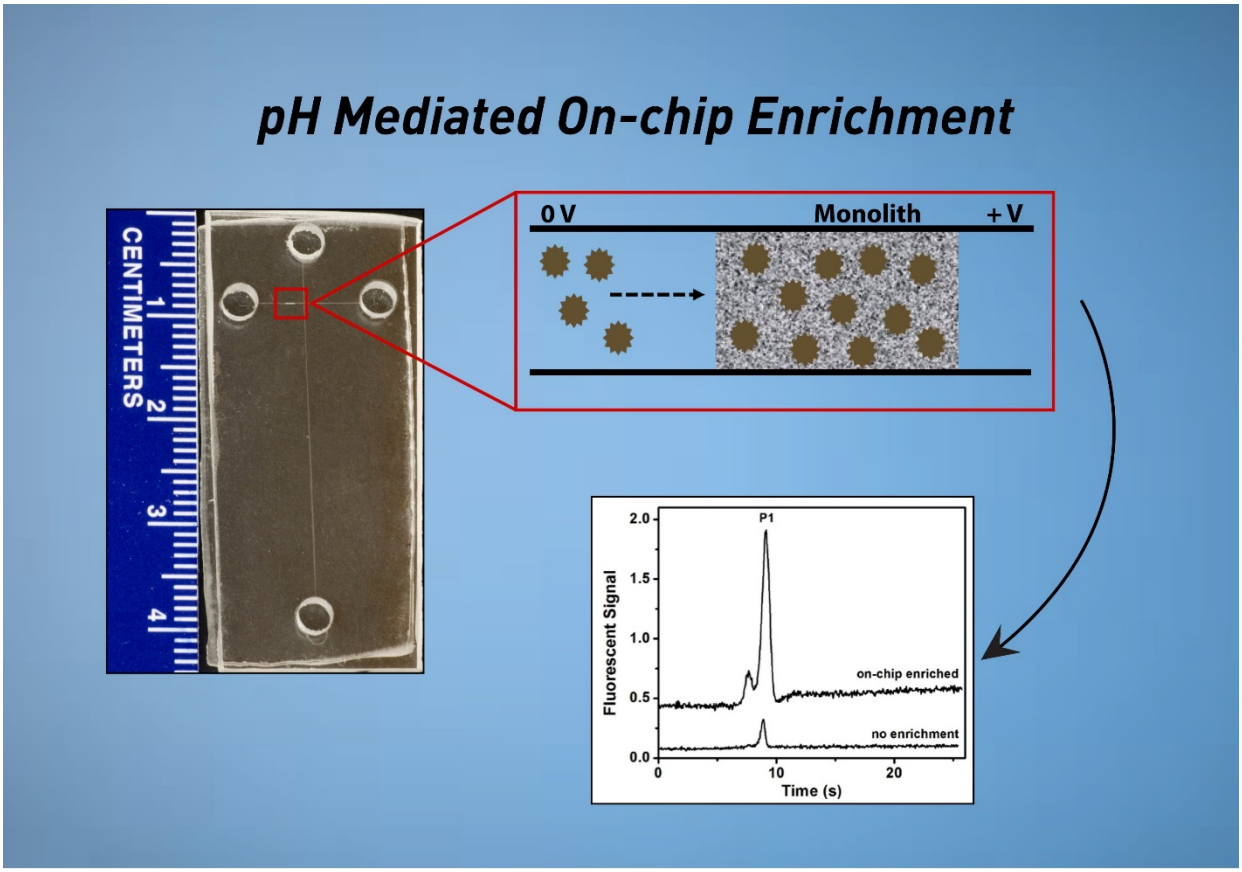

Figure 4.1 Overview of pH mediated SPE.

Here, I have modified a previously reported[44] pH-mediated SPE approach to utilize hydrophobic interaction with the stationary phase and electrokinetic migration of analytes at different pH values to enrich or elute them from a reversed-phase monolithic column in a microfluidic device (overview shown in Fig. 4.1). Related work in conventional capillaries includes preconcentration at a pH junction made using background electrolytes with different pH values[45-46] and pH modulation for preconcentration via stacking and dynamic pH junctions.[47-48] The pH-mediated preconcentration method described here is advantageous over previous microfluidic SPE work,[35, 49-51] as it does not require the use of organic solvents like acetonitrile for extraction that may interfere with analyte separation. I achieved nearly 50-fold pH-mediated SPE enrichment for a PTB biomarker peptide (P1) at low nM concentrations, and found the monolith

binding capacity for this peptide to be 400 pg (0.2 pmol). Importantly, the pH-mediated SPE approach was integrated with μCE to simultaneously enrich and separate multiple analytes, resulting in a ~15-fold increase in PTB peptide peak area in the separation. Moreover, my application of SPE-μCE to a peptide PTB biomarker (P1) expands over published work demonstrating this approach only for a protein PTB biomarker.[50] Overall, this study reports several innovations and lays the foundation for a superior integrated platform for the analysis of PTB biomarkers.

4.2 EXPERIMENTAL SECTION

4.2.1 Chemicals and Materials

Four-inch diameter single side polished silicon wafers were obtained from Desert Silicon (Tempe, AZ). A silicon dioxide layer of ~500 nm was oxidized on these wafers using a Bruce Tube Furnace (Bruce Industrial, New Castle, DE). S1805 positive photoresist and MF 26A photoresist developer were purchased from Dow Chemical (Marlborough, MA). Zeonor 1060R (6”×6”×1 mm thick and 6”×4”×2 mm thick) COC plates were purchased from Zeon Chemicals (Louisville, KY). Polyethylene glycol diacrylate (PEGDA, M_w 575), benzoin methyl ether (BME), 2,2-dimethoxy-2-phenylacetophenone (DMPA), 1-dodecanol, sodium tetraborate decahydrate, ethylene dimethacrylate (EDMA), dimethyl sulfoxide, Phe-Ala (FA, a model peptide), hydroxypropyl cellulose (HPC, M_W 100 kDa), and inhibitor remover packing beads were obtained from Sigma-Aldrich (St Louis, MO). Octyl methacrylate (C8) was from Scientific Polymer Products (Ontario, NY). Tween 20 and sodium hydroxide were obtained from Mallinckrodt Baker (Paris, KY). Cyclohexanol was from J. T. Baker (Phillipsburg, NJ). Isopropyl alcohol (IPA) and acetonitrile

were from Fisher Scientific (Fair Lawn, NJ). Cyclohexane and methanol were purchased from Macron (Center Valley, PA). Anhydrous sodium carbonate, sodium bicarbonate, citric acid, sodium citrate, sodium phosphate monohydrate, anhydrous sodium phosphate, and boric acid were obtained from Merck (Darmstadt, Germany). Sodium chloride was from Columbus Chemicals (Columbus, WI).

All buffers were prepared using deionized water (18.3 MΩ) purified by a Barnstead EASYpure UV/UF system (Dubuque, IA) and filtered through a 0.45 μm Thermo Scientific Nalgene syringe filter (Waltham, MA). A fluorescein labeled PTB peptide (P1, QLGLPGPPDVPDHAAYHPF)[23, 52] was synthesized by GenScript (Piscataway, NJ). Ferritin was purchased from EMD Millipore (Billerica, MA). Fluorescein isothiocyanate (FITC) and Alexa Fluor 488 TFP Ester (AF 488) were obtained from Life Technologies (Carlsbad, CA). FA and ferritin were fluorescently labeled by adding 10 μL of 10 mM FITC in dimethyl sulfoxide to 100 μL of 10 mM FA or 50 μM ferritin and incubating overnight at room temperature. Excess FITC was filtered from ferritin using Amicon ultra 0.5 mL centrifugal filters (EMD Millipore, Billerica, MA). The concentration of filtered FITC-ferritin was determined with a Nanodrop ND-1000 spectrophotometer (Wilmington, DE). Residual, de-identified human serum was obtained from Prof. William Pitt at Brigham Young University.

4.2.2 Device Design and Fabrication

Device designs were made in CleWin software (Phoenix Software, Enschede, Netherlands). Silicon templates were fabricated in the BYU Integrated Microfabrication Lab using photolithographic patterning and wet etching techniques as described previously[53] and in sections

2.2.2 and 3.2.2. Two different devices made from previously characterized masks were used for my experiments. One design was a straight 2-cm-long channel as shown in Figure 4.2A-B, for the optimization of pH-mediated SPE. The channel dimensions were ~80 µm wide and ~20 µm deep. A T-shaped four reservoir design (Fig. 4.2F-H) was used for integrated SPE-µCE experiments, and these channels were designed to be ~50 µm wide and ~20 µm deep.

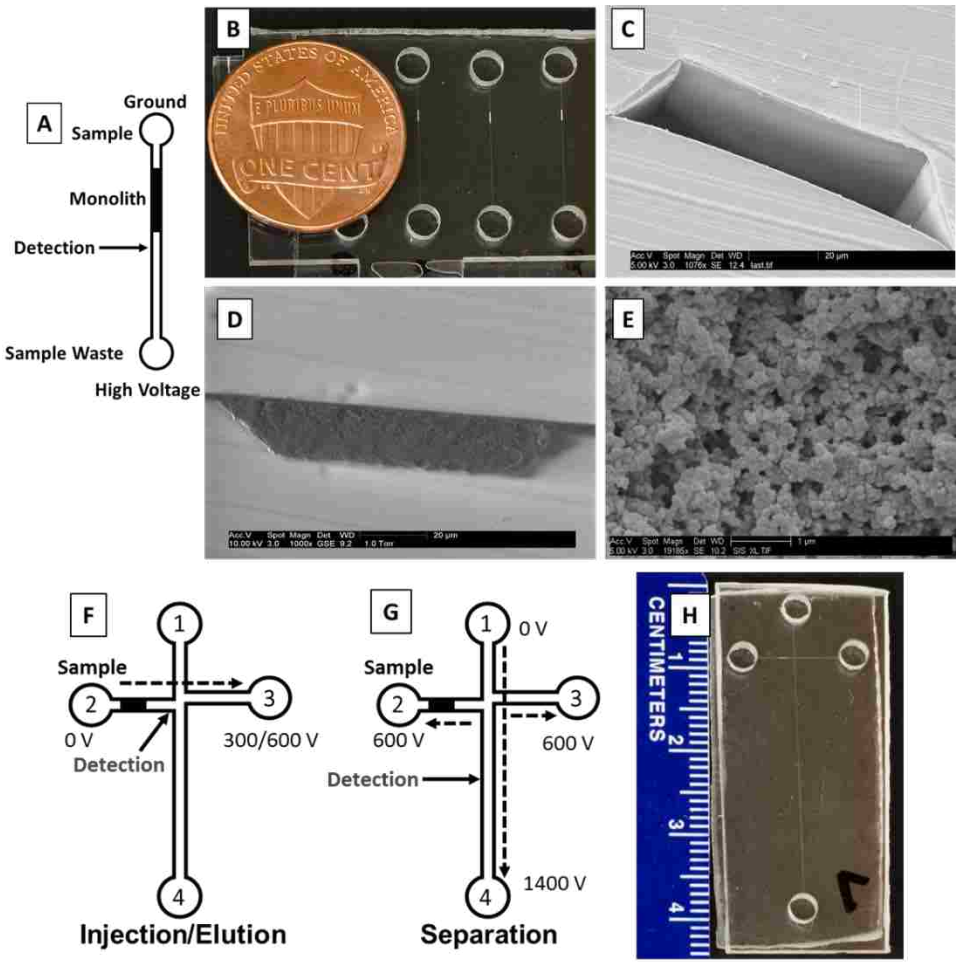

Figure 4.2 Device layout, photograph, operation and SEM images. (A) Single channel SPE device layout showing reservoirs for sample and sample waste, monolith, and voltage configuration for sample injection and elution. (B) Photograph of a device showing reservoirs and monolith (white) in the channels. SEM cross-sectional image of (C) an empty microfluidic channel, (D) a channel containing a C8 monolith, and (E) a magnified view of a C8 monolith prepared in bulk. (F-G) Integrated SPE-µCE device layout showing monolith position, sample flow, detection point and voltage configuration for (F) pinched sample injection/elution and (G) separation with pullback voltages. (H) Device photograph.

4.2.3 Surface Modification with PEGDA

A surface modification step was incorporated to ensure consistent electrokinetic sample flow. Channel surfaces of COC devices were photografted with PEGDA using an approach modified from Ladner et al.[54] First, polymerization inhibitor (methyl ether hydroquinone) was removed from PEGDA by slowly flowing it through a column filled with inhibitor remover packing beads and collecting the purified PEGDA. Methanol (94% w/w) was used to dissolve PEGDA to 3%, 5% or 7% w/w and BME (1% w/w) was used as the photoinitiator. This mixture was sonicated for 10 min and then used to fill the channels. Black tape was used to seal the reservoirs to prevent evaporation of the mixture, and then the whole channel was exposed to UV radiation (>100 mW cm^{-2}) for 8 min using a SunRay 600 UV lamp (Uvitron international, West Springfield, MA). After exposure, the unpolymerized mixture was removed from the channel by applying vacuum, and the channels were cleaned with IPA.

Scanning electron microscopy (SEM) images of the PEGDA coating on channels were taken using a Philips XL30 ESEM FEG instrument in high vacuum mode at 5-20 kV electron beam potential. Devices were cut into small pieces around the channels using a laser cutter (VLS 2.30 Versa Laser, Universal Laser Systems, Scottsdale, AZ) and were glued to glass stubs using epoxy. Cross-sections of the channels were then microtomed using a glass knife. These samples were placed on an aluminum stub and coated with Au-Pd (60:40 ratio, 15-20 nm thickness) using a Q150T ES Sputterer (Quorum Technologies, Lewes, East Sussex, UK) to reduce charging.

Water contact angles were measured for unmodified COC, photografted COC and a standard thermoplastic material, polymethyl methacrylate (PMMA, Evonik, Parsippany, NJ). For water contact angle measurements, ~2 cm × ~0.5 cm wide channels were imprinted on a COC plate using a silicon wafer, and photografting was performed using 3% and 5% PEGDA. COC

layers were pulled apart and contact angle measurements were done on the channel after cleaning the surface with IPA and drying with nitrogen gas. Water contact angles were measured with a Ramé-Hart Contact Angle Goniometer (Model 100-00, Netcong, NJ) fitted with a manual syringe filled with high purity (18 MΩ) water. The droplets for measuring static water contact angles were ~10 μL. The success of photografting was confirmed by an observed increase in hydrophilicity of the surface.

CCD images of the injection region of unphotografted and photografted T-shaped devices were recorded during electrokinetic sample flow using a Photometrics coolSNAP HQ2 (Tucson, AZ) CCD camera. A 488 nm laser (JDSU, Shenzhen, China) was used to excite the desired section of the device using a 4x objective on an inverted Nikon Eclipse TE300 microscope. The CCD images (500 ms exposure time) were processed using NIH ImageJ software (http://imagej.net/ImageJ). These images confirmed the electrokinetic sample flow direction in photografted and unphotografted devices.

Table 4.1: Reversed phase octyl methacrylate prepolymer mixture*

Name	Functional role	Mass (%)
Octyl methacrylate (C8)	Monomer	20%
EDMA	Cross-linker	10%
Cyclohexanol	Porogen	25%
1-dodecanol	Porogen	25%
Tween-20	Surfactant	20%
DMPA	Photoinitiator	1%

*sum >100% due to rounding

4.2.4 Monolith Fabrication

Reversed-phase C8 monoliths were fabricated in the device channels by preparing a mixture of monomer, porogen, and surfactant first (see Table 4.1), and then adding photoinitiator (1% by mass) to the mixture. This polymer mixture was sonicated for 15 min to ensure all components were completely dissolved, and channels were filled with the sonicated solutions. A Cr mask was used to cover the channel and expose only the desired area for UV polymerization. The length of the exposed region was 0.6 mm for all the monoliths used in this study. The observed monolith lengths were slightly longer (0.73 ± 0.10 mm, n =10), either due to scatter of the UV source or minor solution movement at the ends during polymerization. UV exposure was carried out for 11 min and after exposure, the unpolymerized mixture was flushed and the channels were rinsed several times using IPA. SEM was performed on cross-sections of channels with or without polymerized monoliths, using the same conditions as described in section 4.2.3, except the SEM of the channel with a monolith was obtained in low vacuum mode without a sputtered metal coating. Bulk C8 monolith for SEM was prepared by adding 250 µL of pre-polymer solution to a 1 mL Eppendorf tube and polymerizing it as described above. Then, the polymerized monolith was broken into pieces and stored in IPA to dissolve any unpolymerized mixture. These pieces were kept in a vacuum chamber overnight before being placed on a carbon taped aluminum stub for sputtering and SEM imaging.

4.2.5 Data Analysis

The laser induced fluorescence setup used for these experiments has been described in section 2.2.3. Eluted peak heights and areas were determined by OriginPro software (OriginLab Corporation, Northampton, MA).

4.2.6 Device Operation

4.2.6.1 pH-mediated SPE

Before experiments, the monoliths were washed several times using IPA and then preconditioned with (1:1 v/v) IPA and deionized water. The loading/rinsing buffer (20 mM citrate, pH 5) was filled in the reservoirs and channels, which were optically inspected for any trapped bubbles that could interfere with fluid flow. The buffer was flowed electrokinetically through the monolith by applying +400 V (200 V/cm) to the sample waste reservoir and grounding the sample reservoir (Fig. 4.2A) for 2-3 min to fill in any air pockets left in the monolith. After electrokinetically rinsing the monolith and channel with citrate buffer, a blank elution was done to ensure no carryover contamination. Citrate buffer in the sample reservoir was replaced with 50 mM bicarbonate buffer (BCB, pH 10), and the voltage applied on the sample waste reservoir for elution was increased to +800 V (400 V/cm).

SPE samples were diluted in 20 mM citrate buffer (pH 5) and filled in the sample reservoir. The sample was injected electrokinetically on the monolith for the desired interval by applying +400 V (200 V/cm) on the sample waste reservoir and grounding the sample reservoir. After injecting the sample, the reservoirs were emptied, rinsed and refilled with fresh citrate buffer. A monolith rinsing step was carried out for 1 min at +400 V (200 V/cm). After rinsing, buffer in the reservoirs was replaced with 50 mM BCB, and the elution step was carried out as described above for the blank elution. During the elution step laser induced fluorescence was recorded in the channel after the end of the monolith as indicated in Fig. 4.2A. For monolith capacity experiments the detector gain was reduced to keep the signal from going off scale.

4.2.6.2 Integrated SPE-µCE

In the integrated "T" shaped device, a monolith was fabricated in one of the arms of the T (Fig. 4.2 F-H), and was washed and filled as described in section 4.2.6.1. Reservoirs 2 and 3 were filled with citrate buffer (pH 5) while reservoirs 1 and 4 were filled with BCB having 0.05% HPC. Sample injection was carried out for 5 min, and monolith rinsing and sample elution steps were carried out as described in section 4.2.6.1, treating reservoir 2 as the sample reservoir and reservoir 3 as the sample waste reservoir, using +300 V (300 V/cm) for sample injection and rinsing, and +600 V (600 V/cm) for elution. Initially, the elution step was monitored at the intersection of the T (Fig. 4.2F) to determine the time required for the eluted sample plug to reach the intersection. For integrated SPE-µCE, sample was loaded and rinsed as before, but during elution the voltage configuration was switched at the previously determined time to carry out µCE of the eluted and injected plug in the intersection. During µCE, +600 V was applied to reservoirs 2 and 3, +1400 V was applied to reservoir 4, and reservoir 1 was grounded, corresponding to ~400 V/cm on the separation channel. The detection point was positioned 5 mm beyond the intersection in the separation channel as indicated in Fig. 4.2G.

4.3 RESULTS AND DISCUSSION

4.3.1 Surface Modification with PEGDA

COC was chosen as the device material due to its compatibility with organic solvents that are required for monolith fabrication.[35, 49] However, one of the challenges with the use of COC is inconsistency in electrokinetic transport due to its hydrophobic surface. Reliable electrokinetic

transport is an important characteristic to ensure constant sample injection for given parameters and a defined interval. Thus, a surface modification step was incorporated before monolith fabrication. PEGDA was used for photografting of COC channels because it provides an optically transparent, inert, and hydrophilic coating which also decreases nonspecific adsorption.[54-55] Initial photografting tests were performed using 3-7% PEGDA dissolved in methanol with BME (1%, photoinitiator) to modify the COC channels. I found that 3%, 5%, and 7% PEGDA formulations were able to make channels hydrophilic enough to facilitate sample injection. However, 3% PEGDA photografting was not reproducible, while 7% PEGDA photografting resulted in occasional blocking of channels. Thus, 5% PEGDA was used for subsequent channel photografting. SEM images were taken to confirm PEGDA photografting on COC channels (Fig. 4.3A).

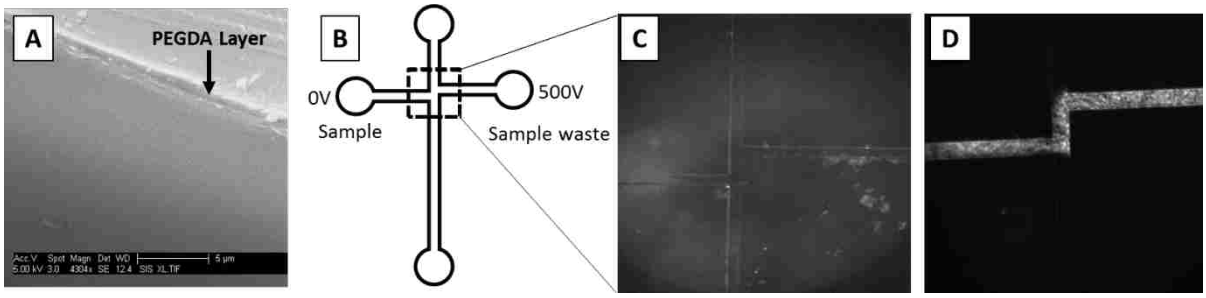

Figure 4.3 PEGDA photografting. (A) SEM image of a channel photografted with 5% PEGDA. (B) Layout of the device and voltage configuration used for sample flow. CCD images of the intersection region for (C) an unphotografted device showing no forward flow, and (D) a photografted device showing forward flow of 10 μM FITC.

Water contact angle was measured for unmodified and photografted COC surfaces to confirm modification. The observed decrease in water contact angle on PEGDA photografted COC indicates an increase in the hydrophilicity of the COC surface (Table 4.2). Additionally, visual inspection confirmed the flow of aqueous buffer by capillary action in photografted channels.

Consistent forward sample flow was recorded in photografted devices by CCD imaging of fluorescence during electrokinetic injection of a fluorescent compound (Fig. 4.3B-D).

Table 4.2: Contact angle measurements

Material	Contact angle (mean ± std. dev.)*
COC	90.7˚ ± 1.5˚
PMMA	71.7˚ ± 2.1˚
3% PEGDA photografted COC	67.7˚ ± 1.5˚
5% PEGDA photografted COC	54.0˚ ± 2.6˚

*n=3

4.3.2 Monolith Characterization

The monolith pre-polymer mixture was previously characterized and consisted of monomer (C8), cross-linker (EDMA), porogen (cyclohexanol and 1-dodecanol), surfactant (Tween 20) and a photoinitiator (DMPA).[35, 49] C8 was chosen as the monomer because of its hydrophobic characteristics that can retain both proteins and peptides. For this study, a porogen-to-monomer ratio of 70:30 was used to ensure high surface area. Fig. 4.2C-D shows cross-sectional SEM images of a photografted channel without and with C8 monolith. The SEM shows that the monolith is well anchored to the PEGDA-photografted COC surface. Additionally, a magnified SEM image of bulk C8 monolith showed high porosity and round nodules of 200-500 nm diameter (Fig. 4.2E). In agreement with previous reports, these monoliths did not dislocate or move upon application of voltage during experiments.

4.3.3 Optimization of pH-mediated SPE

SPE was carried out on a monolithic support by altering the analyte charge, and hence hydrophilicity and electrophoretic mobility, using different pH solutions. Initially, pH 5 solution was used to enrich the sample on the reversed-phase monolith. The pH 5 buffer chosen for capturing P1 and ferritin is slightly above their native isoelectric points (~4.8; and fluorescence labeling moves the isoelectric point lower); at this pH these biomarkers have lower effective mobility and higher hydrophobicity, aiding in retention on the reversed-phase monoliths. Species with similar pI values and hydrophobicities would be similarly retained on these monoliths. Then, this sample was eluted from the monolith by switching to a higher pH buffer in which the analyte became more charged and hydrophilic. This pH-mediated SPE approach was fine-tuned using eluents with different pH and buffer concentrations.

4.3.3.1 Eluent pH

The effect of eluent pH from 7.0-11.5 was observed. The injection time (2 min) and buffer ionic concentration (50 mM) were kept constant. Experiments were carried out as described in section 4.2.6.1, and the elution profile of P1 (loaded at pH 5) was recorded for different pH eluents (Fig. 4.4A). Eluted peak heights and areas were determined for each pH eluent (Fig. 4.4B). Elution buffer at pH 10 showed the highest peak height and peak area for eluting P1 from C8 monoliths, so this pH eluent was chosen for subsequent experiments.

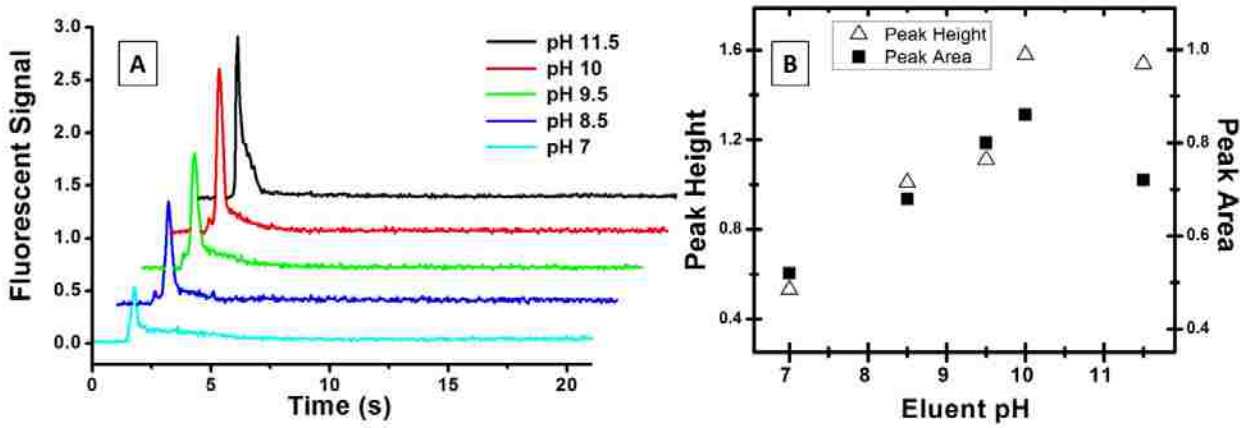

Figure 4.4 Effect of eluent pH on electroelution. (A) Elution of P1 (50 nM loaded concentration) from a C8 monolith with increasing eluent pH. Traces are offset vertically and horizontally. (B) Eluted peak height and area for different pH eluents.

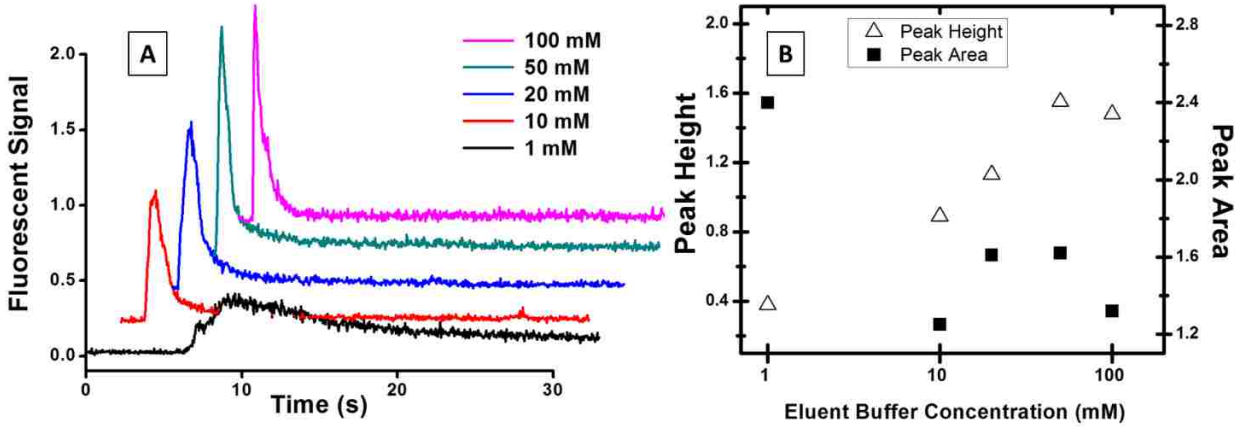

Figure 4.5 Effect of eluent buffer concentration. (A) Elution of P1 (50 nM loaded concentration) from a C8 monolith using different BCB eluent concentrations. Traces are offset vertically and horizontally. (B) Peak height and area for different eluting BCB concentrations.

4.3.3.2 Eluent Buffer Concentration

The effect of pH 10 BCB eluent concentration from 1 to 100 mM was also studied. Sample injection buffer and time were kept consistent from previous experiments. The elution profile for different buffers was recorded (Fig. 4.5A), and the peak height and area were plotted for different

buffer concentrations (Fig. 4.5B). Although 1 mM BCB showed the largest peak area, it also had the lowest eluted peak height. The low ionic strength of 1 mM buffer resulted in a broader plug of P1 due to slow elution. A narrowing of the eluted peak was observed with increasing concentration of eluent. Considering both peak height and area, 50 mM BCB showed the best efficiency for eluting P1 from C8 monoliths, so I used 50 mM BCB in subsequent experiments.

4.3.4 pH-mediated SPE of PTB Biomarkers

Fig. 4.6 shows the elution traces obtained after pH-mediated SPE of blank sample, two model dyes, and two PTB biomarkers (P1 and ferritin), on a C8 monolith under conditions optimized above. A blank run with no fluorescent sample showed only a small bump in the signal indicating a change in background fluorescence in changing from pH 5 to pH 10 buffer. 100 nM FITC showed a small peak and AF 488 showed a peak three times as tall as FITC at the same concentration after eluting from the C8 monolith. An even larger elution peak was observed when FITC-labeled P1 at half the concentration of the dyes was loaded and eluted from the C8 monolith. Ferritin had a lower eluted peak height than P1, but the loaded ferritin concentration was 50-fold lower than P1. Additionally, ferritin showed a broader eluted band than the other analytes. Fluorescent dyes also showed lower peak heights than P1 on the monolith owing both to their higher mobility, which results in elution during electrokinetic loading and rinsing steps, and lower hydrophobicity,[35, 50-51] which makes them less retained on the monolith. Ferritin, being the most hydrophobic, showed the greatest retention. This experiment, done with 1 nM loaded ferritin, indicates potential for enrichment at pM concentrations. The hydrophobic characteristics of ferritin are also responsible for its broader eluted band. This pH-mediated SPE extraction method allows low nM concentration analytes to be enriched and eluted.

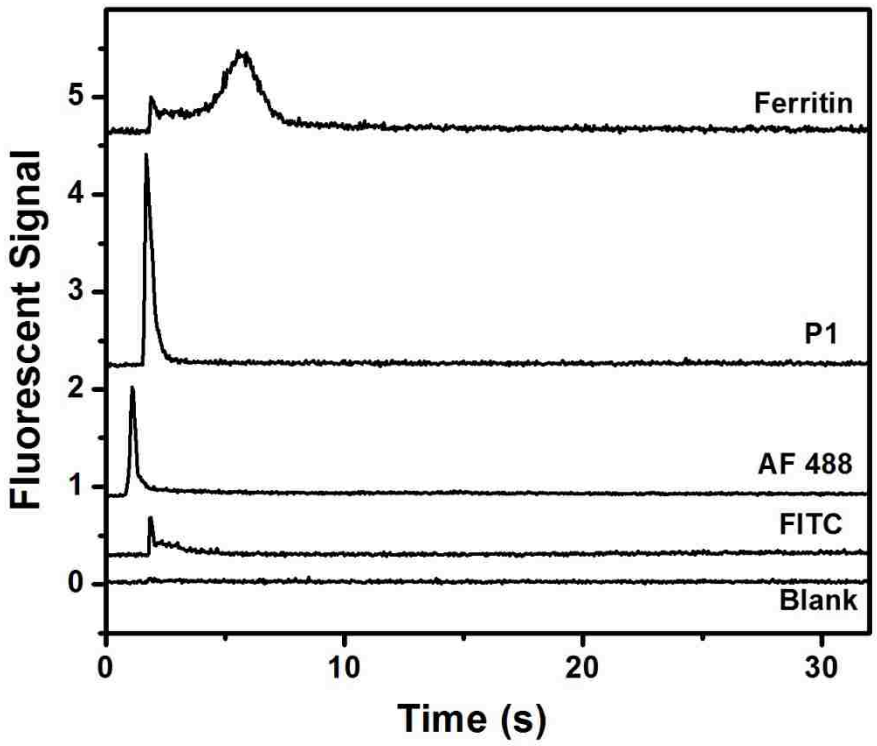

Figure 4.6 pH-mediated SPE of sample dyes and PTB biomarkers for 2 min loading times. Traces are offset vertically. Concentrations: ferritin (1 nM), P1 (50 nM), AF 488 (100 nM), and FITC (100 nM).

4.3.5 Effect of Analyte Concentration on pH-mediated Elution

Different concentrations of FITC-labeled P1 were loaded on a C8 monolith to determine the effect of analyte concentration on pH-mediated electroelution. Fig. 4.7A shows the elution profile from the monolith for different loaded concentrations (50-500 nM) of P1. A linear plot (Fig. 4.7B) was obtained for the peak heights as a function of loaded P1 concentration with an R^2 value of 0.997. The eluted peak migration time RSD for Fig. 4.7A data was determined to 3.9% (n=7). These results demonstrate the ability of pH-mediated SPE with electroelution to provide reproducible and quantitative results, similar to earlier μCE systems that reported quantification either by standard addition or calibration curve.[56]

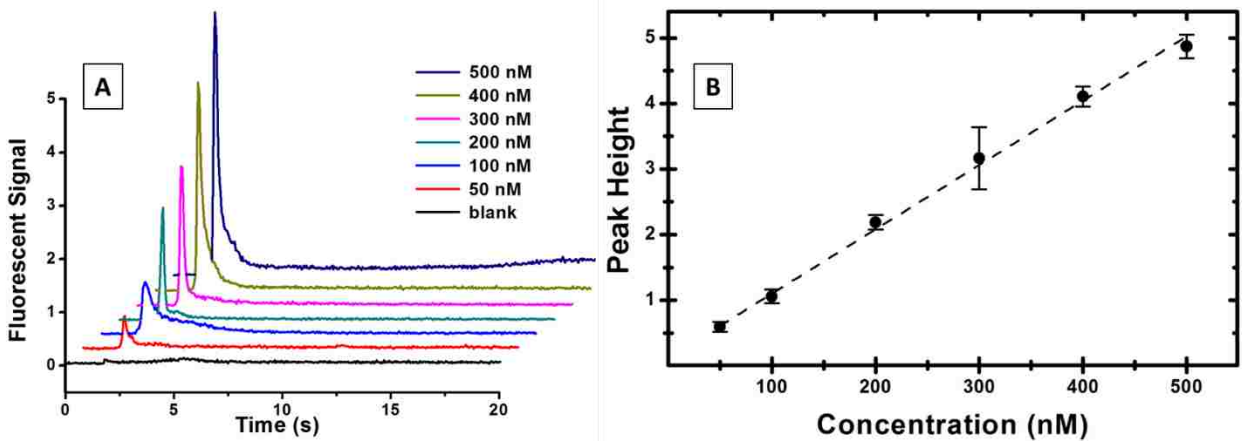

Figure 4.7 Effect of loaded P1 concentration on eluted peaks. (A) Elution from a C8 monolith of different concentrations of P1 loaded for 1 min. Traces are offset vertically and horizontally. (B) The peak height of eluted P1 plotted against concentration (n=3).

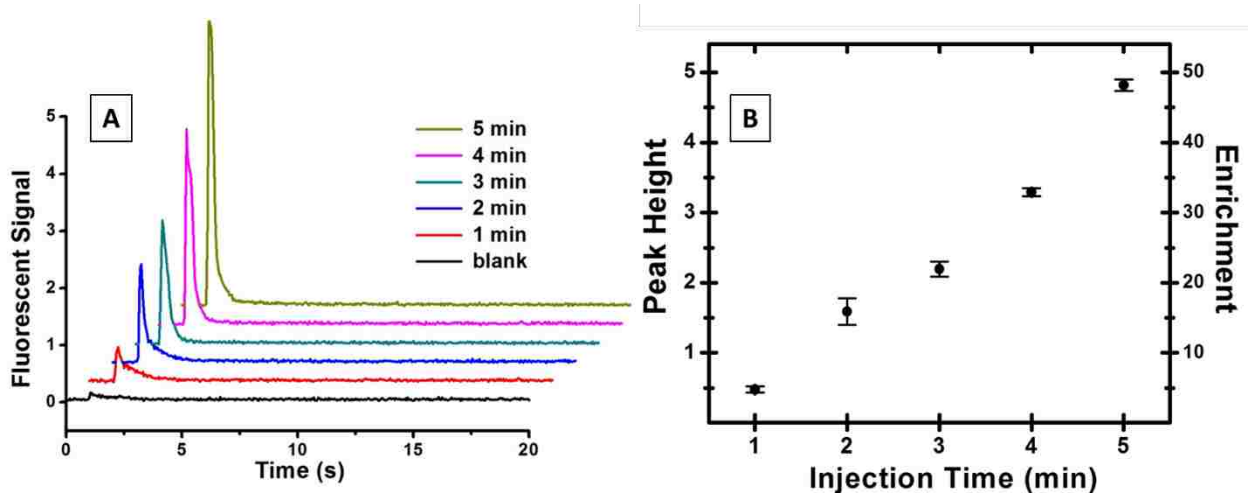

Figure 4.8 P1 (50 nM loaded) enrichment with injection time. (A) Elution profiles. (B) P1 enrichment and peak heights (n=3) with injection time.

4.3.6 Analyte Enrichment

Reversed-phase monoliths can be used for preconcentration of dilute analytes, especially with the use of increased loading time. To determine the analyte enrichment with pH-mediated SPE, 50 nM FITC-labeled P1 was loaded on a C8 monolith for 1-5 min, and elution profiles were recorded as shown in Fig. 4.8A. Peak heights in the elution traces increased with loading time. The peak

heights were used to calculate enrichment based on the average signal obtained from 50 nM P1 injected directly into the channel (see Fig. 4.9).

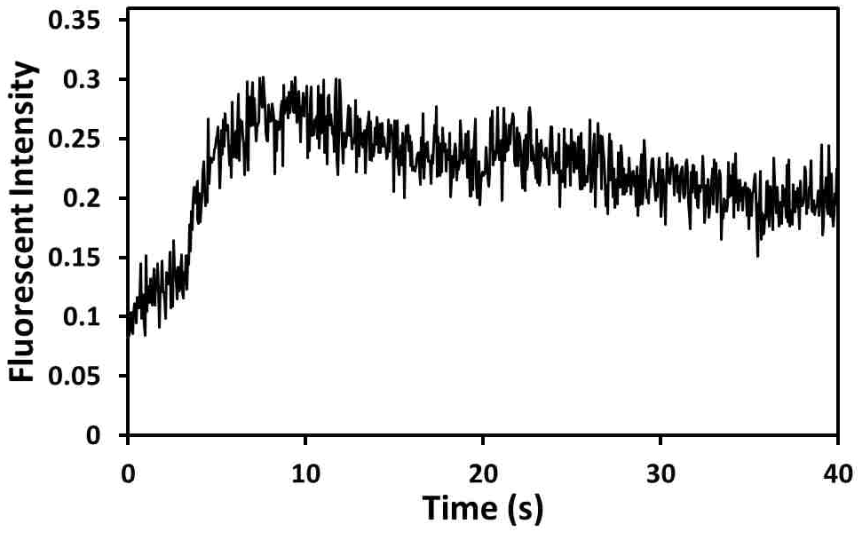

Figure 4.9 Signal from 50 nM P1 injected directly into a channel. The signal increase at 3.1 s marks the introduction of P1 in the channel. The average of the fluorescent signal (taken from 3.1 to 40 s) was found to be 0.21, which after subtracting the baseline signal of 0.11 (obtained from the first 3.0 seconds) yielded a background-subtracted signal of 0.10. This value was used to calculate P1 enrichment in Fig. 4.8B.

Fig 4.8B shows the average peak height and calculated enrichment factor for injection times from 1-5 min. An enrichment of nearly 50-fold was observed for 50 nM P1 with a 5 min injection time. The eluted peak migration time RSD for Fig. 4.8A results was calculated to 6.4% (n=6), indicative of good reproducibility of this approach. Increasing the sample injection time further could lead to even higher enrichment factors.

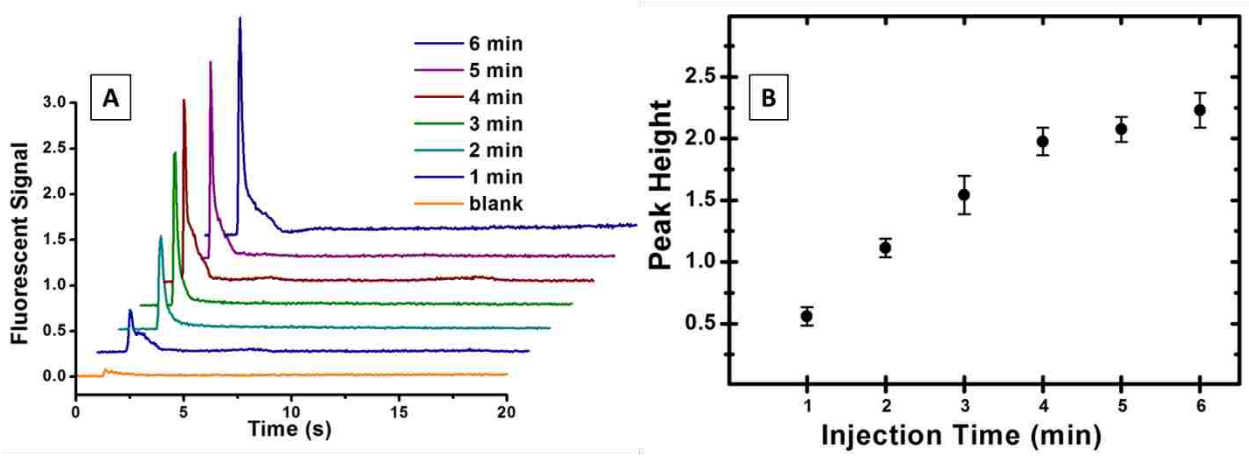

Figure 4.10 Monolith saturation. (A) Elution profiles for P1 (500 nM loaded) for increasing injection times. Traces are offset vertically and horizontally. (B) Peak heights of eluted P1 for increasing injection times (n=3).

4.3.7 Monolith Capacity

Monolith capacity is an important parameter to determine because it gives an estimate of the enrichment capabilities of the system. The monolith capacity was determined by injecting 500 nM FITC-labeled P1 on the C8 monolith for different times and monitoring elution as seen in Fig. 4.10A. A tenfold higher concentration of P1 was used than in Fig. 4.8 so saturation could be achieved more readily. Traces during elution for 1-6 min loading times (Fig. 4.10A) showed narrow peaks, with heights that increased with injection time through a certain range. Fig. 4.10B shows the eluted peak heights as a function of injection time. A plateau in the eluted peak height is seen starting at 4 min injection time, indicating monolith saturation. I adapted a photobleaching flow measurement method previously described by He et al.[57] to determine the migration velocity of P1 under these injection conditions (see Fig. 4.11). A dip in fluorescent signal due to photobleaching was detected at 5.5 s, indicating the time taken for the photobleached plug to migrate 5 mm. The migration velocity of P1 was thus 900 μm s^{-1}, which for 500 nM P1 loaded for 4 min corresponds to a monolith binding capacity of 400 pg or 0.2 pmol. The binding capacity

RSD is <15%, limited by the RSD of the monolith lengths, and consistent with the peak height variations in Fig. 4.10B. Although the binding capacity for P1 is less than 1 ng, for the low nL volumes used in microfluidics this capacity is sufficient for typical SPE experiments.

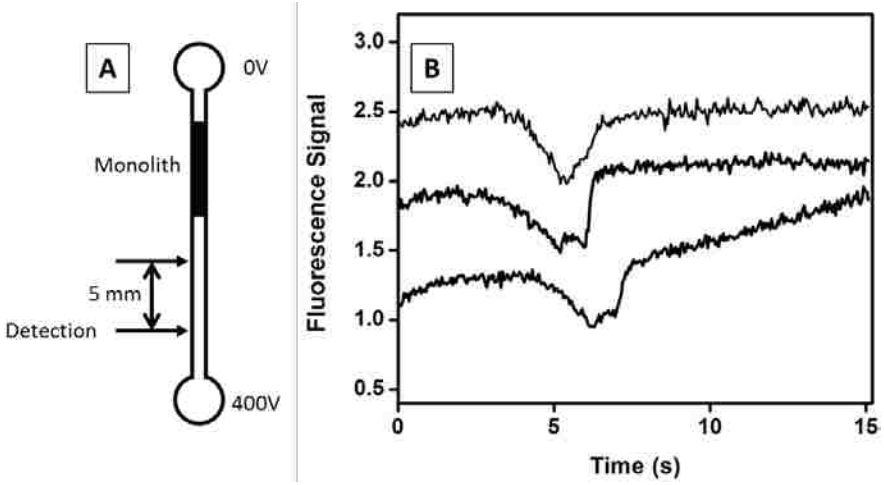

Figure 4.11 Migration velocity of 500 nM P1. (A) Device design and experimental setup to determine the migration velocity of P1. A plug of 500 nM P1 (buffered at pH 5) was injected and photobleached with the injection voltage off for 20 min by focusing the laser (using a 4× lens) at the desired point on the channel. After photobleaching, the detection point was moved 5 mm down the channel and the injection voltage was re-applied. (B) Fluorescence signal from 500 nM P1 shows a dip from photobleaching at an average time (n=3) of 5.5 s. Plots are offset vertically.

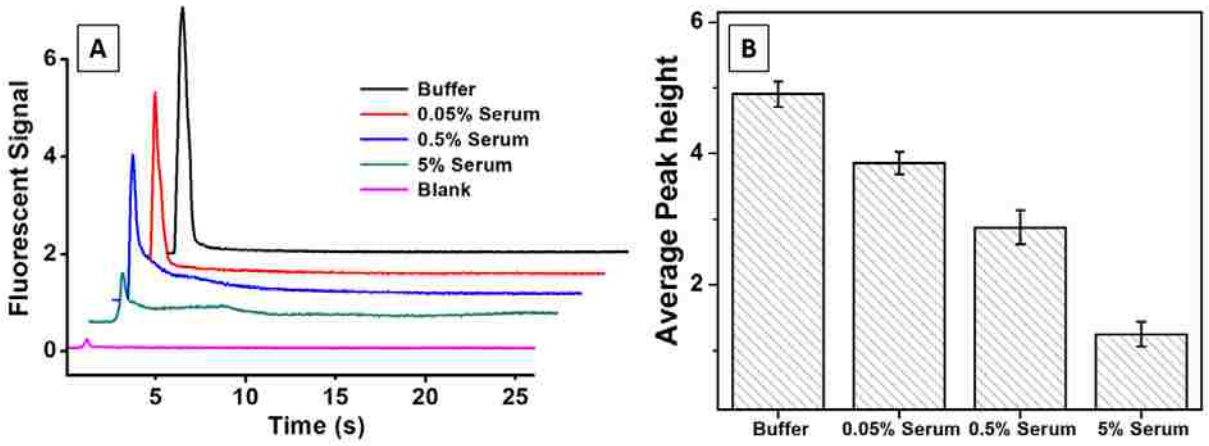

Figure 4.12 Effect of a serum matrix on P1 retention and elution. (A) Elution profiles of P1 (50 nM) loaded on a monolith in buffer and various human serum matrices. (B) Peak heights of eluted P1 for different matrices (n=3).

4.3.8 Effects of Blood Serum on P1 Binding Capacity

Sample matrix affects the retention and elution capabilities of this system. Fig. 4.12A shows the elution profile from these monoliths of 50 nM P1 loaded in buffer and diluted human serum (buffered at pH 5). Fig. 4.12B shows the eluted peak heights of P1 from the monoliths for each sample matrix. For P1 loaded from 0.05%, 0.5% and 5% serum, the eluted peak height was reduced by 20%, 45%, and 75%, respectively, compared to P1 loaded in buffer. This indicates a decrease in binding of P1 to the monolith due to serum components competing for retention. Additionally, more peak tailing was observed in Fig. 4.12A for samples loaded in a serum matrix because interfering components slowed the electroelution of P1 from the monolith. A similar effect was observed for the higher P1 concentrations in Fig. 4.10. Importantly, these results show that pH-mediated extraction and elution could be used to enrich target peptides from diluted serum samples.

4.3.9 Integrated SPE and µCE of a PTB Biomarker

Integration of SPE sample enrichment and µCE can enable automated analysis of low-concentration analytes. To demonstrate this potential, pH-mediated SPE was combined with µCE using the device design detailed in Fig 4.2F-H. Fig. 4.13A shows an electropherogram after extraction, pH-mediated electroelution, injection, and µCE of 50 nM P1 in buffer. As a comparison µCE of 50 nM P1 (unenriched and buffered at pH 9.5; injection time 1 min) run in a standard PMMA device[36, 58] with the same injection volume as these SPE-µCE device is also shown. A 10-fold increase in the peak area of enriched P1 was observed, with a small decrease in the number

of theoretical plates per meter (N/m) from 210,000 to ~140,000. Furthermore, a mixture of FITC-labeled P1 and FA in buffer was used for integrated SPE and μCE to demonstrate the separation ability of this device.

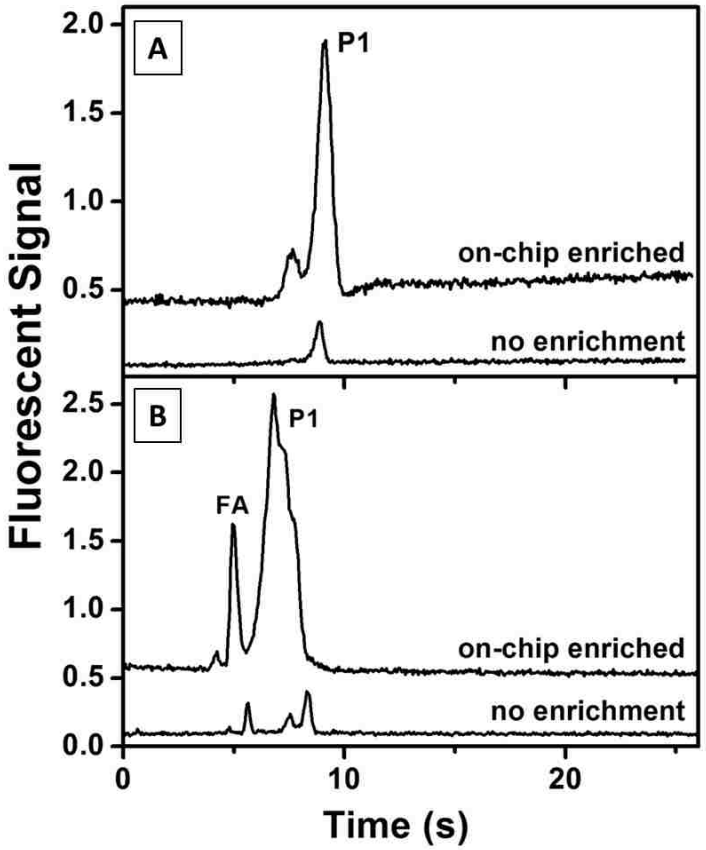

Figure 4.13 Integration of pH-mediated SPE with μCE. (A) Electropherogram of 50 nM P1 loaded with and without on-chip enrichment using a C8 monolith. (B) Electropherogram showing separation of FA and P1 (50 nM each loaded) with and without enrichment. Traces are offset vertically.

Fig. 4.13B shows the electropherogram of a mixture of P1 and FA extracted, eluted, injected, and separated on this device, along with the electropherogram of the same unenriched mixture. An 8.5- and 15-fold increase in peak areas was observed for FA and P1, respectively. Decreases in N/m from ~560,000 to ~140,000 and ~380,000 to ~25,000 were also observed for FA and P1, respectively. The decrease in N/m for P1 is due to a closely migrating impurity peak

that is no longer resolved in the enriched mixture. The enrichment for FA was lower than for P1 due to its higher electrophoretic mobility, which results in its partial elution during the rinsing step. Additionally, the enrichment factor for P1 was less than what was observed in electroelution, because during μCE only a part of the eluted plug is injected into the separation channel. From the 50 μm channel width and ~700 μm eluted plug length, I estimate that ~7% of the eluted plug was injected for μCE. The peptide enrichment reported in this study is comparable to what was recently reported in an integrated pressure-driven microfluidic platform.[50]

This integrated pH-mediated SPE-μCE method shows promising results for peptide enrichment and electrophoretic separation. N/m can be improved by further optimization of buffers and applied voltages. Higher enrichment factors can also be obtained by increasing the length of the monolith or injecting for longer times. Furthermore, this simple pH-mediated SPE approach can be extended for analysis of a wide range of analytes like PTB biomarkers.

4.4 REFERENCES

1. Hayes, J.; Peruzzi, P. P.; Lawler, S., MicroRNAs in cancer: biomarkers, functions and therapy. Trends Mol. Med. 2014, 20 (8), 460-469.

2. Zhou, L.; Wang, R.; Yao, C.; Li, X.; Wang, C.; Zhang, X.; Xu, C.; Zeng, A.; Zhao, D.; Zhang, F., Single-band upconversion nanoprobes for multiplexed simultaneous in situ molecular mapping of cancer biomarkers. Nat. Commun. 2015, 6, 6938.

3. Yotsukura, S.; Mamitsuka, H., Evaluation of serum-based cancer biomarkers: A brief review from a clinical and computational viewpoint. Crit. Rev. Oncol. Hemat. 2015, 93 (2), 103-115.

4. Pavo, N.; Raderer, M.; Hülsmann, M.; Neuhold, S.; Adlbrecht, C.; Strunk, G.; Goliasch, G.; Gisslinger, H.; Steger, G. G.; Hejna, M.; Köstler, W.; Zöchbauer-Müller, S.; Marosi, C.; Kornek, G.; Auerbach, L.; Schneider, S.; Parschalk, B.; Scheithauer, W.; Pirker, R.; Drach, J.; Zielinski, C.; Pacher, R., Cardiovascular biomarkers in patients with cancer and their association with all-cause mortality. Heart 2015, 101 (23), 1874-1880.

5. Manson, J. E.; Bassuk, S. S., Biomarkers of cardiovascular disease risk in women. Metabolism 2015, 64 (3, Supplement 1), S33-S39.

6. Jack Jr., C. R.; Bennett, D. A.; Blennow, K.; Carrillo, M. C.; Feldman, H. H.; Frisoni, G. B.; Hampel, H.; Jagust, W. J.; Johnson, K. A.; Knopman, D. S.; Petersen, R. C.; Scheltens, P.; Sperling, R. A.; Dubois, B., A/T/N: An unbiased descriptive classification scheme for Alzheimer disease biomarkers. Neurology 2016, 87 (5), 539-547.

7. Bateman, R. J.; Xiong, C.; Benzinger, T. L. S.; Fagan, A. M.; Goate, A.; Fox, N. C.; Marcus, D. S.; Cairns, N. J.; Xie, X.; Blazey, T. M.; Holtzman, D. M.; Santacruz, A.; Buckles, V.; Oliver, A.; Moulder, K.; Aisen, P. S.; Ghetti, B.; Klunk, W. E.; McDade, E.; Martins, R. N.; Masters, C. L.; Mayeux, R.; Ringman, J. M.; Rossor, M. N.; Schofield, P. R.; Sperling, R. A.; Salloway, S.; Morris, J. C., Clinical and Biomarker Changes in Dominantly Inherited Alzheimer's Disease. N. Engl. J. Med. 2012, 367 (9), 795-804.

8. Lewczuk, P.; Mroczko, B.; Fagan, A.; Kornhuber, J., Biomarkers of Alzheimer's disease and mild cognitive impairment: A current perspective. Adv. Med. Sci. 2015, 60 (1), 76-82.

9. Mussap, M.; Noto, A.; Cibecchini, F.; Fanos, V., The importance of biomarkers in neonatology. Semin. Fetal Neonatal Med. 2013, 18 (1), 56-64.

10. Ruggeri, B.; Sarkans, U.; Schumann, G.; Persico, A. M., Biomarkers in autism spectrum disorder: the old and the new. Psychopharmacology 2014, 231 (6), 1201-1216.

11. Ross, C. A.; Aylward, E. H.; Wild, E. J.; Langbehn, D. R.; Long, J. D.; Warner, J. H.; Scahill, R. I.; Leavitt, B. R.; Stout, J. C.; Paulsen, J. S.; Reilmann, R.; Unschuld, P. G.; Wexler, A.; Margolls, R. L.; Tabrizi, S. J., Huntington disease: natural history, biomarkers and prospects for therapeutics. Nat. Rev. Neurol. 2014, 10 (4), 204.

12. Carinelli, S.; Martí, M.; Alegret, S.; Pividori, M. I., Biomarker detection of global infectious diseases based on magnetic particles. New Biotechnol. 2015, 32 (5), 521-532.

13. Punyadee, N.; Mairiang, D.; Thiemmeca, S.; Komoltri, C.; Pan-ngum, W.; Chomanee, N.; Charngkaew, K.; Tangthawornchaikul, N.; Limpitikul, W.; Vasanawathana, S.; Malasit, P.; Avirutnan, P., Microparticles Provide a Novel Biomarker To Predict Severe Clinical Outcomes of Dengue Virus Infection. J. Virol. 2015, 89 (3), 1587-1607.

14. Nge, P. N.; Rogers, C. I.; Woolley, A. T., Advances in Microfluidic Materials, Functions, Integration, and Applications. Chem. Rev. 2013, 113 (4), 2550-2583.

15. Araci, I. E.; Brisk, P., Recent developments in microfluidic large scale integration. Curr. Opin. Biotechnol. 2014, 25, 60-68.

16. Kim, H. J.; Park, J. W.; Park, J. W.; Byun, J. H.; Vahidi, B.; Rhee, S. W.; Jeon, N. L., Integrated Microfluidics Platforms for Investigating Injury and Regeneration of CNS Axons. Ann. Biomed. Eng. 2012, 40 (6), 1268-1276.

17. Zhang, H.; Liu, L.; Fu, X.; Zhu, Z., Microfluidic beads-based immunosensor for sensitive detection of cancer biomarker proteins using multienzyme-nanoparticle amplification and quantum dotslabels. Biosens. Bioelectron. 2013, 42, 23-30.

18. Nahavandi, S.; Baratchi, S.; Soffe, R.; Tang, S.-Y.; Nahavandi, S.; Mitchell, A.; Khoshmanesh, K., Microfluidic platforms for biomarker analysis. Lab Chip 2014, 14 (9), 1496-1514.

19. Pagaduan, J. V.; Sahore, V.; Woolley, A. T., Applications of microfluidics and microchip electrophoresis for potential clinical biomarker analysis. Anal. Bioanal. Chem. 2015, 407 (23), 6911-6922.

20. Long, Z.; Shen, Z.; Wu, D.; Qin, J.; Lin, B., Integrated multilayer microfluidic device with a nanoporous membrane interconnect for online coupling of solid-phase extraction to microchip electrophoresis. Lab Chip 2007, 7 (12), 1819-1824.

21. Kang, Q.-S.; Li, Y.; Xu, J.-Q.; Su, L.-J.; Li, Y.-T.; Huang, W.-H., Polymer monolith-integrated multilayer poly(dimethylsiloxane) microchip for online microextraction and capillary electrophoresis. Electrophoresis 2010, 31 (18), 3028-3034.

22. Ramsey, J. D.; Collins, G. E., Integrated Microfluidic Device for Solid-Phase Extraction Coupled to Micellar Electrokinetic Chromatography Separation. Anal. Chem. 2005, 77 (20), 6664-6670.

23. Esplin, M. S.; Merrell, K.; Goldenberg, R.; Lai, Y.; Iams, J. D.; Mercer, B.; Spong, C. Y.; Miodovnik, M.; Simhan, H. N.; van Dorsten, P.; Dombrowski, M., Proteomic identification of serum peptides predicting subsequent spontaneous preterm birth. Am. J. Obstet. Gynecol. 2011, 204 (5), 391.e1-391.e8.

24. Graves, S. W.; Esplin, M. S., 80: Validation of predictive preterm birth biomarkers obtained by maternal serum proteomics. Am. J. Obstet. Gynecol. 2011, 204 (1), S46.

25. Goldenberg, R. L.; Culhane, J. F.; Iams, J. D.; Romero, R., Epidemiology and causes of preterm birth. Lancet 2008, 371 (9606), 75-84.

26. Romero, R.; Dey, S. K.; Fisher, S. J., Preterm labor: One syndrome, many causes. Science 2014, 345 (6198), 760-765.

27. Goldenberg, R. L.; Goepfert, A. R.; Ramsey, P. S., Biochemical markers for the prediction of preterm birth. Am. J. Obstet. Gynecol. 2005, 192 (5), S36-S46.

28. Goldenberg, R. L.; Iams, J. D.; Mercer, B. M.; Meis, P. J.; Moawad, A.; Das, A.; Miodovnik, M.; VanDorsten, P. J.; Caritis, S. N.; Thurnau, G.; Dombrowski, M. P., The Preterm Prediction Study: Toward a multiple-marker test for spontaneous preterm birth. Am. J. Obstet. Gynecol. 2001, 185 (3), 643-651.

29. Augusto, F.; Hantao, L. W.; Mogollón, N. G. S.; Braga, S. C. G. N., New materials and trends in sorbents for solid-phase extraction. TrAC Trends Anal. Chem. 2013, 43, 14-23.

30. Duan, Y.-P.; Dai, C.-M.; Zhang, Y.-L.; Ling, C., Selective trace enrichment of acidic pharmaceuticals in real water and sediment samples based on solid-phase extraction using multi-templates molecularly imprinted polymers. Anal. Chim. Acta 2013, 758, 93-100.

31. Majors, R. E., Solid-Phase Extraction. In Handbook of Sample Preparation, John Wiley & Sons, Inc., Hoboken, NJ, USA: 2010; pp 53-79.

32. Malmstadt, N.; Yager, P.; Hoffman, A. S.; Stayton, P. S., A Smart Microfluidic Affinity Chromatography Matrix Composed of Poly(N-isopropylacrylamide)-Coated Beads. Anal. Chem. 2003, 75 (13), 2943-2949.

33. Yu, C.; Davey, M. H.; Svec, F.; Fréchet, J. M. J., Monolithic Porous Polymer for On-Chip Solid-Phase Extraction and Preconcentration Prepared by Photoinitiated in Situ Polymerization within a Microfluidic Device. Anal. Chem. 2001, 73 (21), 5088-5096.

34. Aggarwal, P.; Tolley, H. D.; Lee, M. L., Monolithic bed structure for capillary liquid chromatography. J. Chromatogr. A 2012, 1219, 1-14.

35. Yang, R.; Pagaduan, J. V.; Yu, M.; Woolley, A. T., On chip preconcentration and fluorescence labeling of model proteins by use of monolithic columns: device fabrication, optimization, and automation. Anal. Bioanal. Chem. 2015, 407 (3), 737-747.

36. Yang, W.; Sun, X.; Pan, T.; Woolley, A. T., Affinity monolith preconcentrators for polymer microchip capillary electrophoresis. Electrophoresis 2008, 29 (16), 3429-3435.

37. Oleschuk, R. D.; Shultz-Lockyear, L. L.; Ning, Y.; Harrison, D. J., Trapping of Bead-Based Reagents within Microfluidic Systems: On-Chip Solid-Phase Extraction and Electrochromatography. Anal. Chem. 2000, 72 (3), 585-590.

38. Vázquez, M.; Paull, B., Review on recent and advanced applications of monoliths and related porous polymer gels in micro-fluidic devices. Anal. Chim. Acta 2010, 668 (2), 100-113.

39. Knob, R.; Sahore, V.; Sonker, M.; Woolley, A. T., Advances in monoliths and related porous materials for microfluidics. Biomicrofluidics 2016, 10 (3), 032901.

40. Stachowiak, T. B.; Rohr, T.; Hilder, E. F.; Peterson, D. S.; Yi, M.; Svec, F.; Fréchet, J. M. J., Fabrication of porous polymer monoliths covalently attached to the walls of channels in plastic microdevices. Electrophoresis 2003, 24 (21), 3689-3693.

41. Liu, K.; Aggarwal, P.; Lawson, J. S.; Tolley, H. D.; Lee, M. L., Organic monoliths for high-performance reversed-phase liquid chromatography. J. Sep. Sci. 2013, 36 (17), 2767-2781.

42. Pruim, P.; Öhman, M.; Schoenmakers, P. J.; Kok, W. T., Methacrylate monolithic stationary phases for gradient elution separations in microfluidic devices. J. Chromatogr. A 2011, 1218 (31), 5292-5297.

43. Ladner, Y.; Crétier, G.; Faure, K., Electrochromatography in cyclic olefin copolymer microchips: A step towards field portable analysis. J. Chromatogr. A 2010, 1217 (51), 8001-8008.

44. Nordman, N.; Barrios-Lopez, B.; Laurén, S.; Suvanto, P.; Kotiaho, T.; Franssila, S.; Kostiainen, R.; Sikanen, T., Shape-anchored porous polymer monoliths for integrated online solid-phase extraction-microchip electrophoresis-electrospray ionization mass spectrometry. Electrophoresis 2015, 36 (3), 428-432.

45. Britz-McKibbin, P.; Bebault, G. M.; Chen, D. D. Y., Velocity-Difference Induced Focusing of Nucleotides in Capillary Electrophoresis with a Dynamic pH Junction. Anal. Chem. 2000, 72 (8), 1729-1735.

46. Britz-McKibbin, P.; Chen, D. D. Y., Selective Focusing of Catecholamines and Weakly Acidic Compounds by Capillary Electrophoresis Using a Dynamic pH Junction. Anal. Chem. 2000, 72 (6), 1242-1252.

47. Baidoo, E. E. K.; Benke, P. I.; Neusüss, C.; Pelzing, M.; Kruppa, G.; Leary, J. A.; Keasling, J. D., Capillary Electrophoresis-Fourier Transform Ion Cyclotron Resonance Mass Spectrometry for the Identification of Cationic Metabolites via a pH-Mediated Stacking-Transient Isotachophoretic Method. Analytical Chemistry 2008, 80 (9), 3112-3122.

48. Imami, K.; Monton, M. R. N.; Ishihama, Y.; Terabe, S., Simple on-line sample preconcentration technique for peptides based on dynamic pH junction in capillary electrophoresis–mass spectrometry. J. Chromatogr. A 2007, 1148 (2), 250-255.

49. Nge, P. N.; Pagaduan, J. V.; Yu, M.; Woolley, A. T., Microfluidic chips with reversed-phase monoliths for solid phase extraction and on-chip labeling. J. Chromatogr. A 2012, 1261, 129-135.

50. Kumar, S.; Sahore, V.; Rogers, C. I.; Woolley, A. T., Development of an integrated microfluidic solid-phase extraction and electrophoresis device. Analyst 2016, 141 (5), 1660-1668.

51. Sonker, M.; Yang, R.; Sahore, V.; Kumar, S.; Woolley, A. T., On-chip fluorescent labeling using reversed-phase monoliths and microchip electrophoretic separations of selected preterm birth biomarkers. Anal. Methods 2016, 8 (43), 7739-7746.

52. Sahore, V.; Kumar, S.; Rogers, C. I.; Jensen, J. K.; Sonker, M.; Woolley, A. T., Pressure-actuated microfluidic devices for electrophoretic separation of pre-term birth biomarkers. Anal. Bioanal. Chem. 2016, 408 (2), 599-607.

53. Kelly, R. T.; Woolley, A. T., Thermal Bonding of Polymeric Capillary Electrophoresis Microdevices in Water. Anal. Chem. 2003, 75 (8), 1941-1945.

54. Ladner, Y.; Bruchet, A.; Crétier, G.; Dugas, V.; Randon, J.; Faure, K., New “one-step” method for the simultaneous synthesis and anchoring of organic monolith inside COC microchip channels. Lab Chip 2012, 12 (9), 1680-1685.

55. Rogers, C. I.; Pagaduan, J. V.; Nordin, G. P.; Woolley, A. T., Single-Monomer Formulation of Polymerized Polyethylene Glycol Diacrylate as a Nonadsorptive Material for Microfluidics. Anal. Chem. 2011, 83 (16), 6418-6425.

56. Yang, W.; Sun, X.; Wang, H.-Y.; Woolley, A. T., Integrated microfluidic device for serum biomarker quantitation using either standard addition or a calibration curve. Anal. Chem. 2009, 81 (19), 8230-8235.

57. He, M.; Bao, J.-B.; Zeng, Y.; Harrison, D. J., Parameters governing reproducibility of flow properties of porous monoliths photopatterned within microfluidic channels. Electrophoresis 2010, 31 (14), 2422-2428.

58. Pagaduan, J. V.; Ramsden, M.; O'Neill, K.; Woolley, A. T., Microchip immunoaffinity electrophoresis of antibody–thymidine kinase 1 complex. Electrophoresis 2015, 36 (5), 813-817.

5. MICROFLUIDIC DEVICES FOR INTEGRATED IMMUNOAFFINITY MONOLITH EXTRACTION AND ELECTROPHORETIC SEPARATION OF PRETERM BIRTH BIOMARKERS

5.1 INTRODUCTION

Microfluidic devices have garnered immense interest for disease diagnosis due to advantages like small sample requirements, low cost, portability, and rapid analysis.[1-5] Microfluidic platforms have been reported recently for detection of biomarkers or molecular indicators of cancers,[6-7] diabetes,[8] cardiac disorders,[9] Alzheimer's[10] and infectious[11-12] diseases. These biomarkers are typically present in complex biological matrices like blood, cerebrospinal fluid or urine, which often require complicated off-chip sample preparation steps prior to analysis.[7-8, 10-12] These processes are a major limitation in automated sample-to-answer microfluidic analysis; thus, numerous microfluidic platforms are being developed that can perform sample preparation processes on-chip, like blood cell/plasma separation,[13] preconcentration,[14-15] and fluorescent labeling[16-17] in an integrated fashion.[6, 10, 18-19]

Preterm birth (PTB), birth prior to 37 weeks of gestation, is the most common complication in pregnancy and the leading cause of neonatal deaths and newborn illnesses.[20-22] Recently, an expanded biomarker panel was identified that can predict a subsequent PTB with 87% sensitivity and 81% specificity.[23-24] Thus, a platform for early detection of PTB risk could offer a substantial medical benefit in preventing preterm births. Woolley's group have previously developed microfluidic devices for various on-chip sample preparation and analytical processes for PTB biomarkers, including electrophoretic separation,[25] combined preconcentration with electrophoretic separation,[14, 26] and on-chip fluorescent labeling[27] integrated with microchip electrophoresis (μCE).[28] Here, I have developed an electrokinetically operated immunoaffinity

monolith microfluidic device integrated with μCE for the extraction and separation of selected PTB biomarkers in a human serum matrix.

Porous polymer monoliths are often used in microfluidic systems as a chromatographic material due to their high surface area, low backpressure and ease of fabrication. Affinity monoliths are especially promising for solid-phase extraction applications in microfluidics.[5, 29] Liu et al.[30] developed a voltage-driven glass microfluidic device with a carbohydrate-modified affinity monolith to study the interaction between polysaccharides and granulocyte colony-stimulating factor. Kang et al.[31] used affinity monoliths made from glycidyl methacrylate (GMA) to carry out microfluidic immunoassays for H1N1 influenza virus. Low nanomolar to micromolar concentrations of target analyte were extracted and detected using these affinity devices; however, these affinity extraction reports could be improved by developing a multiplexed approach for capture of target analytes, and by working directly with biologically relevant sample matrices like blood or urine. Yang et al.[32-33] previously developed an immunoaffinity channel wall coating using GMA copolymerized with polyethylene glycol diacrylate (PEGDA) in poly(methyl methacrylate) (PMMA) microchips. Using these affinity devices, automated extraction, separation, and quantification of low nanomolar concentrations of multiple cancer biomarkers was reported in human serum, but the biomarker panel was not designed for diagnostic potential. Additionally, the PMMA device material had poor compatibility towards organic solvents, which limited the ability to form and optimize monoliths. Finally, the wall-coated affinity column had limited binding capacity and was less effective for analyte capture compared to what could be achieved with a monolith polymerized across the full channel cross-section.

In this work, I improved over these major limitations of prior work with three key advances. First, I developed cyclic olefin copolymer (COC) devices which offer greater solvent

compatibility than PMMA. Second, with this solvent compatibility I developed new affinity monoliths with low enough backpressure for filling via capillary action such that they could be polymerized within the full channel volume instead of only using a wall coating. Third, these high surface area monoliths were used to immobilize antibodies (Abs) specific to biomarkers correlated with preterm birth to develop a targeted diagnostic application. I also tested two different elution strategies for immunoaffinity extraction optimization. This immunoaffinity extraction system was further integrated with μCE for the combined extraction and separation of two PTB biomarkers in a human serum matrix in <30 min analysis time. This work is a promising step towards an integrated microfluidic platform for the analysis of PTB biomarkers, which could be used for determining risk for a subsequent preterm birth.

5.2 EXPERIMENTAL SECTION

5.2.1 Materials and Reagents

Four-inch-diameter silicon wafers (single-side polished) were purchased from Desert Silicon (Tempe, AZ). PMMA sheets (1-mm and 3-mm thick) were from Evonik (Parsippany, NJ). Zeonor 1060R (6”×6”×1 mm and 6”×4”×2 mm) COC plates were purchased from Zeon Chemicals (Louisville, KY). GMA, ethylene glycol dimethacrylate (EGDMA), PEGDA (M_w 575), benzoin methyl ether (BME), 2,2-dimethoxy-2-phenylacetophenone (DMPA), 1-dodecanol, sodium tetraborate decahydrate, and dimethyl sulfoxide (DMSO) were from Sigma-Aldrich (St. Louis, MO). Tween 20 and sodium hydroxide were purchased from Mallinckrodt Baker (Paris, KY). Cyclohexanol was from J. T. Baker (Phillipsburg, NJ). Tris base, isopropyl alcohol (IPA), and acetonitrile were from Fisher Scientific (Fair Lawn, NJ). Cyclohexane and methanol were bought

from Macron (Center Valley, PA). Anhydrous sodium carbonate, sodium bicarbonate, citric acid, sodium citrate, sodium phosphate monohydrate, anhydrous sodium phosphate, and boric acid were obtained from Merck (Darmstadt, Germany). Sodium chloride was obtained from Columbus Chemicals (Columbus, WI).

All buffers used in sample preparation and experiments were prepared using deionized water (18.3 MΩ) from a Barnstead EASYpure UV/UF system (Dubuque, IA) and further filtered with 0.45 μm syringe filters (Thermo Scientific Nalgene, Waltham, MA). Ferritin (Fer) was purchased from EMD Millipore (Billerica, MA) and Sigma (St. Louis, MO). Lactoferrin (LF), anti-lactoferrin (anti-LF, produced in rabbit), and anti-ferritin (anti-Fer, produced in rabbit) were purchased from Sigma. Nitrocellulose paper and labeled secondary antibody (IRDye 800CW goat anti-rabbit IgG) were obtained from LI-COR, Inc. (Lincoln, NE). Tris hydrochloride, fluorescein isothiocyanate (FITC), and Alexa Fluor 488 TFP ester (AF 488) came from Life Technologies (Carlsbad, CA). Residual, de-identified human blood serum was provided by Prof. William Pitt at Brigham Young University.

5.2.2 Device Design and Fabrication

First, the device designs were transferred to silicon wafers at the Integrated Microfabrication Laboratory at Brigham Young University using standard photolithography and etching techniques described previously.[34-35] PMMA and COC devices were fabricated from these silicon templates following hot embossing and thermal bonding protocols reported previously.[16, 27] Briefly, the patterns from silicon templates were transferred to 1-mm thick PMMA and COC sheets by hot embossing at 138 ˚C for 27 min. Holes for reservoirs were drilled into 2-mm-thick COC plates

using a 2-mm-diameter bit with a drill press (Cameron, Sonora, CA). For PMMA, holes were cut into 2-mm-thick sheets using a laser cutter (VLS 2.30 Versa Laser, Universal Laser Systems, Scottsdale, AZ). These plates were then thermally bonded to 1-mm-thick sheets for 25 min at 110 ˚C. Devices were further sealed by applying acetonitrile (PMMA) or cyclohexane (COC) around the edges. Two different device designs were used for these experiments; straight channels for optimization of immunoaffinity extraction (Figure 5.1A) and a "T" shaped layout for integrated immunoaffinity extraction and μCE (Figure 5.1B). A photograph of these devices is shown in Figure 5.1C.

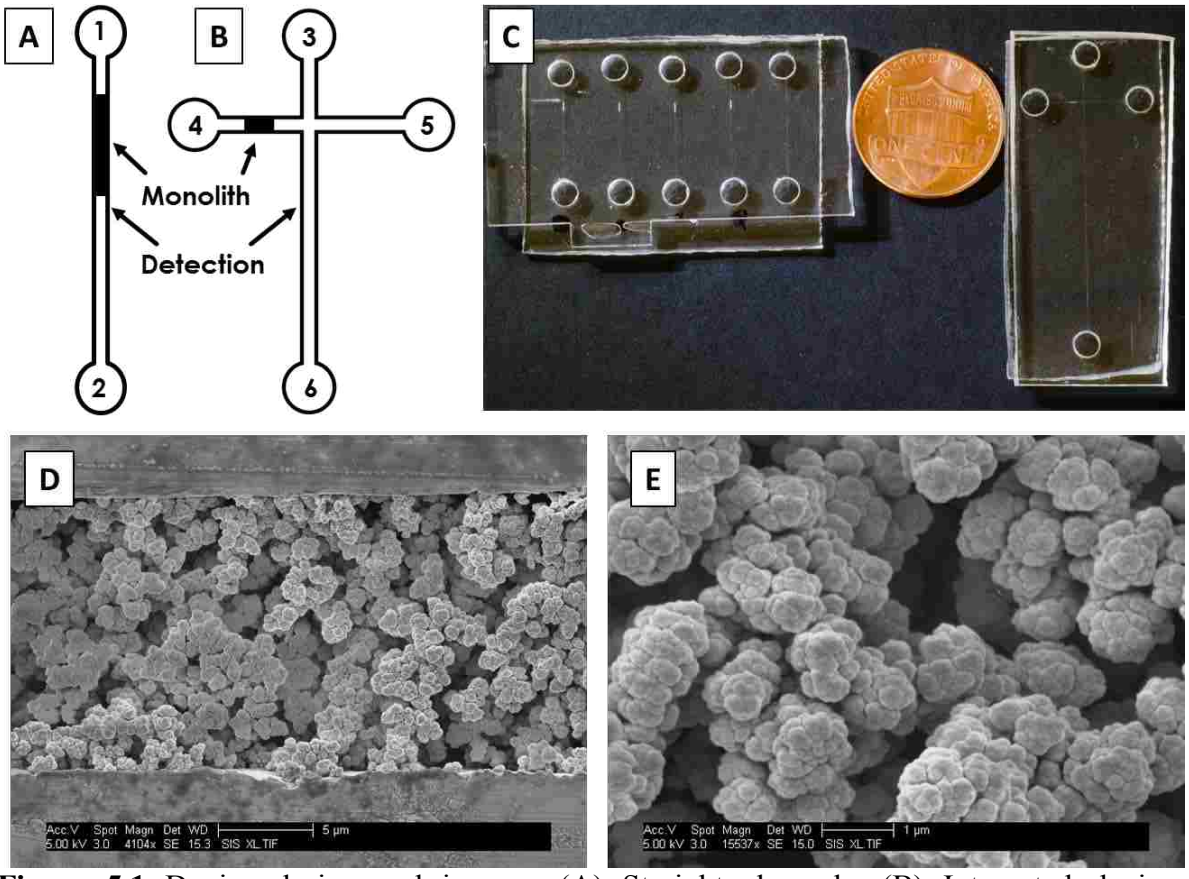

Figure 5.1 Device design and images. (A) Straight channels. (B) Integrated device. (C) Photographs of straight channel (left) and integrated devices (right). (D) SEM of a channel cross-section with GMA-EGDMA monolith polymerized inside. (E) Zoomed SEM image of the monolith.

5.2.3 Monolith Fabrication

A GMA-EGDMA monolith was polymerized in the microfluidic channels. For COC devices, a photografting step with PEGDA was done prior to monolith polymerization as described previously.[26, 36] The pre-polymer mixture was prepared using the following recipe: reactive monomer (GMA, 20%), crosslinker (EGDMA, 10%), porogen (cyclohexanol and 1-dodecanol, each 25%), and surfactant (Tween 20, 20%). This polymer mixture was sonicated for 10 min until a uniform solution was obtained; then, photoinitiator (DMPA, 1%) was added and the mixture was further sonicated for 10 min. This sonicated solution was transferred to device reservoirs and allowed to flow through channels by capillary action. A Cr mask with a 0.6-mm-wide opening was used to expose the desired part of the channel for polymerization of the monolith. UV exposure (~100 mW cm^2) was carried out for 11 min using a SunRay 600 UV lamp (Uvitron International, West Springfield, MA). After exposure, the unpolymerized solution was flushed from the channels using IPA and a vacuum pump, after which the monolith was stored dry.

For scanning electron microscopy (SEM) images, devices were cut into small pieces around the monoliths with an industrial bandsaw. These pieces were then glued to glass stubs using epoxy, and cross sections of the channels were microtomed with a glass knife. These pieces were placed on aluminum stubs using carbon tape and coated with ~15 nm Au-Pd (60:40) using a Q150T ES Sputterer (Quorum Technologies, Lewes, East Sussex, UK) to reduce charging during imaging. SEM images were taken using a Philips XL30 ESEM FEG instrument (Hillsboro, OR) in high vacuum mode at 5 kV electron beam potential.

5.2.4 Antibody Characterization and Immobilization

The Abs were evaluated in a dot blot test to determine their specificity for and compatibility with their respective analytes. First, 10 µL of analyte solution was dotted on nitrocellulose paper (see the Figure 5.2 caption for the amount of protein). After drying the dot, a blocking step was performed using 5% milk in 10× Tris buffer saline (TBS) for 1 h to block other sites. Then, the paper was washed thoroughly using TBS plus 0.1% Tween 20 (TBST) for 15 min. Next, 2 mL of 10 µg/mL antibody solution was added to the nitrocellulose paper, which was sealed in a plastic bag and left overnight for incubation on an electric rotor at 4 ˚C. Then, the paper was washed again using TBST for 15 min, and 2 mL of 1 µg/mL secondary antibody was added to it and incubated for 1 h. Then, the paper was washed again with TBST for 15 min. Finally, scans of dot blots were taken using a LI-COR ODYSSEY imaging system (Lincoln, NE).

Abs were immobilized on the monolith using the epoxy groups present on the reactive monomer, GMA, as described previously.[32-33, 37-38] A solution of Ab (5 µL, 2 mg/mL) was added to the reservoir and flowed through the monolith by capillary action. After adding the Ab, the reservoirs were filled with 20 mM borate buffer (pH 8) and sealed using tape to prevent evaporation. Devices were left overnight at room temperature to provide ample time for the primary amines on the Ab to react with epoxy groups on the GMA monolith. Next, the remaining epoxy groups were blocked by flowing 0.1 M Tris buffer (pH 8.5) through the monoliths for 1 h. After blocking, the monoliths were thoroughly washed with 20 mM phosphate buffer (pH 7.2). Control experiments were carried out by blocking the whole monolith with Tris buffer without immobilizing any Ab.

5.2.5 Fluorescent Labeling

PTB biomarkers, serum, and Abs were fluorescently labeled off-chip using FITC and AF 488. Briefly, 10 mM FITC and 6 mM AF 488 solutions were prepared in DMSO. Unlabeled analyte solutions were prepared in 0.1 M bicarbonate buffer (BCB, pH 9.5). For anti-Fer labeling, 5 µL of 10 mM FITC was added to 50 µL of anti-Fer (2 mg/mL). For Fer and LF labeling, 5 µL of AF 488 solution was added to 50 µL of Fer (1 mg/mL) and LF (2 mg/mL) solutions. These solutions were left overnight at room temperature on an electric shaker (VWR, Radnor, PA) to facilitate mixing. Unreacted FITC or AF 488 was removed from these solutions using 10 kDa cut-off Amicon ultra 0.5 mL centrifugal filters (EMD Millipore). The concentrations of filtered, labeled analytes were determined with a Nanodrop ND-1000 spectrophotometer (Wilmington, DE). For labeling of spiked human serum, 50 µL of serum were mixed with 50 µL of 0.1 M BCB and 5 µL each of unlabeled Fer (10 µM) and LF (20 µM). Then, 10 µL of 6 mM AF 488 in DMSO was added to this mixture, which was left overnight on an electric shaker at room temperature. Unattached AF 488 was not filtered from labeled serum samples to avoid removal of low molecular weight labeled components; after labeling, the serum samples were further diluted ten-fold in 20 mM phosphate buffer (pH 7.2). Other fluorescently labeled samples were also diluted in 20 mM phosphate buffer (pH 7.2) to the desired concentration prior to experiments.

5.2.6 Data Analysis

The laser induced fluorescence setup used for these experiments has been described in section 2.2.3. Eluted peak heights and areas were determined by OriginPro software (OriginLab

Corporation, Northampton, MA). A 5 point boxcar average was used to remove high frequency noise in some electropherograms.

5.2.7 Device Operation

5.2.7.1 Immunoaffinity Extraction

For optimization of immunoaffinity extraction the straight channel design in Figure 5.1A was used. First, the monoliths were thoroughly rinsed with 20 mM phosphate buffer (pH 7.2) flowed using vacuum to make sure no bubbles that could interfere with flow were present. Next, monoliths were electrokinetically rinsed for 2 min by placing electrodes in the reservoirs and applying +300 V to reservoir 2 while keeping reservoir 1 grounded. This step ensured the distribution of pH 7.2 buffer throughout the channel and filled residual air pockets in the monolith. Then, the buffer in reservoir 1 was replaced with labeled analyte, which was loaded onto the monolith for 2 min by applying +500 V to reservoir 2 while keeping reservoir 1 grounded. After loading, the voltages were turned off for a 15 min incubation period where analyte could interact with the corresponding Ab. Meanwhile, reservoir 1 was cleaned thoroughly, fresh phosphate buffer (pH 7.2) was added, and then a 2 min rinsing step was carried out using the same voltage configuration as for the loading step. After rinsing, elution of retained analyte was carried out by replacing the buffer in reservoir 1 with elution solution and applying the same voltage configuration for 1 min. Detection was done after the end of the GMA monolith as indicated in Figure 5.1A.

5.2.7.2 Integrated Immunoaffinity Extraction and μCE

A four reservoir offset "T" design was used for integrated experiments as shown in Figure 5.1B. Reservoirs 4 and 5 were filled with phosphate buffer (pH 7.2), and reservoirs 3 and 6 were filled with separation buffer (50 mM BCB, 0.02% HPC, pH 10). The monolith was rinsed electrokinetically by applying +500 V on reservoir 5 for 2 min while keeping all other reservoirs grounded to ensure no air pockets were left in the monolith. After rinsing, sample was pipetted into reservoir 4 and loaded onto the monolith for 2 min by using the same voltage configuration followed by a no voltage incubation period of 15 min. During incubation, sample in reservoir 4 was replaced with phosphate buffer (pH 7.2) and after 15 min unattached analyte was rinsed as above. After rinsing, phosphate buffer was replaced with elution solution in reservoir 4 and elution was carried out with the same voltages applied as described previously for rinsing and loading. After a time determined by measuring the average of how long it took the eluted analyte to reach the injection intersection (25 s for Fer, n=4; 7 s for LF, n=4), +500 V was applied to reservoirs 4 and 5, reservoir 3 was grounded, and +1200 V was applied to reservoir 6 for μCE separation. The detection point was 0.5 cm beyond the injection intersection as shown in Figure 5.1B. Standard T-shaped PMMA devices[27, 34] were also used for μCE of samples under similar experimental conditions (buffer composition, voltage configuration and detection point) for comparison.

5.3 RESULTS AND DISCUSSION

5.3.1 Monolith Characterization

SEM images of GMA-EGDMA monoliths are shown in Figure 5.1D-E. The monoliths were found to be well polymerized and anchored to the microfluidic channel walls. Pores were randomly

distributed across the monolith, which aided in mixing of sample and increasing interaction with the Ab-modified monolith surface. Additionally, monolith nodules had diameters in the range of 200-500 nm. Monoliths did not detach from the channel walls or break during application of electric field or vacuum, consistent with previous reports.[37-38]

5.3.2 Antibody Immobilization

Antibodies are used extensively in microfluidic systems because of their high selectivity towards target proteins and ease of immobilization within microfluidic environments.[39] Compatibility of the antibody-antigen pairs used in this study was determined using a dot-blot test (see Figure 5.2). The dot blot shows high affinity of anti-LF towards LF and to LF spiked into serum; some binding of anti-LF was also observed for unspiked serum because of LF naturally present in serum. Higher affinity of anti-Fer was observed for Fer obtained from Calbiochem compared to Fer from Sigma, so Fer from Calbiochem was used for subsequent studies.

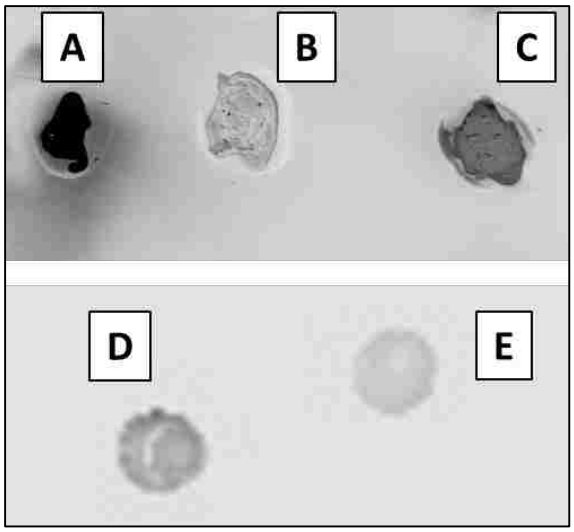

Figure 5.2 Dot blots. (A) LF (2 µg), (B) serum diluted 100× in TBS, and (C) serum spiked with 0.2 µg LF, all incubated with anti-LF. (D) Fer (10 µg, Calbiochem), and (E) Fer (10 µg, Sigma) incubated with anti-Fer.

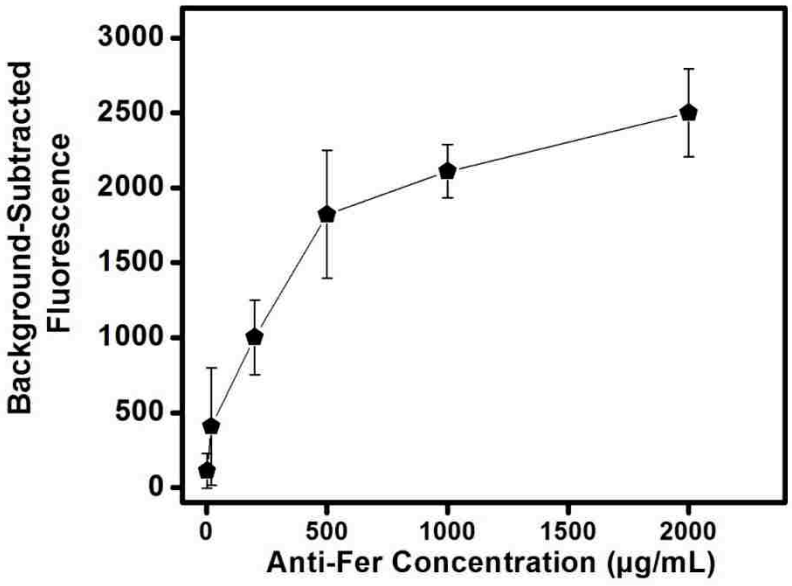

Figure 5.3 Background-subtracted fluorescence on a GMA-EGDMA monolith after immobilization of different concentrations of FITC-labeled anti-Fer (n=3) followed by rinsing.

Antibodies were immobilized in a single step by reacting the GMA epoxy groups on the monolith surface with amine groups present on Abs. I note that these epoxy groups can be converted to more reactive species for faster reaction kinetics, but that introduces additional monolith preparation steps that can reduce the overall device yield.[38] Initially, different concentrations of FITC-labeled anti-Fer were used for immobilization to determine optimal binding conditions. Figure 5.3 shows the background-subtracted fluorescence obtained from monoliths after immobilizing FITC-anti-Fer concentrations ranging from 2-2000 µg/mL followed by a rinsing step. A leveling off in the fluorescence signal from around 500-2000 µg/mL loaded Ab was observed, which indicates saturation of the monolith. Thus, for subsequent studies an Ab concentration of 2000 µg/mL was used in monolith modification. Additionally, the effect of repeating the Ab immobilization process for three consecutive days was also observed. Figure 5.4 shows no increase in fluorescence signal after the first day of immobilization, confirming that a single day of immobilization time is sufficient.

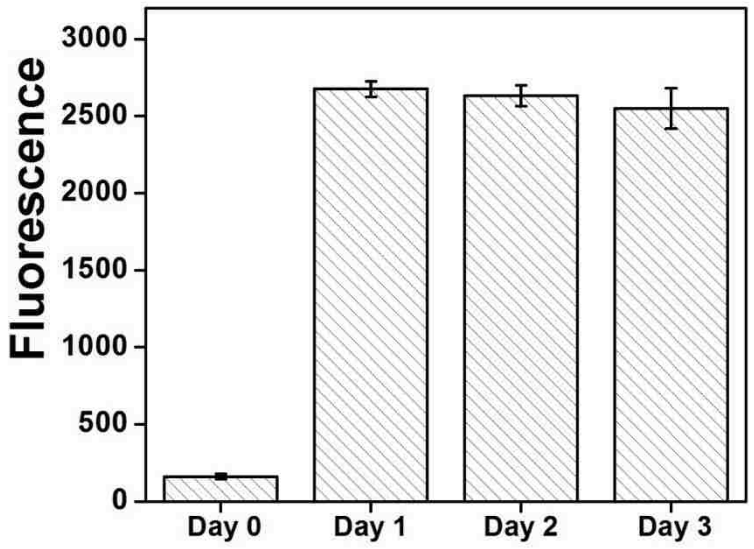

Figure 5.4 Effect of repeating immobilization of anti-Fer (2 mg/mL) on the same GMA-EGDMA column for three consecutive days (n=3).

5.3.3 Optimization of Immunoaffinity Extraction

Next, the pH for elution of target biomarker after affinity extraction on monoliths was determined. I used a straight channel design (Figure 5.1A) with the monolith modified with anti-Fer. Elution with either low pH (20 mM phosphoric acid, pH 2) or high pH (20 mM BCB, 25 mM NaCl, pH 11) was tested using 50 nM AF 488-labeled Fer. Fluorescent signal was recorded after the end of monolith as indicated in Figure 5.1A. AF 488 was used for labeling due to its more stable fluorescence across a wide pH range than FITC. Figure 5.5A shows elution traces of Fer from the monolith with both eluents. A delayed but steady elution of Fer was observed with low pH eluent. A more intense signal for eluted Fer was observed with high pH eluent, and the signal returned to background rapidly, indicating the higher elution efficiency at pH 11. Additionally, background-subtracted fluorescence was measured from CCD images of the monolith to show the effect on signal after each step (see Figure 5.5B). Images were taken after filling the column with pH 7

buffer to eliminate pH-dependent changes in fluorescence signal. No statistically significant change in the fluorescence was observed after elution at pH 2, indicating poor elution. In contrast, a 47% decrease in the fluorescence signal was observed after elution at pH 11, indicating much better elution efficiency at this pH, also consistent with the results in Figure 5.5A. Thus, pH 11 eluent was used for subsequent experiments.

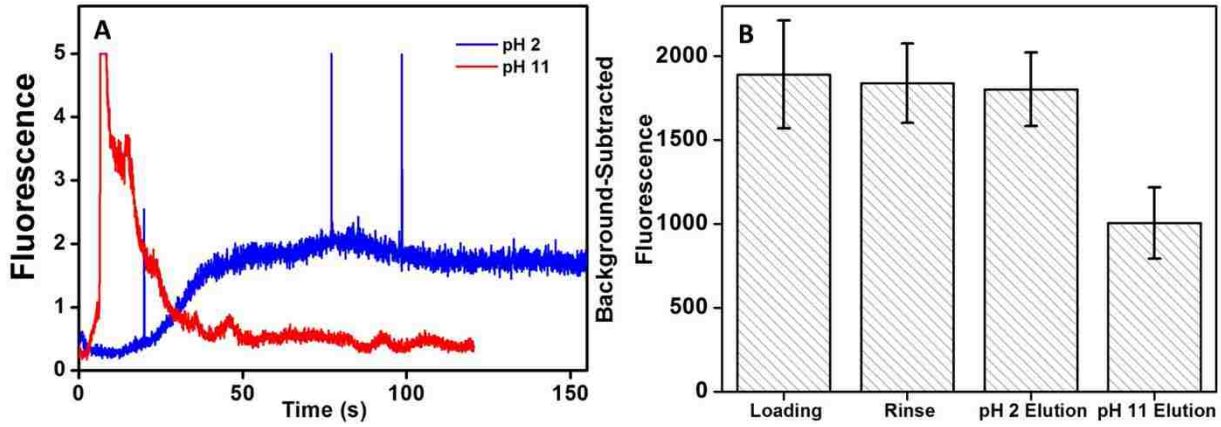

Figure 5.5 Effect of pH on extracted Fer (50 nM, AF 488 labeled) elution from an anti-Fer monolith. (A) Elution traces. (B) Background-subtracted fluorescence on the monolith after each step. Error bars represent the standard deviation in the mean fluorescence signal from the monolith obtained using ImageJ.

5.3.4 Immunoaffinity Extraction of PTB biomarkers

Figure 5.6 shows immunoaffinity extraction of two AF 488-labeled PTB biomarkers, Fer and LF from GMA-EGDMA columns with or without their corresponding Abs. Figure 5.6A-B shows elution traces for 10 and 1 nM Fer loaded on a monolith with or without anti-Fer. An initial peak at ~3-5 s was observed in these elution traces, which indicates either nonspecifically adsorbed AF 488 present in the sample or unretained Fer located in the monolith pores. In the columns modified with anti-Fer, a second peak was observed at 15-30 s, indicating elution of retained Fer; in contrast, no peak was observed for experiments on columns without anti-Fer. In Figure 5.6C-D, a similar

initial peak was obtained at ~2 s for all columns. However, a second peak for retained LF at 3-8 s was observed only when anti-LF was immobilized on the column, corresponding to the elution of retained LF. Two different concentrations of Fer and LF were loaded on the column for these experiments; for a 10-fold increase in concentration 9- and 8-fold increases in eluted peak area were observed for Fer and LF, respectively, showing promise for quantitative analysis[32] in the future. The eluted peaks were also broader for higher loaded concentrations. These results indicate the ability to extract PTB biomarkers with concentration-dependent elution using Ab-modified monolithic columns.

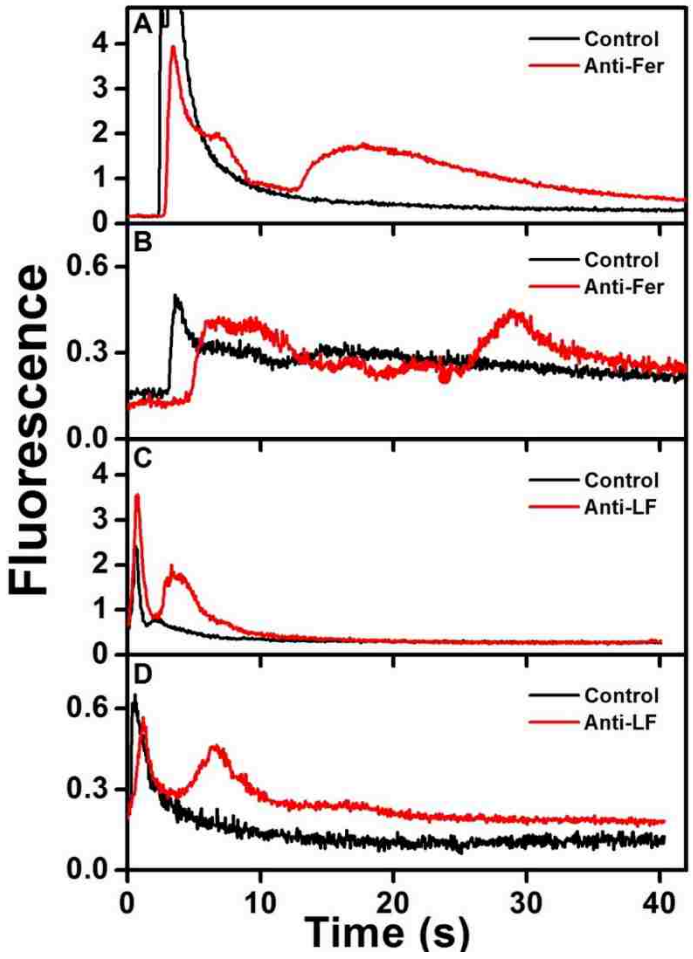

Figure 5.6 Elution traces after immunoaffinity extraction of PTB biomarkers on control and Ab-modified monoliths. Loaded concentrations: (A) 10 nM Fer, (B) 1 nM Fer, (C) 25 nM LF, and (D) 2.5 nM LF.

5.3.5 Integrated Immunoaffinity Extraction and μCE

The ability to multiplex biomarkers is essential; in these studies, integration with μCE can be used to separate multiple extracted biomarkers. Figure 5.7A shows μCE of 10 nM AF 488-labeled Fer using a standard device with pinched injection for 1 min.[27, 34, 40] When this same sample was first extracted on an anti-Fer modified monolith in an integrated device, the peak for free AF 488 was not observed at ~6 s and the Fer peak area increased by 6 fold (Figure 5.7B). Similarly, in Figure 5.7C a peak for free AF 488 was observed in μCE of 25 nM LF. When this sample was first extracted on an integrated anti-LF column and then analyzed by μCE (Figure 5.7D), the LF peak area increased by 2.5 fold, and the unbound AF 488 peak area decreased by 7 fold. In the integrated devices, small variations in the distance between the polymerized monolith and injection intersection can lead to variations in the migration time for the eluted analyte plug to reach the intersection. Thus for each integrated device, eluted analyte was initially detected at the injection intersection to determine the migration/elution time, as described in section 2.7.2. The elution times for Fer and LF ranged from 15-20 s and 5-10 s (n=6), respectively, in these integrated devices, and the elution/injection times used to obtain data like that shown in Figure 5.7B and 5.7D were 20 s and 7 s (n=2), respectively. These results show that the integrated affinity monolith devices can be used for capture and elution of analytes with good run-to-run and device-to-device reproducibility. Addiotnally, this work demonstrates the ability to combine immunoaffinity extraction, specific elution, and electrophoretic separation of PTB biomarkers from buffered samples using an integrated device.

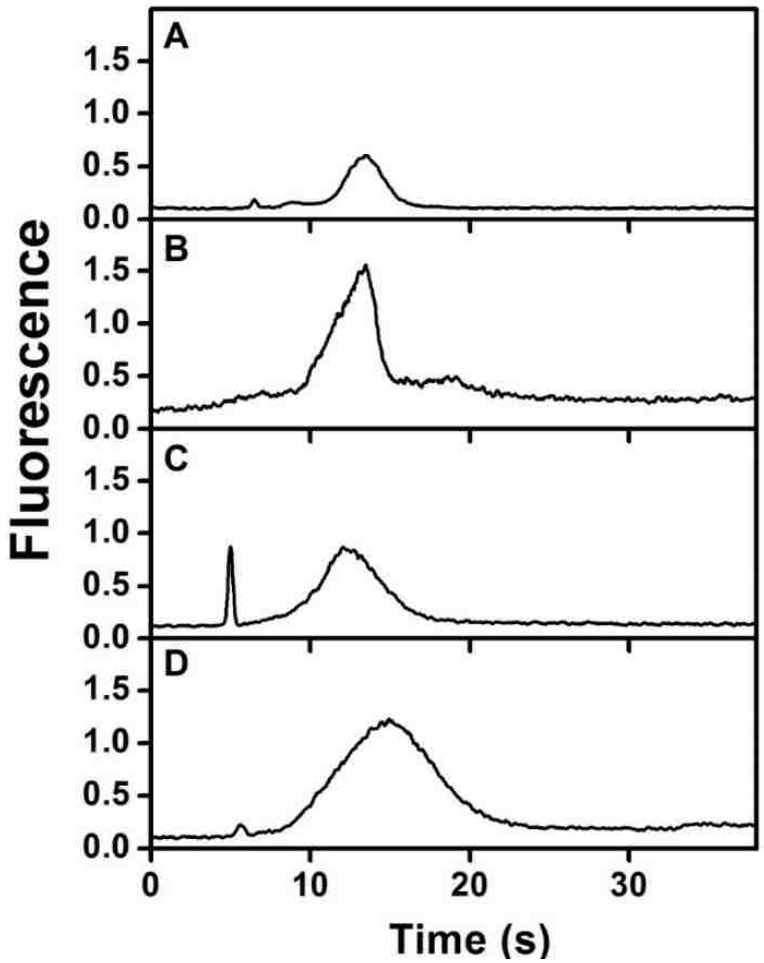

Figure 5.7 Integrated immunoaffinity extraction and μCE of PTB biomarkers. Electropherograms of 10 nM AF 488-labeled Fer (A) before and (B) after on-chip immunoaffinity extraction. Electropherograms showing μCE of 25 nM AF 488-labeled LF (C) before and (D) after on-chip immunoaffinity extraction. Elution/injection times were: (A) 1 min, (B) 20 s, (C) 1 min, and (D) 7 s.

5.3.6 Extraction and μCE Separation of PTB Biomarkers in a Human Serum Matrix

Biological matrices like blood often require multiple sample preparation steps prior to analysis that increase time and costs. Thus, after optimizing the integrated devices for analyzing samples in buffer, I analyzed spiked serum samples. Figure 5.8A shows μCE of AF 488-labeled spiked human serum prepared as described in Section 5.2.5. Multiple overlapping peaks from amine-labeled components present in serum mask the Fer and LF peaks. This same sample was then

extracted on a monolith modified with both anti-LF and anti-Fer in an integrated device, eluted to the injection intersection, and analyzed by μCE. As above, the migration times for eluted Fer and LF were determined to have overlap at 15 s (n=4) for the eluted plug at the injection intersection. In the electropherogram after on-chip sample processing (Figure 5.8B), essentially all non-target peaks were removed and only peaks for LF and Fer were observed, indicating the sample purification capabilities of these devices. Notably, the total analysis time for this experiment was <30 min. The LF and Fer peaks were not baseline resolved because they have similar migration times (see Figure 5.7), and as also observed in a previous report.[27]

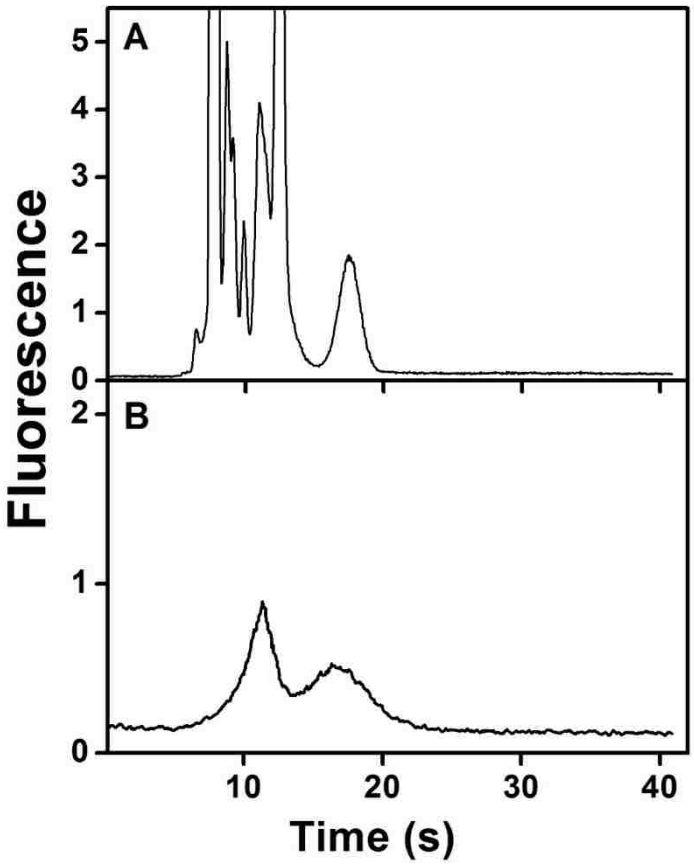

Figure 5.8 Integrated immunoaffinity extraction and μCE of PTB biomarkers spiked in human blood serum. Electropherograms of AF 488-labeled spiked human serum, (A) before and (B) after on-chip immunoaffinity extraction. Elution/injection times were: (A) 1 min and (B) 15 s.

Additionally, the fluorescence signal for the extracted LF and Fer peaks was lower than in Figure 5.7 because the fluorescence labeling was affected by the presence of other abundant amine-reactive species in blood serum seen in Figure 5.8A. Importantly, integration with a downstream fluorescent labeling process[16, 27-28] could improve signal. These results clearly indicate that these integrated microfluidic devices can extract, specifically elute and separate target biomarkers from complex biological matrices, offering potential for future point-of-care applications.

5.4 REFERENCES

1. Nge, P. N.; Rogers, C. I.; Woolley, A. T., Advances in Microfluidic Materials, Functions, Integration, and Applications. *Chem. Rev.* **2013,** *113* (4), 2550-2583.

2. Nahavandi, S.; Baratchi, S.; Soffe, R.; Tang, S.-Y.; Nahavandi, S.; Mitchell, A.; Khoshmanesh, K., Microfluidic platforms for biomarker analysis. *Lab Chip* **2014,** *14* (9), 1496-1514.

3. Pagaduan, J. V.; Sahore, V.; Woolley, A. T., Applications of microfluidics and microchip electrophoresis for potential clinical biomarker analysis. *Anal. Bioanal. Chem.* **2015,** *407* (23), 6911-6922.

4. Sanjay, S. T.; Fu, G.; Dou, M.; Xu, F.; Liu, R.; Qi, H.; Li, X., Biomarker detection for disease diagnosis using cost-effective microfluidic platforms. *Analyst* **2015,** *140* (21), 7062-7081.

5. Sonker, M.; Sahore, V.; Woolley, A. T., Recent advances in microfluidic sample preparation and separation techniques for molecular biomarker analysis: A critical review. *Anal. Chim. Acta* **2017,** *Doi: 10.1016/j.aca.2017.07.043*.

6. Shadfan, B. H.; Simmons, A. R.; Simmons, G. W.; Ho, A.; Wong, J.; Lu, K. H.; Bast, R. C.; McDevitt, J. T., A Multiplexable, Microfluidic Platform for the Rapid Quantitation of a

Biomarker Panel for Early Ovarian Cancer Detection at the Point-of-Care. *Cancer Prev. Res.* **2015,** *8* (1), 37-48.

7. Ali, M. A.; Mondal, K.; Jiao, Y.; Oren, S.; Xu, Z.; Sharma, A.; Dong, L., Microfluidic Immuno-Biochip for Detection of Breast Cancer Biomarkers Using Hierarchical Composite of Porous Graphene and Titanium Dioxide Nanofibers. *ACS Appl. Mater. Interfaces* **2016,** *8* (32), 20570-20582.

8. Li, J.; Chang, K.-W.; Wang, C.-H.; Yang, C.-H.; Shiesh, S.-C.; Lee, G.-B., On-chip, aptamer-based sandwich assay for detection of glycated hemoglobins via magnetic beads. *Biosens. Bioelectron.* **2016,** *79*, 887-893.

9. Shin, S. R.; Zhang, Y. S.; Kim, D.-J.; Manbohi, A.; Avci, H.; Silvestri, A.; Aleman, J.; Hu, N.; Kilic, T.; Keung, W.; Righi, M.; Assawes, P.; Alhadrami, H. A.; Li, R. A.; Dokmeci, M. R.; Khademhosseini, A., Aptamer-Based Microfluidic Electrochemical Biosensor for Monitoring Cell-Secreted Trace Cardiac Biomarkers. *Anal. Chem.* **2016,** *88* (20), 10019-10027.

10. Mohamadi, R. M.; Svobodova, Z.; Bilkova, Z.; Otto, M.; Taverna, M.; Descroix, S.; Viovy, J.-L., An integrated microfluidic chip for immunocapture, preconcentration and separation of b-amyloid peptides. *Biomicrofluidics* **2015,** *9* (5), 054117.

11. Piraino, F.; Volpetti, F.; Watson, C.; Maerkl, S. J., A Digital–Analog Microfluidic Platform for Patient-Centric Multiplexed Biomarker Diagnostics of Ultralow Volume Samples. *ACS Nano* **2016,** *10* (1), 1699-1710.

12. Garg, N.; Vallejo, D.; Boyle, D.; Nanayakkara, I.; Teng, A.; Pablo, J.; Liang, X.; Camerini, D.; Lee, A. P.; Felgner, P., Integrated On-Chip Microfluidic Immunoassay for Rapid Biomarker Detection. *Procedia Eng.* **2016,** *159*, 53-57.

13. Mohammadi, M.; Madadi, H.; Casals-Terré, J.; Sellarès, J., Hydrodynamic and direct-current insulator-based dielectrophoresis (H-DC-iDEP) microfluidic blood plasma separation. *Anal. Bioanal. Chem.* **2015,** *407* (16), 4733-4744.

14. Kumar, S.; Sahore, V.; Rogers, C. I.; Woolley, A. T., Development of an integrated microfluidic solid-phase extraction and electrophoresis device. *Analyst* **2016,** *141* (5), 1660-1668.

15. Cong, Y.; Katipamula, S.; Geng, T.; Prost, S. A.; Tang, K.; Kelly, R. T., Electrokinetic sample preconcentration and hydrodynamic sample injection for microchip electrophoresis using a pneumatic microvalve. *Electrophoresis* **2016,** *37* (3), 455-462.

16. Yang, R.; Pagaduan, J. V.; Yu, M.; Woolley, A. T., On chip preconcentration and fluorescence labeling of model proteins by use of monolithic columns: device fabrication, optimization, and automation. *Anal. Bioanal. Chem.* **2015,** *407* (3), 737-747.

17. Herzog, C.; Poehler, E.; Peretzki, A. J.; Borisov, S. M.; Aigner, D.; Mayr, T.; Nagl, S., Continuous on-chip fluorescence labelling, free-flow isoelectric focusing and marker-free isoelectric point determination of proteins and peptides. *Lab Chip* **2016,** *16* (9), 1565-1572.

18. Cui, F.; Rhee, M.; Singh, A.; Tripathi, A., Microfluidic Sample Preparation for Medical Diagnostics. *Annu. Rev. Biomed. Eng.* **2015,** *17* (1), 267-286.

19. Karle, M.; Vashist, S. K.; Zengerle, R.; von Stetten, F., Microfluidic solutions enabling continuous processing and monitoring of biological samples: A review. *Anal. Chim. Acta* **2016,** *929*, 1-22.

20. Goldenberg, R. L.; Culhane, J. F.; Iams, J. D.; Romero, R., Epidemiology and causes of preterm birth. *Lancet* **2008,** *371* (9606), 75-84.

21. Blencowe, H.; Cousens, S.; Oestergaard, M. Z.; Chou, D.; Moller, A.-B.; Narwal, R.; Adler, A.; Vera Garcia, C.; Rohde, S.; Say, L.; Lawn, J. E., National, regional, and worldwide

estimates of preterm birth rates in the year 2010 with time trends since 1990 for selected countries: a systematic analysis and implications. *Lancet* **2012,** *379* (9832), 2162-2172.

22. Romero, R.; Dey, S. K.; Fisher, S. J., Preterm labor: One syndrome, many causes. *Science* **2014,** *345* (6198), 760-765.

23. Esplin, M. S.; Merrell, K.; Goldenberg, R.; Lai, Y.; Iams, J. D.; Mercer, B.; Spong, C. Y.; Miodovnik, M.; Simhan, H. N.; van Dorsten, P.; Dombrowski, M., Proteomic identification of serum peptides predicting subsequent spontaneous preterm birth. *Am. J. Obstet. Gynecol.* **2011,** *204* (5), 391.e1-391.e8.

24. Graves, S. W.; Esplin, M. S., 80: Validation of predictive preterm birth biomarkers obtained by maternal serum proteomics. *Am. J. Obstet. Gynecol.* **2011,** *204* (1), S46.

25. Sahore, V.; Kumar, S.; Rogers, C. I.; Jensen, J. K.; Sonker, M.; Woolley, A. T., Pressure-actuated microfluidic devices for electrophoretic separation of pre-term birth biomarkers. *Anal. Bioanal. Chem.* **2016,** *408* (2), 599-607.

26. Sonker, M.; Knob, R.; Sahore, V.; Woolley, A. T., Integrated electrokinetically driven microfluidic devices with pH-mediated solid-phase extraction coupled to microchip electrophoresis for preterm birth biomarkers. *Electrophoresis* **2017,** *38* (13-14), 1743-1754.

27. Sonker, M.; Yang, R.; Sahore, V.; Kumar, S.; Woolley, A. T., On-chip fluorescent labeling using reversed-phase monoliths and microchip electrophoretic separations of selected preterm birth biomarkers. *Anal. Methods* **2016,** *8* (43), 7739-7746.

28. Sahore, V.; Sonker, M.; Nielsen, A. V.; Knob, R.; Kumar, S.; Woolley, A. T., Automated Microfluidic Devices Integrating Solid-Phase Extraction, Fluorescent Labeling and Microchip Electrophoresis for Preterm Birth Biomarker Analysis. *Anal. Bioanal. Chem.* **2017,** *DOI: 10.1007/s00216-017-0548-7*.

29. Knob, R.; Sahore, V.; Sonker, M.; Woolley, A. T., Advances in monoliths and related porous materials for microfluidics. *Biomicrofluidics* **2016,** *10* (3), 032901.

30. Liu, X.; Wang, H.; Liang, A.; Li, Y.; Gai, H.; Lin, B., Determination of binding constants between one protein and multiple carbohydrates by affinity chromatography on a microchip. *J. Chromatogr. A* **2012,** *1270*, 340-343.

31. Kang, Q.-S.; Shen, X.-F.; Hu, N.-N.; Hu, M.-J.; Liao, H.; Wang, H.-Z.; He, Z.-K.; Huang, W.-H., A 3D porous polymer monolith-based platform integrated in poly(dimethylsiloxane) microchips for immunoassay. *Analyst* **2013,** *138* (9), 2613-2619.

32. Yang, W.; Sun, X.; Wang, H.-Y.; Woolley, A. T., Integrated microfluidic device for serum biomarker quantitation using either standard addition or a calibration curve. *Anal. Chem.* **2009,** *81* (19), 8230-8235.

33. Yang, W.; Yu, M.; Sun, X.; Woolley, A. T., Microdevices integrating affinity columns and capillary electrophoresis for multibiomarker analysis in human serum. *Lab Chip* **2010,** *10* (19), 2527-2533.

34. Kelly, R. T.; Woolley, A. T., Thermal Bonding of Polymeric Capillary Electrophoresis Microdevices in Water. *Anal. Chem.* **2003,** *75* (8), 1941-1945.

35. Nge, P. N.; Pagaduan, J. V.; Yu, M.; Woolley, A. T., Microfluidic chips with reversed-phase monoliths for solid phase extraction and on-chip labeling. *J. Chromatogr. A* **2012,** *1261*, 129-135.

36. Ladner, Y.; Bruchet, A.; Crétier, G.; Dugas, V.; Randon, J.; Faure, K., New "one-step" method for the simultaneous synthesis and anchoring of organic monolith inside COC microchip channels. *Lab Chip* **2012,** *12* (9), 1680-1685.

37. Sun, X.; Yang, W.; Pan, T.; Woolley, A. T., Affinity monolith-integrated poly (methyl methacrylate) microchips for on-line protein extraction and capillary electrophoresis. *Anal. Chem.* **2008,** *80* (13), 5126-5130.

38. Yang, W.; Sun, X.; Pan, T.; Woolley, A. T., Affinity monolith preconcentrators for polymer microchip capillary electrophoresis. *Electrophoresis* **2008,** *29* (16), 3429-3435.

39. Mairhofer, J.; Roppert, K.; Ertl, P., Microfluidic Systems for Pathogen Sensing: A Review. *Sensors* **2009,** *9* (6), 4804-4823.

40. Jacobson, S. C.; Hergenroder, R.; Koutny, L. B.; Warmack, R.; Ramsey, J. M., Effects of injection schemes and column geometry on the performance of microchip electrophoresis devices. *Anal. Chem.* **1994,** *66* (7), 1107-1113.

6. CONCLUSIONS AND FUTURE WORK

6.1 CONCLUSIONS

6.1.1 μCE OF Selected PTB Biomarkers

In chapter 2, I demonstrated the ability to use μCE for separation of model analytes and more importantly PTB biomarkers. Device fabrication protocols were developed, and fabricated PMMA devices were used for μCE of several off-chip labeled model analytes along with selected PTB biomarkers. Separation protocols, voltage configurations, and buffer compositions were developed and characterized for the separation of selected PTB biomarkers in <2 min. These electropherograms further show the ability to separate PTB biomarkers, a capability that can be further utilized in the future to develop integrated microfluidic devices with upstream immunoaffinity extraction[1-2] and on-chip labeling[3-5] processes for PTB diagnosis.

6.1.2 On-Chip Fluorescent Labeling of PTB Biomarkers

Sample preparation is a challenge in automation of analysis. In chapter 3, I demonstrated on-chip SPE and fluorescent labeling of PTB biomarkers. Reversed-phase monoliths were studied, and an octyl methacrylate formulation was found to provide desired retention and elution characteristics for on-chip labeling of PTB peptide and protein biomarkers. I successfully performed on-chip solid-phase extraction and fluorescent labeling of three PTB biomarkers with comparable results compared to off-chip labeled samples. Importantly, on-chip labeling used 10-fold smaller reagent volumes (~10 μL) in 30-fold faster times (15-20 min) for sample preparation compared to off-chip labeling procedures (~100 μL volumes and >10 hr reaction times). Although the dye and analyte

peaks were not completely resolved in electroelution, better resolution can be achieved on integration with μCE.

6.1.3 Integrated pH-mediated SPE and Electrophoretic Separation of PTB Biomarkers

In chapter 4, a pH-mediated SPE method was developed using hydrophobicity and electrophoretic mobility modulation in different pH buffers, and applied in preconcentration of biomarkers related to preterm birth. Surface modification of COC microchannels was performed using PEGDA to increase the hydrophilicity to make electrokinetic flow more reproducible. Porous, reversed-phase C8 monoliths polymerized in COC channels were used for SPE. Eluents of different pH and ionic concentrations were used to determine the best elution conditions. The optimized eluent was then used to preconcentrate multiple analytes on C8 monoliths. An enrichment factor of nearly 50 was observed for a PTB peptide biomarker (P1) eluted from a monolith after 5 min of injection, with reproducible elution (~6% or better migration time RSD). A linear relation between peptide concentration and eluted peak height was also observed, indicating the potential for this approach to be used for quantitative analysis. The monolith binding capacity for P1 in these devices was determined to be 400 pg (0.2 pmol). Importantly, this pH-mediated SPE approach was integrated with μCE to enable combined enrichment (~15-fold) and μCE separation of a peptide biomarker related to preterm birth (P1).

6.1.4 Immunoaffinity Extraction and Separation of PTB Biomarkers

In chapter 5, I reported immunoaffinity monolith microfluidic devices integrated with μCE for extraction and separation of PTB biomarkers directly from a human serum matrix. The microchips

were electrokinetically operated, and a reactive GMA-EGDMA monolith was polymerized in microfluidic channels to immobilize antibodies specific to PTB biomarkers. Antibody immobilization and biomarker extraction protocols were optimized, and two PTB biomarkers were extracted at low nM concentrations using these affinity columns. These immunoaffinity extraction monoliths were further integrated with μCE for combined extraction and separation of two PTB biomarkers directly in a blood serum matrix in <30 min analysis time.

6.2 FUTURE WORK

6.2.1 Integration of Immunoaffinity Extraction, On-chip Labeling and μCE

Our ultimate goal is to develop a microfluidic platform that can electrokinetically extract, fluorescently label, separate and quantify PTB biomarkers directly from blood samples. To achieve this goal, all the processes described in chapters 2-5 should be integrated into one microchip as shown schematically in Figure 6.1. Combining multiple steps can also be important for minimizing or avoiding human error during sample handling. The devices and methods I developed show potential for integrated on-chip sample preparation, including purification, preconcentration, fluorescent labeling and separation of PTB bioamrkers. This could enable the analysis of low concentrations of PTB biomarkers directly from serum samples using an affinity monolith[1, 6] for selective capture, and then enriching these biomarkers on a reversed-phase monolith for fluorescent labeling,[3-4, 7] followed by electrophoretic separation.[8] Additional reservoirs can also be introduced as required for different reagents used in immunoaffinity extraction, on-chip labeling and separation of PTB biomarkers to automate the analysis. After optimization and integration of all three modules, one should be able to put a sample (~10 μL) into this device and extract, label,

separate and quantify all nine PTB biomarkers (down to 1 ng/mL) within an hour. Such a device could offer a prompt and cost-effective analysis platform for PTB biomarkers.

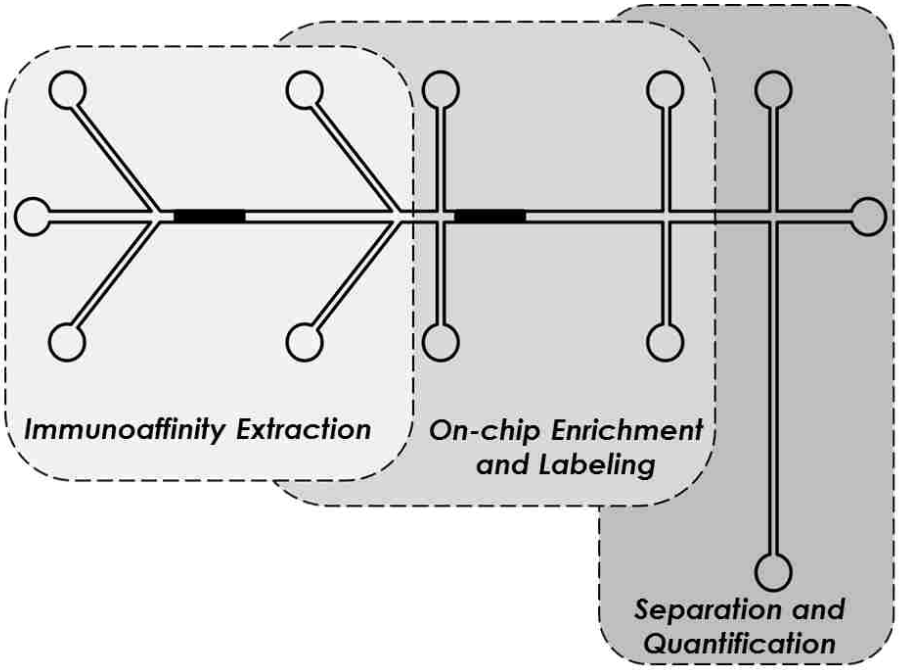

Figure 6.1 Schematic for proposed integrated microfluidic device for PTB diagnosis.

6.2.2 Integrated Analysis for PTB Diagnosis

To be able to predict PTB risk, an integrated microfluidic device like the one in Figure 6.1 should be optimized for work with serum samples to enable this platform to be used in PTB risk assessment. Serum samples spiked with commercially obtained PTB peptides and proteins can be analyzed initially. Once adequate results are achieved with serum samples, testing on blind samples will follow. These serum samples can be used to quantify PTB biomarkers at their known blood concentrations. Once quantification is reproducibly achieved in several devices, results can

be validated by comparing to standard LC-MS quantification. This will establish the performance of this platform on serum samples, demonstrating its potential for PTB risk assessment.

6.2.3 3D Printed Integrated Microfluidic Devices for PTB Diagnosis

3D printing has gained immense interest recently for developing microfluidic devices due to its high fabrication rate and low barrier to editing, which could hasten innovation.[9-11] Many researchers have reported 3D printed fluidic devices for analytical applications,[10, 12-13] but most have fluidic features at the mm or sub-mm scale, while very few publications have achieved the ~100 μm size range for 3D printed microfluidic features.[14-16] Thus, improvement in critical dimensions is still required to develop truly microfluidic devices.[16-17] Additionally, diagnostic applications for biomarker detection using 3D printed microfluidics[17] will need to be expanded and improved upon significantly in the future.

Recently, Nordin and Woolley's groups developed an optical approach to resin formulation for making truly microfluidic 3D printed devices[14, 18] and characterization of these 3D printed devices for μCE and immunoaffinity extraction is currently underway. For example, Figure 6.2A shows a 3D printed T-shaped microfluidic device being developed for μCE. Porous polymer monoliths or other solid support media can also be incorporated into 3D printed devices, as seen in Figure 6.2B, which shows a 3D printed device being used for optimization of immunoaffinity extraction monoliths. Additionally, 3D printed on-chip valves, pumps and multiplexers were also shown recently for facilitating fluid manipulation and automation, as shown in Figure 6.2C.[15, 19] 3D printed valves and pumps could be used to restrict, mix, and move samples within immunoaffinity extraction, on-chip labeling and separation modules of an integrated device, as

shown previously using PDMS valves and pumps.[8, 20-21] In the future, these 3D printed components could be specifically developed and integrated for the analysis of PTB biomarkers.

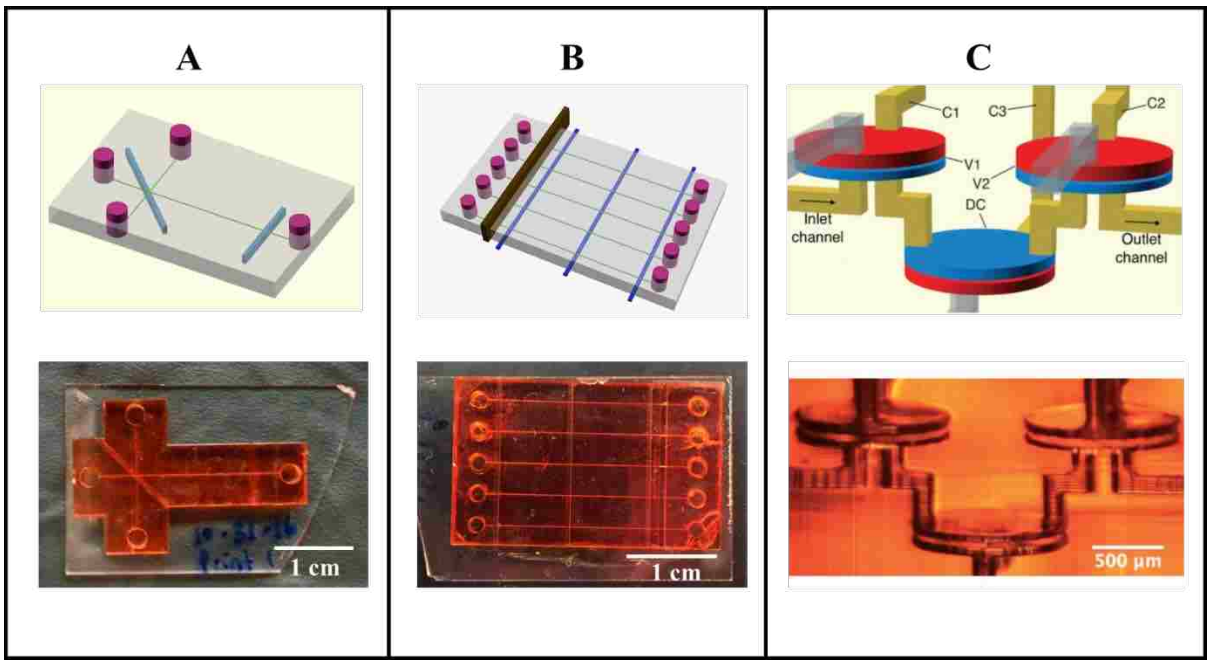

Figure 6.2 3D printed microfluidic devices. A. Schematic (top) and photograph (bottom) of a 3D printed µCE device. Images provided by Michael Beauchamp. B. Schematic (top) and photograph (bottom) of a 3D printed straight channel microfluidic device for immunoaffinity extraction. Images provided by Ellen Parker. C. Schematic (top) and micrograph (bottom) of 3D printed valves in a microfluidic device. Adapted with permission from Gong, H. *et al. Lab Chip* 2016, *16* (13), 2450-2458.

The integrated microfluidic systems described here offer potential for early diagnosis of PTB through biomarker analysis. Early diagnosis can potentially limit PTB related complications by enabling therapeutic interventions to delay birth or expedite fetal development, reducing costs and improving the quality of life. Finally, the general approach for this platform is not restricted to PTB biomarker analysis but can also be implemented for diagnosis of other diseases.

6.3 REFERENCES

1. Yang, W.; Yu, M.; Sun, X.; Woolley, A. T., Microdevices integrating affinity columns and capillary electrophoresis for multibiomarker analysis in human serum. *Lab Chip* **2010,** *10* (19), 2527-2533.

2. Sun, X.; Yang, W.; Pan, T.; Woolley, A. T., Affinity monolith-integrated poly (methyl methacrylate) microchips for on-line protein extraction and capillary electrophoresis. *Anal. Chem.* **2008,** *80* (13), 5126-5130.

3. Sonker, M.; Yang, R.; Sahore, V.; Kumar, S.; Woolley, A. T., On-chip fluorescent labeling using reversed-phase monoliths and microchip electrophoretic separations of selected preterm birth biomarkers. *Anal. Methods* **2016,** *8* (43), 7739-7746.

4. Yang, R.; Pagaduan, J. V.; Yu, M.; Woolley, A. T., On chip preconcentration and fluorescence labeling of model proteins by use of monolithic columns: device fabrication, optimization, and automation. *Anal. Bioanal. Chem.* **2015,** *407* (3), 737-747.

5. Nge, P. N.; Pagaduan, J. V.; Yu, M.; Woolley, A. T., Microfluidic chips with reversed-phase monoliths for solid phase extraction and on-chip labeling. *J. Chromatogr. A* **2012,** *1261*, 129-135.

6. Yang, W.; Sun, X.; Wang, H.-Y.; Woolley, A. T., Integrated microfluidic device for serum biomarker quantitation using either standard addition or a calibration curve. *Anal. Chem.* **2009,** *81* (19), 8230-8235.

7. Sonker, M.; Knob, R.; Sahore, V.; Woolley, A. T., Integrated electrokinetically driven microfluidic devices with pH-mediated solid-phase extraction coupled to microchip electrophoresis for preterm birth biomarkers. *Electrophoresis* **2017,** *38* (13-14), 1743-1754.

8. Sahore, V.; Kumar, S.; Rogers, C. I.; Jensen, J. K.; Sonker, M.; Woolley, A. T., Pressure-actuated microfluidic devices for electrophoretic separation of pre-term birth biomarkers. *Anal. Bioanal. Chem.* **2016,** *408* (2), 599-607.

9. Bishop, G. W., 3D Printed Microfluidic Devices. In *Microfluidics for Biologists: Fundamentals and Applications*, Dixit, C. K.; Kaushik, A., Eds. Springer International Publishing: Cham, 2016; pp 103-113.

10. Bhattacharjee, N.; Urrios, A.; Kang, S.; Folch, A., The upcoming 3D-printing revolution in microfluidics. *Lab on a Chip* **2016,** *16* (10), 1720-1742.

11. Reza, A.; Stephanie, K.; Alexander, H.; Bekir, Y.; Fariba, G.; Sara, K.; Michael, M.; Ali, K.; Savas, T., 3D-printed microfluidic devices. *Biofabrication* **2016,** *8* (2), 022001.

12. Lee, W.; Kwon, D.; Choi, W.; Jung, G. Y.; Au, A. K.; Folch, A.; Jeon, S., 3D-Printed Microfluidic Device for the Detection of Pathogenic Bacteria Using Size-based Separation in Helical Channel with Trapezoid Cross-Section. *Sci. Rep.* **2015,** *5*, 7717.

13. Ho, C. M. B.; Ng, S. H.; Li, K. H. H.; Yoon, Y.-J., 3D printed microfluidics for biological applications. *Lab on a Chip* **2015,** *15* (18), 3627-3637.

14. Gong, H.; Beauchamp, M.; Perry, S.; Woolley, A. T.; Nordin, G. P., Optical approach to resin formulation for 3D printed microfluidics. *RSC Adv.* **2015,** *5* (129), 106621-106632.

15. Gong, H.; Woolley, A. T.; Nordin, G. P., High density 3D printed microfluidic valves, pumps, and multiplexers. *Lab Chip* **2016,** *16* (13), 2450-2458.

16. Beauchamp, M. J.; Nordin, G. P.; Woolley, A. T., Moving from millifluidic to truly microfluidic sub-100-μm cross-section 3D printed devices. *Anal. Bioanal. Chem.* **2017,** *409* (18), 4311-4319.

17. Waheed, S.; Cabot, J. M.; Macdonald, N. P.; Lewis, T.; Guijt, R. M.; Paull, B.; Breadmore, M. C., 3D printed microfluidic devices: enablers and barriers. *Lab on a Chip* **2016,** *16* (11), 1993-2013.

18. Gong, H.; Bickham, B. P.; Woolley, A. T.; Nordin, G. P., Custom 3D printer and resin for 18 μm × 20 μm microfluidic flow channels. *Lab Chip* **2017,** *DOI: 10.1039/C7LC00644F*.

19. Rogers, C. I.; Qaderi, K.; Woolley, A. T.; Nordin, G. P., 3D printed microfluidic devices with integrated valves. *Biomicrofluidics* **2015,** *9* (1), 016501.

20. Kumar, S.; Sahore, V.; Rogers, C. I.; Woolley, A. T., Development of an integrated microfluidic solid-phase extraction and electrophoresis device. *Analyst* **2016,** *141* (5), 1660-1668.

21. Sahore, V.; Sonker, M.; Nielsen, A. V.; Knob, R.; Kumar, S.; Woolley, A. T., Automated Microfluidic Devices Integrating Solid-Phase Extraction, Fluorescent Labeling and Microchip Electrophoresis for Preterm Birth Biomarker Analysis. *Anal. Bioanal. Chem.* **2017,** *DOI: 10.1007/s00216-017-0548-7*.